Sapienza University of Rome

Antimycobacterial compounds targeting MmpL3 and tryptophan biosynthetic pathway

Pharmaceutical Sciences XXXI

PhD candidate

Giulia Venditti

Tutor

Prof. Mariangela Biava

Abstract

Tuberculosis (TB) remains the main cause of death for infectious diseases with 10.4 million new cases in 2016. The spreading of resistant strain of *Mycobacterium tuberculosis* makes the discovery of innovative anti-TB drugs a global urgency.

The present thesis concerned the development of new antimycobacterial agents targeting MmpL3 and the tryptophan biosynthesis.

In the first study we synthetized a novel series of pyrazole derivatives in order to improve the drug-like properties and safety profile of the potent MmpL3 inhibitor **BM635.** Several synthetized pyrazoles showed better activity and drug-like properties compared to hit and the best one proved to be also effective in a mouse model of TB infection.

In the second study, we synthetized analogues of the 2-amino-6-fluorobenzoic acid (6-FABA), as promising new antimycobacterial compounds acting on tryptophan (Trp) biosynthetic pathway. The synthetized aryl hydrazides analogues showed better activities than 6-FABA and good cytotoxicities, making them good candidates for *in vivo* studies. Moreover, the inhibition of Trp biosynthetic pathway was confirmed by target studies on aryl hydrazides.

Altogether, presented results demonstrated MmpL3 and Trp biosynthesis inhibitions as new promising pharmacological approaches for the treatment of TB.

Abbreviations: TB, tuberculosis; WHO, World Health Organization; PIMs, phosphatidylinositol mannosides; LAM, lipoarabinomannan; TDM, treahlose mono-mycolate; TNF, tumour necrosis factor; IL-1β, interleukin 1β; IL-6, interleukin 6; LTB, latent tuberculosis; MDR-TB, multidrug-resistant tuberculosis; XDR-TB, extensively drug-resistant TB; MTB, *M. tuberculosis*; HIV, human immunodeficiency virus; RR-TB, rifampicin resistant tuberculosis; INH, isoniazid; RIF, rifampin; EMB, ethambutol; PZ, pyrazinamide; ARV, antiretroviral; DprE1, decaprenylphosphoryl-β-D-ribose-2'-epimerase ; FDA, food and drugs administration; EMA, European medicines agency; PMF, proton motive force, ROS, reactive oxygen species; LeuRS, leucyl-tRNA synthetase, PK, pharmacokinetic; ATP, adenosine triphosphate; NADH, nicotinamide adenine dinucleotide; PDE6, phosphodiesterase 6; HepG2, human hepatic carcinoma cell line; LORA, low oxygen recovery assay, ED_{99}, efficacious dose in 99% of treated mice; AUC, area under the curve; DNA, deoxyribonucleic acid; WGS, whole genome sequencing; MmpL3, mycobacterium membrane protein Large 3; RND, resistance, nodulation and division; Trp, tryptophan; TLC, thin layer chromatography; MIC, minimum inhibitory concentration; THF, tetrahydrofuran; TEA, trimethylamine; DCM, dichloromethane; DCE, dichloroethane; TOX_{50}, concentration of compound resulting in 50% inhibition; HSA, human serum albumin; CLND, chemiluminescent nitrogen detection; FaSSIF, fasted state simulated intestinal fluid; hERG, human ether-a-go-go-related gene; SAR, structure activity relationship, CFU, colony forming unit; AnPRT, anthranilate phosphoribosyl transferase; TrpAB, tryptophan synthase, 6-FABA, 6-fluoro anthranilic acid; PRPP, phosphor ribosyl phosphate; PRA, phosphor ribosyl anthranilate; PPi, pyrophosphate; DMF, dimethyl formamide; Tw, tween80; Tx, tyloxapol; BSA, bovine serum albumin; ADC, alanine-dextrose-catalase; DPPC, dipalmitoyl phosphatidyl choline; CC_{50}, cytotoxic concentration against 50% of treated cells; BCG, *M. bovis* Bacillus of Calmette-Guerlain; FIC, fractional inhibitory concentration; FICI,

fractional inhibitory concentration index; KatG, catalase peroxidase G; TMS, tetramethyl silane.

Table of Contents

Chapter 1. Introduction

Mycobacterium tuberculosis (MTB) is the causative agent of tuberculosis (TB), ranking above HIV as the first cause of death for infectious disease in 2016 [1]. It is considered "the most successful" pathogen in the world [2, 3] killing more people than any other infectious disease in the history of humanity. The emergence of multi-drug-resistant strains and co-infection with HIV virus make the discovery of new anti-TB drugs a high priority for global health.

1.1 *Mycobacterium tuberculosis* profile

MTB is a slow growing mycobacterium and could survive in latent state both in oxygen-deprived and nutrient-deprived environments [4].

The distinguishing feature of mycobacteria is the complex waxy cell wall (Fig. 1), that is composed of three main components covalently bounded: the cross-linked peptidoglycan, the highly branched arabinogalactan and the long-chain mycolic acids. Glycophospholipids (phosphatidylinositol mannosides (PIMs), lipoarabinomannan (LAM)) and inert waxes (phthiocerol dimycocerosate, threalosomomycolate and threalosodimycolate (TDM)) intercalate the mycolate layer, forming the outer membrane. The capsule is the outermost layer and is mainly composed of proteins and polysaccharides. The lipid- and carbohydrate-rich envelope plays a critical role in pathogenesis and drug resistance [5].

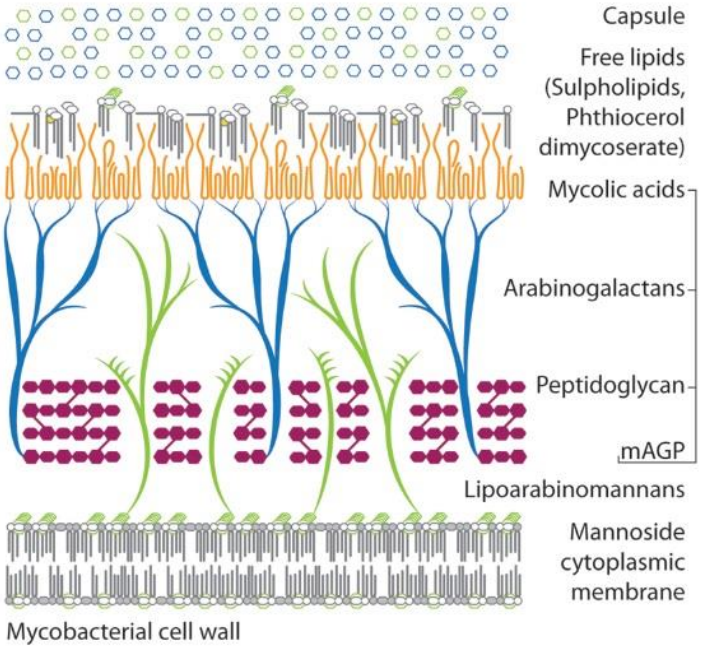

Figure 1. Adapted from *Microbiology*, **164**, 2018**.** Mycobacterial cell wall composition. The inner layer is the cytoplasmic membrane (grey), where lipoarabinomannan (LAM) (green) is anchored. The cytoplasmic membrane is linked to the macropolymer, formed by peptidoglycan (P) (purple), arabinogalactan (A) (blue) and mycolic acids (m) (orange). The outer layer is the capsule composed by glycolipids and proteins [6].

1.2 Pathogenesis of infection

Tuberculosis is a highly infectious airborne disease caused by *M. tuberculosis complex* mycobacteria and is transmitted by the inhalation of infected aerosol droplets. Following inhalation, MTB reaches the lung airways and is internalized by the macrophages using the receptor-mediated phagocytosis [7]. Macrophages recognize bacteria by surface exposed LAM, PIMs and TDM that bind different pattern recognition receptors [8-11].

Once internalized into the phagosome, MTB blocks the phagosome-lysosome fusion, disrupts the phagosome membrane to translocate into the macrophage cytosol [12-14]. When the primary infection is established, infected macrophages transport MTB to pulmonary lymph nodes for T-cell priming [7] (Fig. 2).

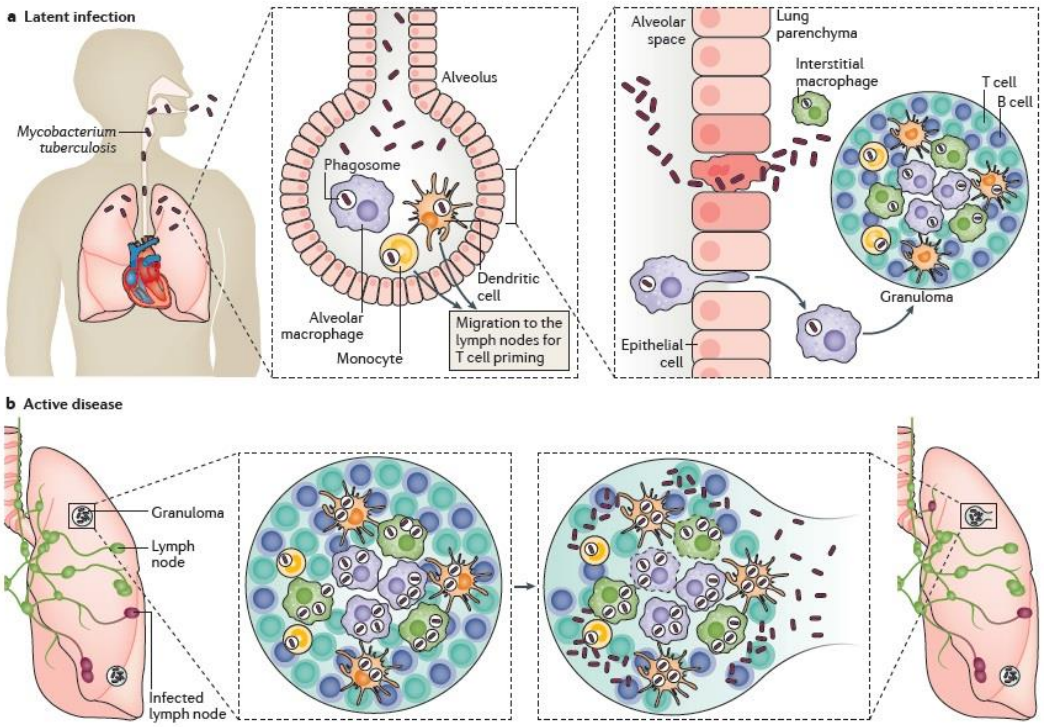

Figure 2. From *Nat Rev Dis Primers*, **2**, 2016. MTB infection. a) Latent state: mycobacteria are inhaled and reach the alveolar space where they are phagocyted by

alveolar macrophages. The infected macrophages migrate to pulmonary lymph nodes for T cell priming. The granuloma is formed by the recruitment of immune cells in the locus of infection. b) Active state: mycobacteria replicate into the granuloma. If the bacterial burden becomes too high, the granuloma will no longer be able to contain the infection. In this status MTB could disseminate in the blood stream and infect other organs [7].

When T-cells are activated, they stimulate the macrophages by the secretion of interferon-γ and tumor necrosis factor-α to bring bacillary replication under control [15]. Indeed, activated macrophages contain the infection by producing reactive oxygen species, nitric oxide and pro-inflammatory cytokines (TNF, IL-1β, IL-6) [16]. The secretion of cytokines leads to the recruitment of an increasing number of immune cells to the focus of infection. The immune cells surround the infected macrophages to inhibit infection spreading, forming the granuloma [16] (Fig. 2, 3).

At the beginning, granuloma is highly vascularized, and the cell recruitment is accompanied by the differentiation of macrophages into foamy macrophages. With the development of inflammation and immune response, the granuloma evolves into caseous granuloma. Caseous granuloma is characterized by a fibrous cuff, loss of vascularization and accumulation of lipids and necrotic macrophages (*caseum)* within the core (Fig. 3) [17]. An excessive pro-inflammatory immune response could lead to tissue destruction and pulmonary cavitation [18]. If the granuloma fails to contain the infection, mycobacteria can reach the blood stream and produce extra pulmonary infections.

In nearly 90% of cases, MTB generates a latent infection and remains in a quiescent status, to overcome host immune response [19]. Latent TB (LTB) can be reactivated into active TB (5-15% of cases) [1, 20], in the presence of different risk factors (i.e. immunodeficiency, cancer, organ transplantation, or immune system diseases).

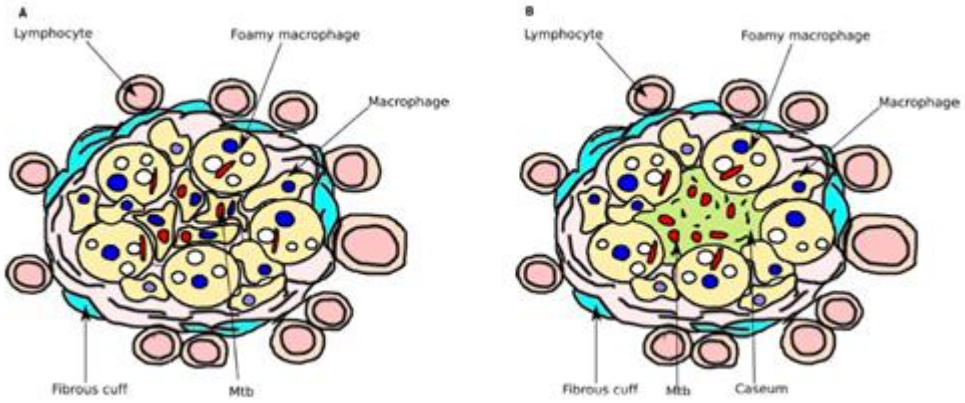

Figure 3. From *Chem. Rev.*, **4**, 2018. The two stages of granuloma: (A) cellular granuloma, with the infected macrophages with MTB (red) at the centre, surrounded by foamy macrophages, (B) necrotic granuloma, died macrophages released MTB into the necrotic hypoxic centre, filled with lipid *caseum* [17].

1.3 TB epidemiology

Although there is an effective treatment, TB remains the leading cause of death worldwide from a single infectious agent. In 2016 10.4 million new TB-cases were registered (10% of which among HIV-infected people) (Fig. 4), along with 1.3 million TB deaths among HIV negative people and an additional 374 000 deaths among HIV-positive people. In 2016 the incident cases mostly occurred in the South-East Asia Region (45%), the African Region (25%) and the Western Pacific Region (17%). The top five countries, with 56% of the total estimated cases, were India, Indonesia, China, the Philippines and Pakistan.

The main challenge for global TB surveillance is the persistent spread of drug-resistant TB. Multidrug-resistant (MDR) strains, resistant to isoniazid and rifampicin, and rifampicin-resistant (RR) strains are hard to detect and to eradicate by standard first-line treatment. In 2016, there were 600 000 incident cases of MDR/RR-T, 4.1% of the new cases. China, India and the Russian Federation were the countries with the largest numbers of MDR/RR-TB cases (47% of the global total). Based on the most updated WHO data, the MDR-TB cases increase as a proportion of all TB cases in these countries [1].

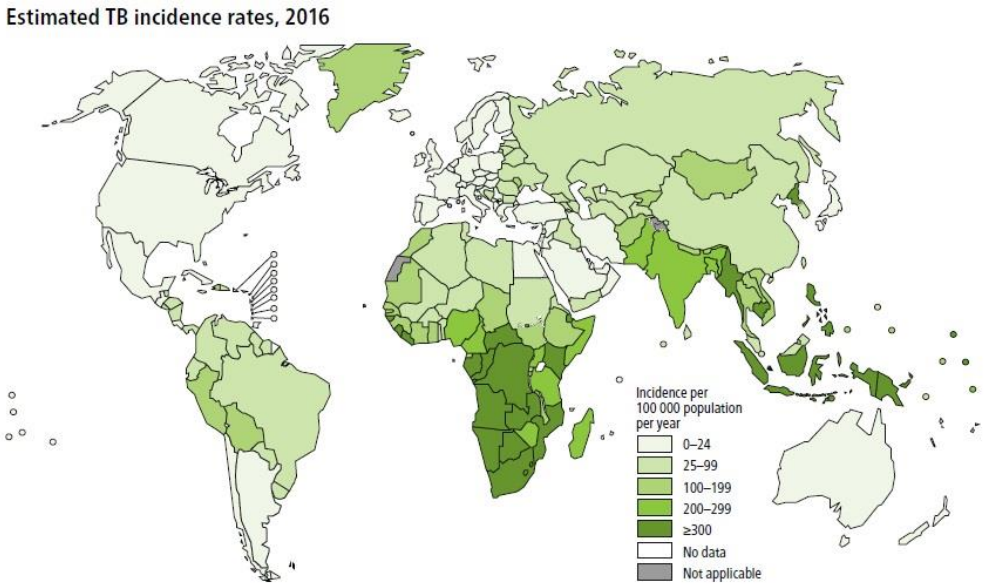

Figure 4. From *WHO Global tuberculosis report* 2017. TB incidence in 2016 [1].

1.4 Current therapies

The current treatment for drug susceptible TB, recommended by WHO guidelines, includes an intensive first phase of 2 months with a daily co-administration of four first line drugs (isoniazid (INH), rifampicin (RIF), ethambutol (EMB), pyrazinamide (PZ), Tab. 1), followed by a continuation phase of 4 months with INH and RIF [21]. Instead, MDR-TB and RR-TB treatment is based on drug susceptibility test but generally consists of a combination of first and second line drugs indicated in the *WHO treatment guideline for drug-resistant tuberculosis* [22] (Tab. 1).

Table 1. First and second line drugs in TB therapeutic treatment.

Class of therapeutic agents	Drugs
First line oral anti-TB drugs	INH, RIF, EMB, PZ
Second line oral anti-TB drugs	ethionamide, prothionamide, cycloserine, *para*-amino salicylic acid.
Fluoroquinolones	levofloxacin, moxifloxacin, gatifloxacin
Second line injectable anti-TB drugs	streptomycin, kanamycin, amikacin, capreomycin
Add-on agents	bedaquiline, delamanid, linezolid, iminipenem, meropenem

The longest MDR-TB regimen lasts 18 months with at least five effective TB medicines during the intensive phase, including second-line TB medicines. Recently a shorter regimen of 9-12 months was also standardized to improve the patient compliance and prevent the insurgence of resistance [22, 23].

Different regimens are recommended to manage LTB and avoid the progression to active disease [24]. LTB represents an important risk especially for HIV-positive

people, in which TB is the most common opportunistic infection and the leading cause of death. Unfortunately, the use of antiretroviral (ARV) drugs makes the TB eradication more difficult because of the overlapping of ARV and anti-TB drugs toxicity and pharmacokinetics [25].

Although current treatment can achieve 83% success in treating susceptible TB [1], the current regimens show several limitations:

- duration and complexity of treatment cause poor compliance to the therapy,
- common drug adverse effects contribute to nonadherence,
- exposure to subtherapeutic doses of anti- TB drug promotes the insurgence of resistant strains.

To overcome patient compliance, the new drug candidates and the new regimens should be more potent and safer than the current ones. Reducing the number of drugs in the regimens and the duration, as well as the occurrence of adverse reactions, the patient adherence to the therapy could be encouraged. Instead, drug candidates with innovative target and mechanism of action are needed to eradicate the drug-resistant TB infection.

1.5 Novel drug candidates in clinical development

In the last decades, many efforts in the anti-TB drug discovery field led to the identification of new targets and new chemical entities endowed with different mechanisms of action compared to the standard anti-TB drugs. According to the 2018 TB drug pipeline (Fig. 7) several drug candidates are currently in the clinical development phases (Tab. 2). The main issue in anti-TB drug discovery is satisfying all the following requirements:

- a novel mechanism of action to ensure activity against MDR- and XDR-TB,
- a favourable metabolism profile and good oral availability to increase patient compliance,
- pharmacokinetic (PK) and pharmacodynamic profiles compatible with HIV treatment.

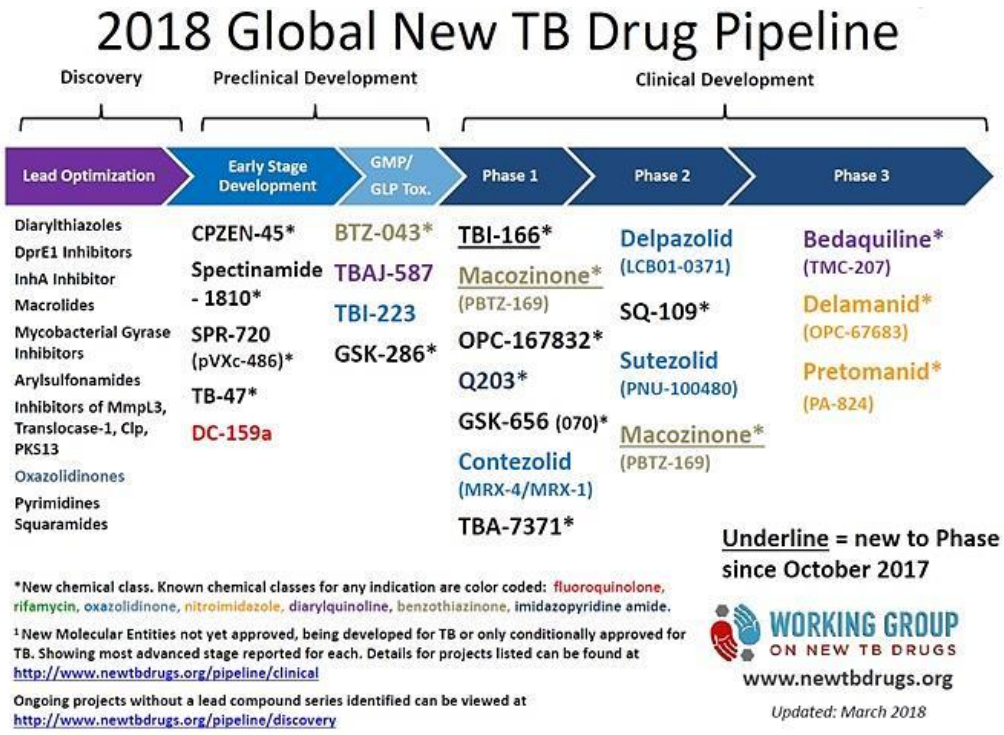

Figure 7. From *www.newtbdrug.org*. Global new TB drug pipeline 2018.

Table 2. New anti-TB drugs in clinical development.

Name	Owner	Target	Therapeutic use	Phase of clinical development	References
bedaquiline	Jhonson&Jhonson	ATP-synthase	MDR-TB	3	[30-33]
delamanid	Otshuka Phamaceutical	Mycolic acids synthesis	MDR-TB	3	[34, 35]
pretomanib	Global TB Alliance	Mycolic acids synthesis, respiratory chain	MDR-TB	3	[1, 36-38]
delpazolid	LegoChem Bioscences	Protein synthesis	MDR-TB	2	[44-46]
SQ-109	Sequella Inc.	Mmpl3, MenA/MenG	MDR-TB	2	[54-59]
sutezolid	Sequella Inc., Pfizer	Protein synthesis	MDR-TB	2	[40-43]
macozinone	Nearmedic plus, iM4TB	DprE1	MDR-TB	1-2	[51-53]
TBI-166	Global TB Alliance, Institute of Materia Medica	Oxidoreductive balance	MDR-TB	1	[63-67]
telacebec (Q203)	Qurient	Cytochrome *bc1*	MDR-TB	1	[69-71]
GSK-656	GSK	LeuRS	MDR-TB	1	[75]
contezolid	MicuRX Pharmaceuticals	Protein synthesis	MDR-TB	1	[47]
TBA-7371	AstraZeneca, Global TB Alliance	DprE1	MDR-TB	1	[78]

Bedaquiline (Fig. 8) and delamanid (Fig. 9) are the only two agents approved by FDA and EMA in the last 10 years for the treatment of only pulmonary MDR-TB [26], since both showed an alarming cardiotoxicity, producing the Q-T prolongation of ECG [27-29].

1.5.1 Diarylquinolines

Bedaquiline (TMC207) (Fig. 8) is the lead compound of diarylquinoline series, with a chemical scaffold identified by whole-cell screening by Andries *et al.* in 2005 [30]. *In vitro* studies revealed its potent bactericidal activity against replicating and quiescent mycobacteria including different clinical multidrug-resistant isolates, with MIC values ranging from 0.002 to 0.120 µg/mL [31]. Since bedaquiline displayed a higher efficacy than INH and RIF in a TB murine model and passed clinical studies, it was approved in 2012 by the FDA.

The diarylquinolines target the mycobacterial ATP-synthase. Bedaquiline inhibits selectively the ATP-synthase proton pump binding the *c* subunit and causing ATP depletion [30, 32, 33].

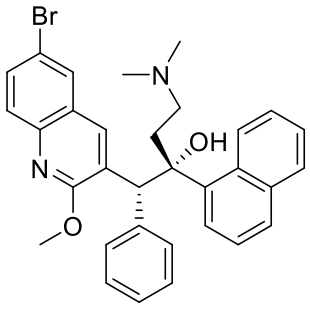

bedaquiline (TMC-207)

Figure 8. Chemical structure of bedaquiline.

1.5.2 Nitroimidazoles

Nitroimidazoles inhibit the methoxy and ketomycolic acid synthesis, after the reductive activation by a deazaflavin-dependent nitroreductase [34]. Delamanid (OPC-67683) (Fig. 9) showed potent *in vitro* (MIC= 0.012 µg/mL) and *in vivo* activities against both drug-susceptible and drug-resistant MTB strains [34], including dormant mycobacteria [35]. Although delamanid was approved by EMA in 2014 for the treatment of MDR-TB, it is currently undergoing Phase III clinical trials.

Pretonamid (PA-824) is another nitroimidazole in Phase III clinical trials (Fig. 9). It showed to be a potent bactericidal agent in *in vitro* (MIC = 0.13 µg/mL) and in *in vivo* studies [36, 37]. In addition to mycolic acid synthesis inhibition, the reduction of the nitro group produces radical species that block the mycobacterial respiratory chain [38]. Pretonamid is currently tested as part of three different combination therapies for both drug-susceptible and drug-resistant TB [1].

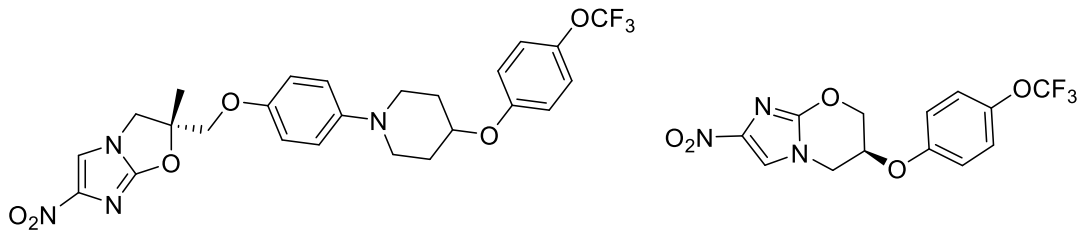

delamanid (OPC-67683) **pretomanid (PA-824)**

Figure 9. Chemical structures of delamanid (OPC-67683) and pretomanid (PA-824).

1.5.3 Oxazolidinones

Oxazolidinones are a class of protein synthesis inhibitors, targeting the 50s ribosomal subunit of 23S rRNA and blocking the early step of protein synthesis [39]. According to the last Global anti-TB drug pipeline (www.newtbdrugs.org) (Fig.10), sutezolid and delpazolid are currently in phase II of clinical development and cotezolid is in phase I.

Sutezolid showed good bactericidal activity *in vitro* against MTB (MIC= 0.125 µg/mL), good *in vivo* efficacy in a TB murine model [40, 41] and successfully completed several safety studies [42, 43]. Identified in 2010 as a new potent antibacterial agent against different clinical isolates of Gram-positive and Gram-negative bacteria, delpazolid showed to be active *in vitro* against drug-susceptible and resistant MTB strains (MIC= 2 µg/mL) [44, 45]. Moreover, delpazolid is effective in a murine model of infection and well tolerated in toxicological studies [46]. Another oxazolidinone, contezolid, recently entered Phase I clinical trials because of its promising *in vivo* biological profile [47].

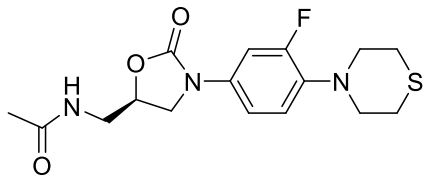

sutezolid (PNU-100480)

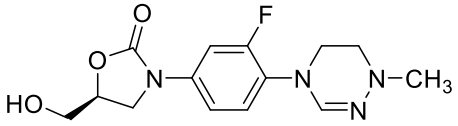

delpazolid (LCB01-0371)

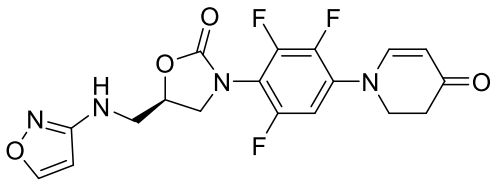

contezolid (MRX-4/MRX-1)

Figure 10. Chemical structures of sutezolid (PNU-100480), delpazolid (LCB01-0371), contezolid (MRX-4/MRX-1).

1.5.4 Benzothiazinones

Benzothiazinones are a class of antimycobacterial compounds targeting the cell wall synthesis by inhibition of decaprenylphosphoryl-β-D-ribose-2'-epimerase (DprE1). DrpE1 is a flavoenzyme that catalyzes the epimerization of decaprenylphosphoryl-β-D-ribose to decaprenylphosphoryl-β-D-arabinose, a crucial step for the synthesis of arabino-furanose [48, 49]. Benzothiazinones are reduced by DprE1producing nitroso electrophilic species that react with an essential cysteine residue in the active-site of DprE [49, 50].

BTZ-04 (Fig. 11) was the first member of this series that displayed an outstanding *in vitro* activity against MTB (MIC= 1ng/mL), including MDR and XDR clinical isolates, and showed to be more effective in acute and chronic murine model of TB infection than INH [49]. The lead optimization of BTZ-043 led to identify macozinone (PBTZ-169) (Fig. 11) with a better *in vitro* and *in vivo* activity against MTB (MIC= 0.19 ng/mL) than BTZ-043, due to an improvement stability from nitro reductase as well as an improvement of DprE1 binding [51, 52]. The co-administration of macozinone, bedaquiline and PZ showed to reduce the bacterial load more rapidly than the current tri-therapy (RIF, INH, PZA) in chronic TB infection [52]. In 2017 macozinone started the phase I clinical trial financed by EPFL no profit Innovative Medicines for Tuberculosis (iM4TB) and the Bill and Melinda Gates foundation [53].

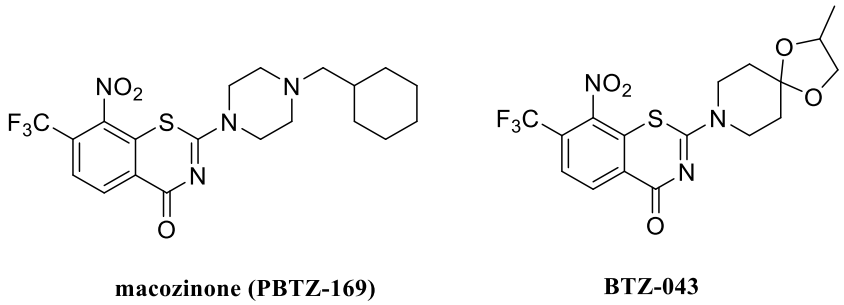

Figure 11. Chemical structures of macozinone (PBTZ-169) and BTZ-043.

1.5.5 1,2-Ethylenediamine

SQ109 (Fig. 12), in Phase II, is a 1,2-ethylenediamine identified as EMB analogue by a combinatorial solid-phase synthetic approach, with an improved *in vitro* activity against drug-susceptible and drug-resistant MTB (MIC ranging from 0.70 to 1.5 µM), better *in vivo* efficacy and lower *in vivo* toxicity compared to EMB [54, 55]. Surprisingly, SQ109 and EMB have completely different mechanisms of action. SQ109 seems to be a multi-target agent that blocks cell wall synthesis by MmpL3 (*Mycobacterium* membrane protein Large 3) inhibition [56, 57] and menaquinone synthesis by MenA/MenG protein inhibition. MmpL3 is an attractive target for anti-TB drug discovery. MmpL3 is a transmembrane proton antiport responsible of the trehalosemonomycolate export and the heme uptake into the cell [58]. SQ109 disrupts the proton motive force (PMF) used by MmpL3 to execute the TMM transfer [57, 59].

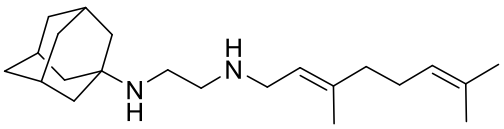

SQ-109

Figure 12. SQ-109 chemical structure.

1.5.6 Riminophenazines

Although the anti-leprosy drug clofazimine is effective against MTB infection [60], it presents extremely high lipophilicity, responsible of low solubility, long half-life and high accumulation in tissues with consequent side effects [61, 62]. A clofazimine lead optimization led to the identification of TBI-166 (Fig. 13), a less lipophilic riminophenazine with a good *in vitro* antimycobacterial activity (MIC= 0.016 μg/mL) and improved physicochemical and pharmacokinetic properties as well as limited side effects [63]. TBI-166 entered Phase I clinical trials in January 2018. Several studies were performed to clarify the riminophenazine mechanism of action [64-67]. Recently Yano *et al.* revealed that clofazimine is reduced by mycobacterial NADH-quinone oxidoreductase type II and the spontaneous re-oxidation generates bactericidal concentration of ROS [68].

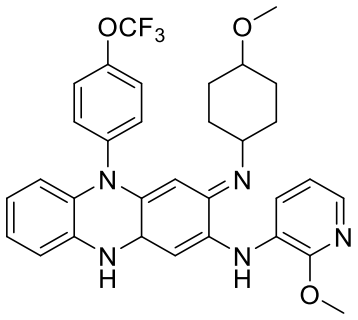

TBI-166

Figure 13. TBI-166 chemical structure.

1.5.7 Imidazopyridine amides

Telacebec (Q-2013) is a promising drug candidate currently undergoing Phase I clinical trials. Telacebec was obtained through the optimization of the imidazopyridine amide (IPA) scaffold (Fig. 14) [69] and displayed an *in vitro* nanomolar activity against MTB (MIC_{50}= 2.7 nM), a sub-nanomolar intramacrophage activity (MIC_{50}= 0.28 nM) and activity against MDR and XDR clinical isolates [70]. The *in vivo* efficacy in a mouse model of TB revealed that telacebec is effective at doses below 1mg/Kg. Telacebec targets the MTB cytochrome *bc1* complex of the respiratory chain, involved in ATP synthesis, that catalyzes the electron transfer from ubiquinol to cytochrome *c*. Telacebec interacts with the ubiquinol oxidation site (Q_p) of cytochrome *b* subunit, then blocking ATP synthesis [70]. A recent study proved that telacebec is a bacteriostatic agent, since MTB seems to maintain respiration and ATP synthesis by using electron flow through the cytochrome *bd* oxidase [71].

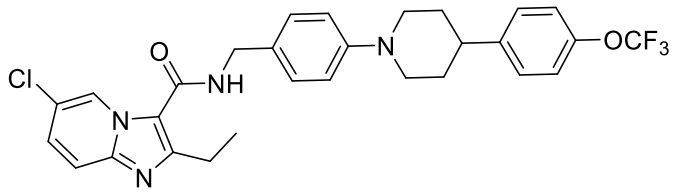

telacebec (Q-203)

Figure 14. Telacebec chemical structure.

1.5.8 Oxaboroles

Based on the fungal cytoplasmic leucyl-tRNA synthetase (LeuRS) inhibitors [72, 73], promising antimycobacterial benzoxaboroles (1.8 µg/mL <MIC< 0.02 µg/mL) were identified, showing to be efficacious in *in vivo* murine model of acute and chronic TB infection [74]. The optimization of 3-aminomethylbenzoxaboroles chemical scaffold led to the synthesis of GSK-656 (Fig. 15) with an improved antimycobacterial activity (MIC= 0.08 µM), a high selectivity for MTB LeuRS and a superior *in vivo* efficacy in acute and chronic TB. Because of excellent *in vivo* efficacy and good pharmacokinetic and safety profile, GSK-656 progressed to the first phase of clinical development [75].

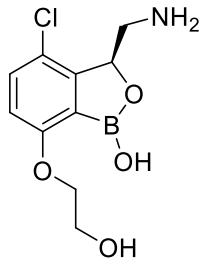

GSK-656 (070)

Figure 15. GSK-656 (070) chemical structure.

1.5.9 1,4-Azaindoles

The 1,4-azaindoles are a class of antimycobacterial compounds non-covalent inhibitors of DprE1 [76]. The first 1,4-azaindoles series showed good *in vitro* activities against MTB (0.156 μM <MIC< 6.25 μM), a moderate bactericidal activity (0.39 μM <MBC< 12.5 μM), a dose-dependent efficacy assessed in BALB/c mouse acute and chronic TB infection models [76]. Despite the excellent *in vitro* and *in vivo* efficacies against MTB, these compounds showed low water solubility, high clearance in mice and inhibitory activity against PDE6 eye protein, which may lead to impaired visual acuity [77]. The lead optimization of 1,4-azaindoleamides produced derivatives characterized by an improved PK and limited PDE6 activity [78]. Among them, TBA-7371 (Fig. 16) was selected for phase I clinical trials.

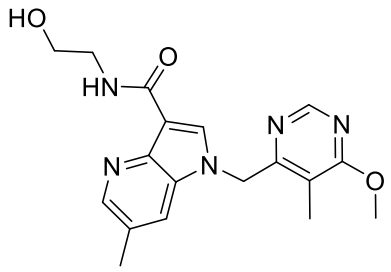

TBA-7371

Figure 16. TBA-7371 chemical structure.

Chapter 2. New pyrazole derivatives of BM635 inhibiting MmpL3

2.1 From the "soft" hit to the hit

The research group of Prof M. Biava developed a new series of antimycobacterial agents endowed with an innovative mechanism of action. **BM212** (Fig. 17), the soft hit of this new class of compounds, was identified through a phenotypic screening of a small library of azole compounds [79].

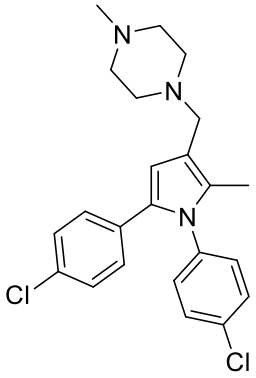

BM212

Figure 17. BM212 chemical structure.

Although **BM212** showed a good *in vitro* activity against MTB (MIC= 5.0 μM), it suffered from high cytotoxicity against HepG2 cells (TOX_{50}= 7.8 μM). In order to improve the potency and the safety profile of **BM212,** systematic modifications around the central pyrrole core were introduced (Fig. 18), preparing several **BM 212** derivatives.

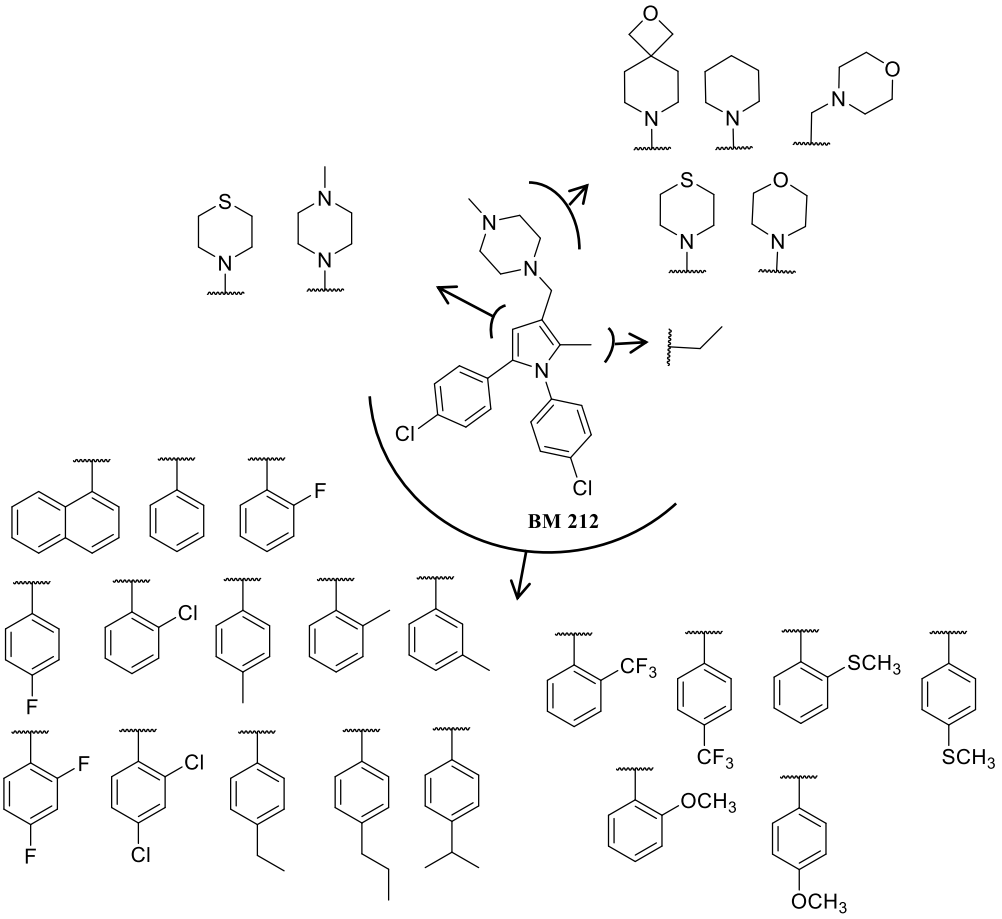

Figure 18. BM 212 modifications around the pyrrole core.

The chemical optimization of **BM212** led to the identification of **BM635** (Fig. 19) that displayed a remarkable improvement of activity against H37Rv (MIC= 0.12 µM) compared to **BM212** (MIC= 5.0 µM). Therefore, **BM635** was selected as the new hit of this class of 1,5-diaryl pyrroles [80]. Furthermore, **BM635** gave additional important results:

a) activity under anaerobic condition (LORA=28.73 µM);

b) activity against intramacrophagic mycobacteria (MIC_{80} = 0.16 µM);

c) acceptable cytotoxicity against HepG2 cells (Tox_{50}= 15.3µM);

d) good mouse microsomal stability with clearance values of 1.4mL/min/g;

e) no inhibition of the cytochrome P450 isoform 3A4 (IC_{50}> 40µM) [80].

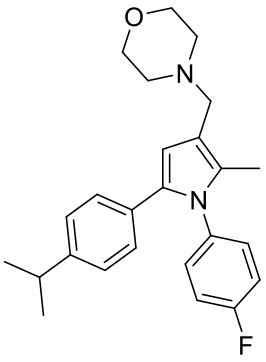

BM635

Figure 19. BM635 chemical structure.

Because of the promising biological profile, **BM635** was selected to determine the pharmacokinetic profile (Fig. 20) and to evaluate the *in vivo* efficacy in a murine model of acute TB infection (Fig. 21) [80]. **BM635** was tested at multiple doses in an acute murine infection model and exhibited an ED_{99} (Efficacious Dose that results in 99% CFU reduction in the lung) of 49 mg/Kg. The oral pharmacokinetic profile was then determined at active dose of 50 mg/Kg. The correlation between the ED_{99} and the respective area under the curve (AUC_{inf}) proved as the **BM635** potency per effective *in vivo* concentration is comparable to that of moxifloxacin. These results highlight **BM635** as being competitive with standard anti-tubercular drugs currently used in therapy [80].

Dose (mg/kg)	Tmax (h)	Cmax (µM)	AUC 0-∞ (µM.h)
50	1.00	1.62	11.6

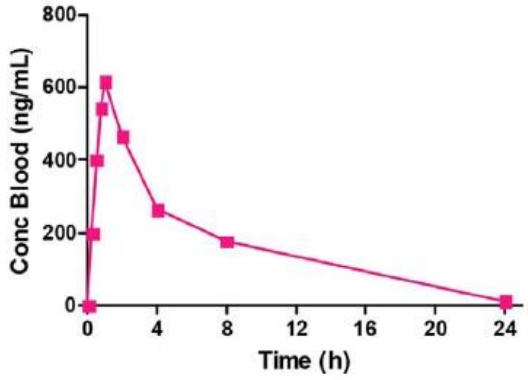

Figure 20. From *PlosOne*, **2**, 2013. Peripheral blood levels after oral administration of **BM635 (**50 mg /Kg) to C57BL/6 mice (n=3) [80].

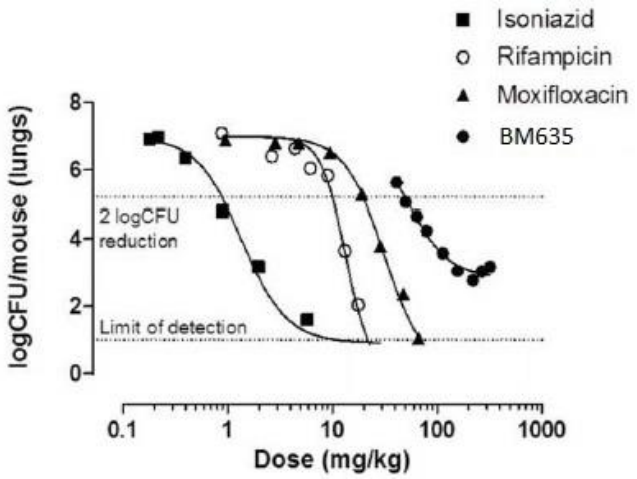

Figure 21. From *PlosOne*, **2**, 2013. Acute infection model dose-response curve correlating logCFU count reduction in the lungs of mice with different doses of rifampicin, isoniazid, moxifloxacin and **BM635** [80].

Unfortunately, **BM635** reported some issues about drug-like properties and toxicity. Because of a significant lipophilicity (Chrom log$D_{pH7.4}$= 8.1), **BM635** presents a relevant percentage of binding to the Human Serum Albumin (%HSA= 97.7%) and very low water solubility determined by Chemi Luminescent Nitrogen Detection (CLND < 1μM). Moreover, **BM635** is active against human ether-a-go-go related gene (hERG) ion channels (IC_{50}= 10 μM) that could originate a cardiotoxicity, especially in a long-term treatment, such as the anti-tubercular one [80].

Therefore, different strategies were followed for improving those issues:

- preparing different pharmaceutical salts of **BM635** to improve water solubility [81];
- introducing modifications around the central pyrrole core (Fig. 22): *i)* synthesis of alkyl derivatives to decrease the aromaticity of the molecule, responsible of low solubility and hERG activity [82], *ii)* introduction of a carboxylic substituent in the chemical structure of **BM635** to decrease hERG activity [82], *iii)* reduction of the nitrogen basicity of the morpholine moiety, which might be responsible of hERG activity [82].

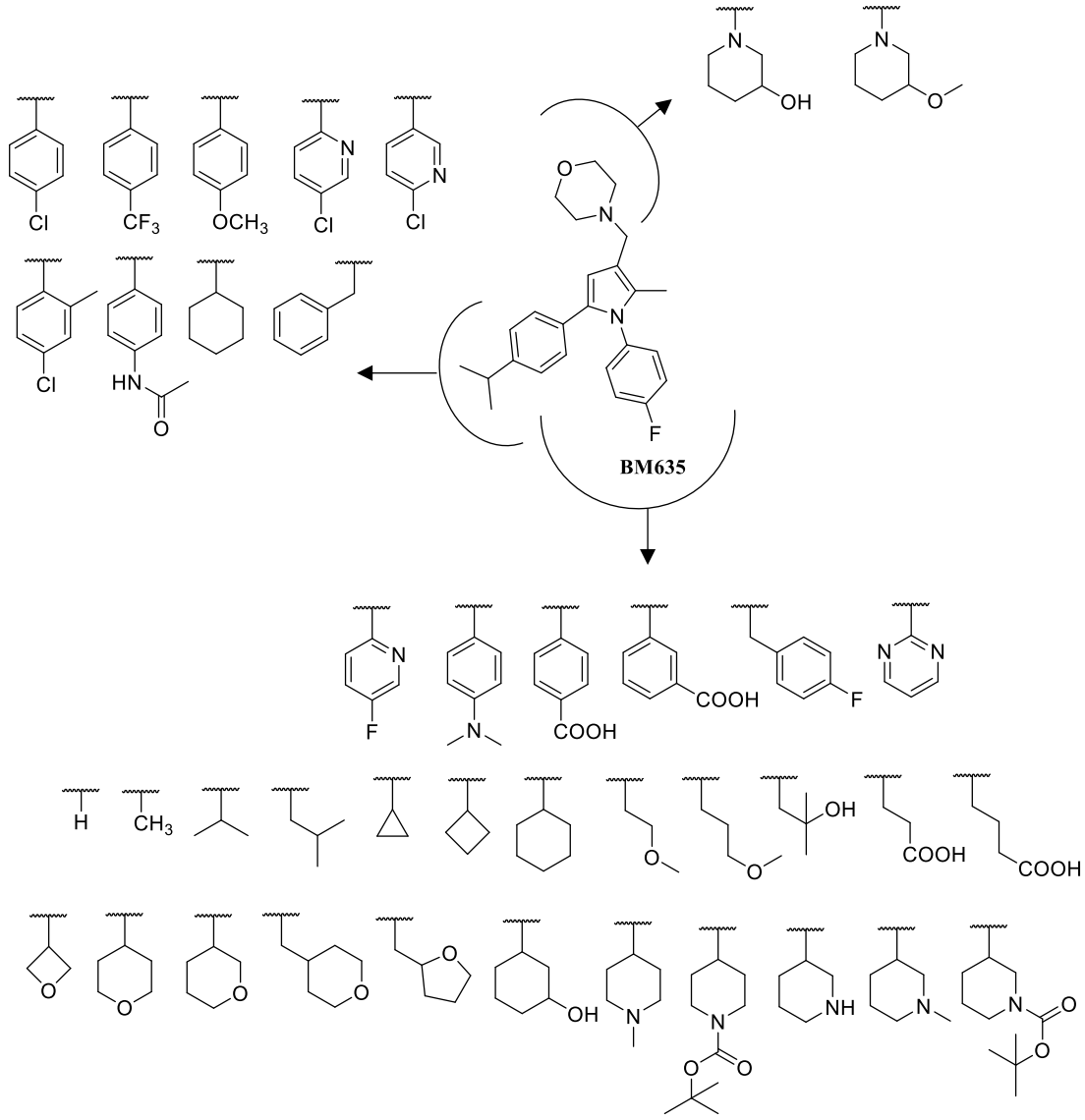

Figure 22. All the substitutions introduced to the **BM635** chemical scaffold.

Based on the biological results of the new **BM635** pyrrole derivatives, the following structure-activity relationships (SARs) were obtained:

- **C5 modification.** The 4-trifuoromethyl phenyl group proved to be tolerated, showing good values of activity (0.60 μM ≤MIC ≤ 2.50 μM).
- **N1 modifications.** The replacement of the 4-F-phenyl ring with the 4-F-pyridin-2-yl, 4-F-benzyl ring as well as with alkyl, cycloalkyl or hetero cycloalkyl

ones led to derivatives with good activity (0.08 μM ≤ MIC ≤ 0.6 μM) and improved drug-like properties (6.85 ≤ Chrom log$D_{pH=7.4}$ ≤ 8.13, CLND ≥ 24)

- **C3 modifications.** The incorporation of 3-hydroxy piperidine and 3-methoxy piperidine led to a partial loss of activity (2.0 μM ≤ MIC ≤ 7.5 μM) [82]**.**

Thereafter, the central pyrrole core was replaced by two five-membered isosteric heterocycles: imidazole and pyrazole (Fig. 23). Only the 1,3,5-trisubstituted pyrazoles proved to maintain the activity against MTB, whereas imidazoles and 1,3,4,5-tetrasubstitued pyrazoles proved to be inactive.

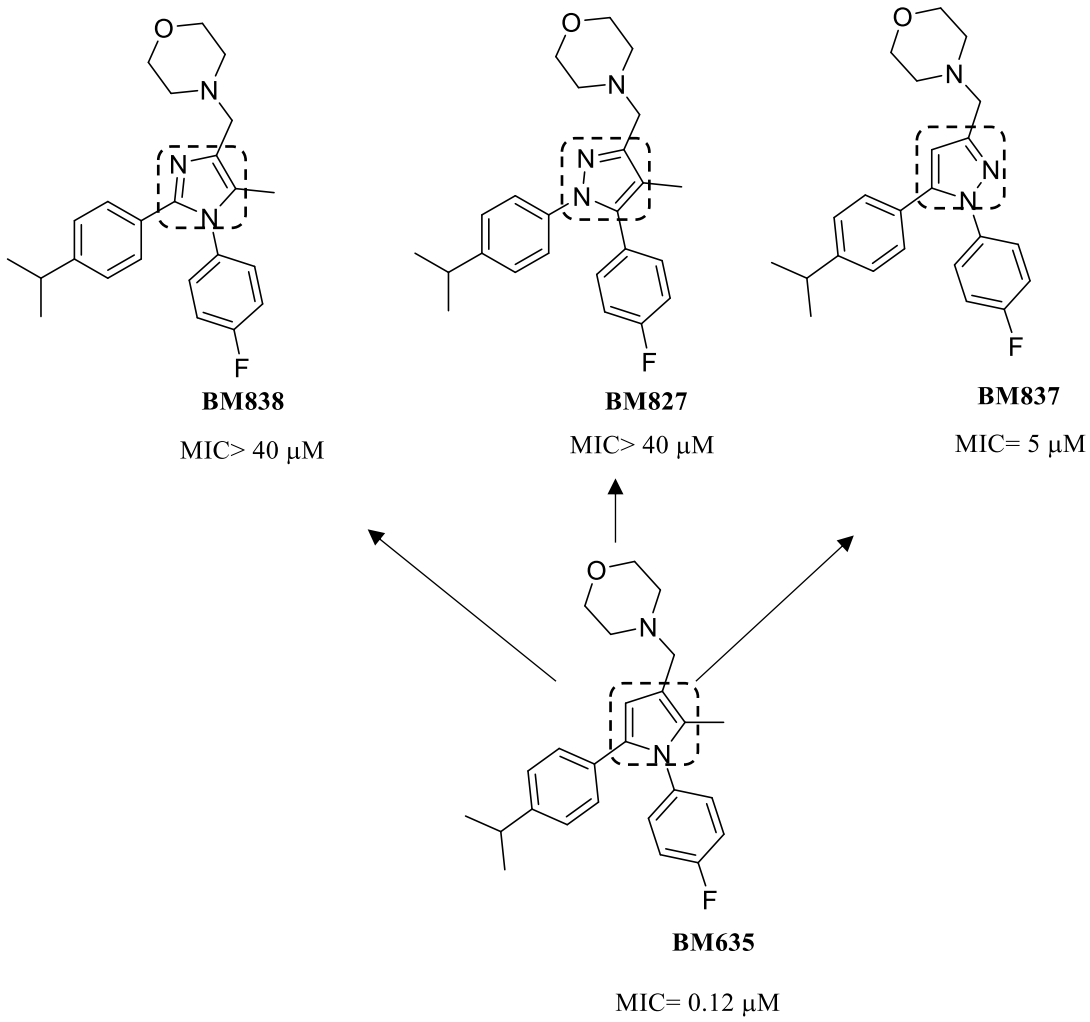

Figure 23. Replacement of **BM635** pyrrole core with imidazole, 1,3,4,5-tetrasubstitued and 1,3,4-trisubstitued pyrazoles.

Therefore, a first series of 1,3,5-trisubstituted pyrazoles was synthetized (Fig. 24) decorating both N1 and C5 with the substituents that furnished the best results in the pyrrole series and introducing hydroxyl an methoxyl piperidines at C3.

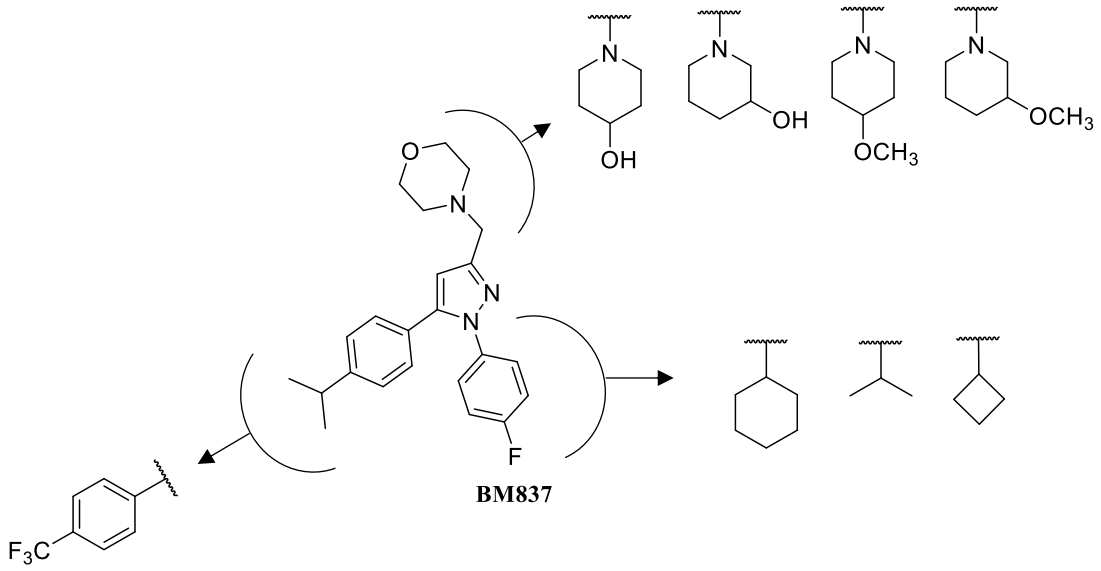

Figure 24. First **BM635** pyrazole derivatives.

Pyrazole **BM859**, **BM840** and **BM850** (Fig. 25) showed comparable anti-mycobacterial activity to that of **BM635** but a significant improvement of solubility in water and in FaSSIF medium (Tab. 3). In addition, **BM859**, **BM840** and **BM850** provided lower activities against hERG channels (Tab. 3).

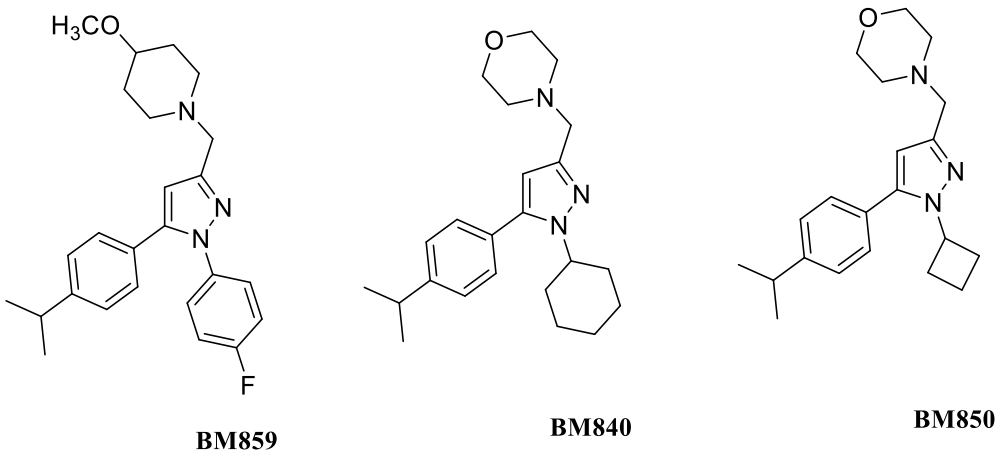

Figure 25. Chemical structures of **BM859**, **BM840** and **BM850**.

Table 3. Minimum Inhibitory Concentration (MIC) against *M. tuberculosis*, cytotoxicity (TOX_{50}) on HepG2 cell line, lipophilicity (Chrom log$D_{pH7.4}$), membrane permeability, percentage of binding to the HSA, water solubility assessed via CLND, solubility in FaSSIF medium, activity against hERG channels (IC_{50}) of compounds **BM859**, **BM840**, **BM850** and **BM635**.

Compound	MIC MTB (µM)[a]	Tox_{50} (µM) HepG2[b]	Chrom log$D_{pH7.4}$[c]	Membrane permeability cm/sec[d]	%HSA binding[e]	CLND (µM)[f]	FaSSIF (µg/ml)[g]	hERG IC_{50} (µM)[h]
BM859	0.3	32	8.29	4.40×10^{-5}	96.42	152	-	6.31
BM840	0.4	64	8.68	3.50×10^{-5}	97.11	78.50	100	>50
BM850	0.4	50	7.70	6.10×10^{-5}	96.72	306	139	32
BM635	0.12	50	8.10	2.4×10^{-5}	98.37	>1	5	10

[a]activity against MTB H37Rv.
[b]cytotoxicity in HepG2 cell line.
[c]hydrophobicity by Chrom Log$D_{pH7.4.}$
[d]membrane permeability.
[e]percentage of binding to the human serum albumin.
[f]water solubility by Chemi Luminescent Nitrogen Detection.
[g]solubility in Fast State Simulating Intestinal Fluid.
[h]activity on hERG channels.

Therefore the *in vivo* efficacy of **BM859**, **BM840** and **BM850** was assessed in a murine model of TB infection (Tab. 4). **BM859** proved to be active *in vivo*, reducing the mycobacterial count of 1.5 log CFU in the lungs, compared to untreated mice.

Table 4. Therapeutic efficacy of derivative **BM840**, **BM850**, **BM859** and moxifloxacin. Differences in the lung microorganism burden (log10 CFUs/lungs) with respect to untreated controls (Day 9 after infection).

Compound	Dose (mg/kg)[a]	Administration	Difference in logCFU/lungs
BM840	200	Once a day	0.4
BM850	200	Once a day	0.1
BM859	200	Once a day	1.5
moxifloxacin	30	Once a day	3.1

[a]Dose administered daily.

2.2 Target identification

Having identified the 1,5-diaryl pyrroles as a potent antimycobacterial class, the cellular target was determined through complementary genetic approaches. **BM212** *M. smegmatis, M. bovis* BCG, and MTB resistant mutants were generated in solid and liquid media containing different concentrations of drug. Then the resistant colonies were isolated for whole genome sequencing to identify polymorphism linked to resistance. The characterization of resistors showed several mutations in *mmpl3* gene resulting in different amino acidic residues in the protein transmembrane domain (i.e. all **BM212** BCG resistant strains displayed a common mutation L320P) [83]. As mentioned above, MmpL3 is a mycolic acids transporter via proton antiport mechanism. It was speculated that **BM212** acts by inhibiting MmpL3 and TMM transfer. MmpL3 is the target of different drugs with diverse chemical scaffolds reported in Fig. 26 [59, 84-86]. The inhibitors share a protonatable nitrogen that could be responsible for the PMF collapse, dissipating the transmembrane proton concentration gradient (ΔpH).

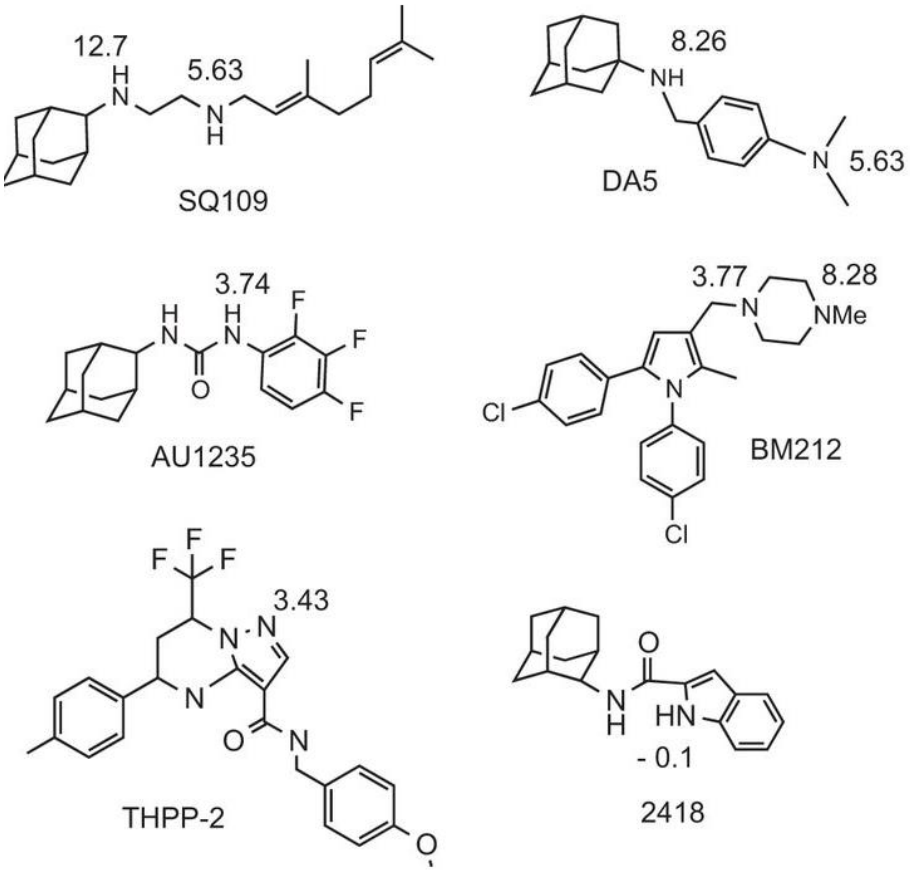

Figure 26. Adapted from *Antimicrob.Agents Chemoter*. **58**, 2014. MmpL3 inhibitors chemical structure and their extimated pK_a values [59].

Because both **BM212** and SQ109 are also active against hypoxic and nutrient-starved non-replicating mycobacteria, it was speculated that they could be able to dissipate the membrane potential [87].

On the contrary, Xu Z. *et al*. had recently demonstrated that **BM212** has no effect on PMF but inhibits TMM transport across the membrane binding MmpL3. Indeed, it was observed that **BM212** binds purified MmpL3 protein in a specific and saturable manner. Furthermore, the mutations, that confer resistance to the drug, mostly cluster in a specific region, revealing a possible binding site (Fig. 27) [88]. Afterwards,

MmpL3 was confirmed as the target also of the other 1,5-aryl pyrroles and **BM635,** using the same approaches [80].

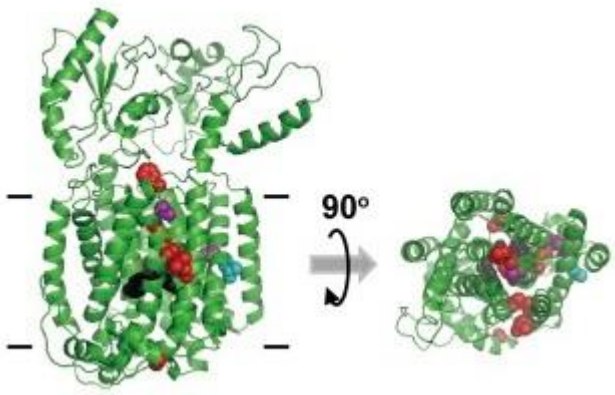

Figure 27. From *PNAS* **30**, 2017: Mutations that confer resistance against **BM212** cluster on a structural model of MmpL3, suggesting a possible binding site. Residues that conferred resistance against **BM212** are highlighted in red, purple and cyan, when mutated in MmpL3 from *M. smegmatis*, *M. bovis bacillus Calmette–Guérin*, and *M. tuberculosis* respectively [88].

2.3 Rationale and aims of the project

The first part of my PhD thesis was focused on the development of a second series of pyrazole derivatives (**1-25**) (Fig. 28). Once the 1,3,5- trisubstituted pyrazole was identified as an effective alternative to the pyrrole core, systematic modifications were carried out to meet the following goals:

- improve water solubility, assuring accurate activity assays and accurate absorbance prediction;
- reduce activity against hERG channels and limit the possible cardiotoxicity during treatment;
- maintain good TOX_{50}/MIC values.

Compounds **1-25** bear either 4-F-phenyl, cyclohexyl or isopropyl substituents at N1 or 4-isopropylphenyl and 4-trifluoromethylphenyl rings at C5, while our attention was devoted to evaluate the influence of the different cyclic amines at C3 on both activity and drug-like properties. Therefore, different small subsets of compounds were prepared by insertion of the following amines:

- *thiomorpholine* (**6**, **13**, **19**), *N-methyl piperazine* (**1**, **7**), *piperazine* (**9**) *and piperidine* (**15**, **21**). Because the presence of thiomorpholine, *N*-methyl piperazine, piperazine and piperidine led to active compounds in the pyrrole series, their activity was assessed within the pyrazole scaffold.
- *4,4-Dimethyl-1,4-azasilane* (**4**, **11**, **18**, **24**). The incorporation of this moiety was suggested by the recent work by Ramesh and co-workers that highlighted as the presence of silicon amines into the **BM212** chemical scaffold leads to an improvement of the anti-mycobacterial activity [89].

- *2-Pyridyl piperazine* (**3**, **10**, **17**, **23**), introduced to increase the aqueous solubility by harnessing an aromatic heterocycle with a protonatable nitrogen that shows the right balance between hydrophilicity and lipophilicity.

Moreover, given that the presence of both a positively ionizable group and a wide aromatic-hydrophobic planar region are the main features of hERG pharmacophore, amines with low nitrogen basicity and amines that can break the planarity were introduced:

- *tert-butylpiperazine-1-carboxylate* (**2**, **8**, **16**, **22**). The electron withdrawing effect of the carboxylate group should decrease the nitrogen basicity.

- *2-Oxa-7-azaspiro [3.5] nonane* (**5**, **12**). As reported by Wuitschik and co-workers, spirooxetane is a bioisostere of carbonyl group. Like carbonyl, the spirooxetane decreases the nitrogen basicity of the morpholine by electronic effect [90, 91].

- *4-Methoxy-piperidine* (**14**, **20**, **25**). A hindered morpholine bioisoster could promote a different spatial arrangement, breaking the planarity of hydrophobic region.

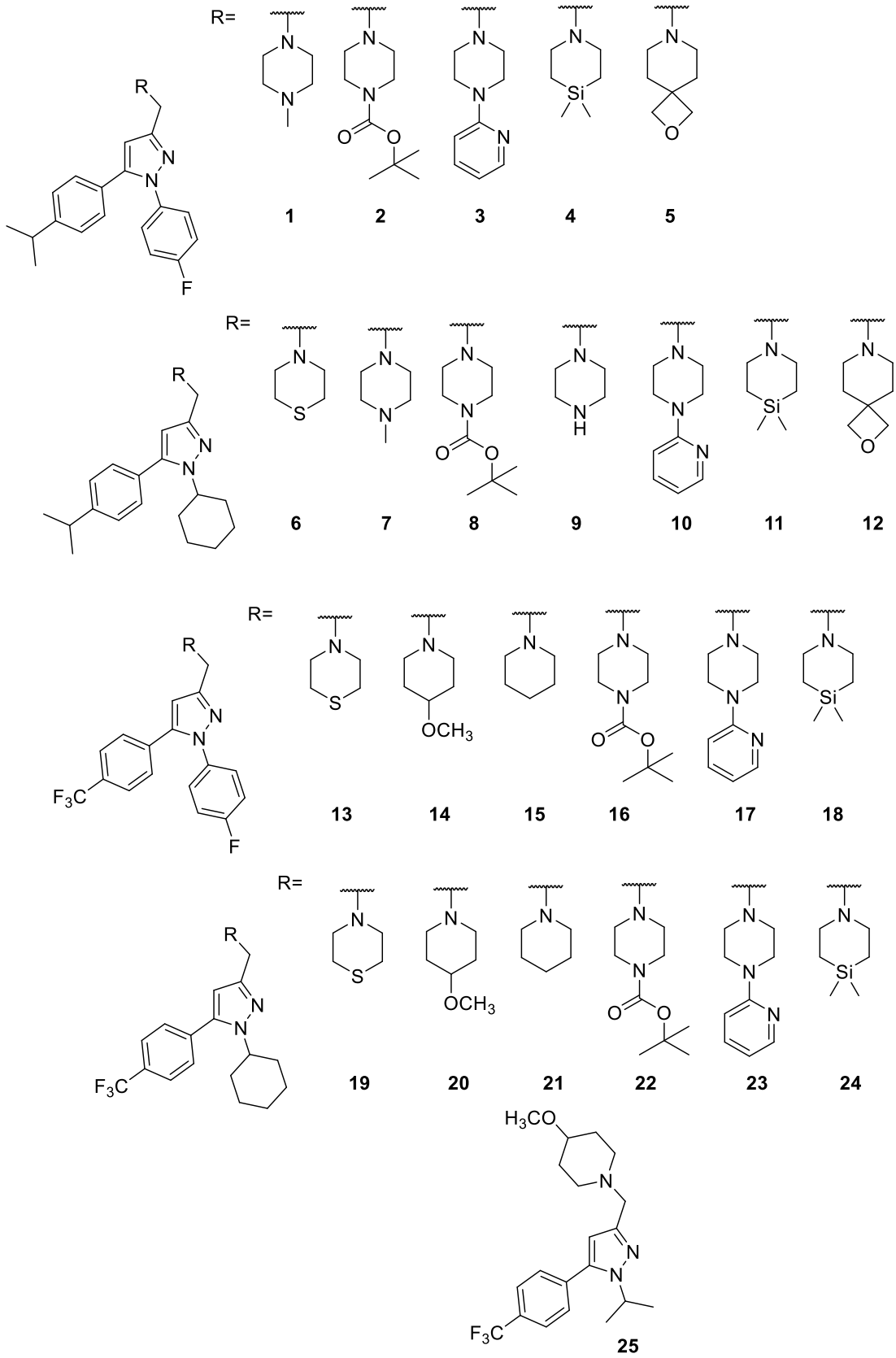

Figure 28. Chemical structure of pyrazole compounds **1-25**.

2.4 Chemistry

Compounds **1-25** were prepared as shown in Scheme 1. The reaction between acetophenones (**26 a-b**) and diethyloxalate (**27**) in the presence of litium bis (trimethylsilyl)-amide gave the desired litium salts (**28 a-b**) [92] that were in turn cyclized with the appropriate hydrazines (**29 a-c**) to afford the corresponding pyrazoles (**30 a-e**) [93]. Ethyl esters (**30 a-e**) were reduced to the corresponding alcohols (**31 a-e**) with litium aluminium hydride [94] and oxidized with Dess-Martin periodinane to obtain the appropriate pyrazole-3-carbaldehydes (**32 a-e**) [95]. Finally, the aldehyde reductive amination in the presence of sodium triacetoxyborohydride gave the desired products **1-25** [96].

Scheme 1. Synthetic pathway for compounds **1-25.**

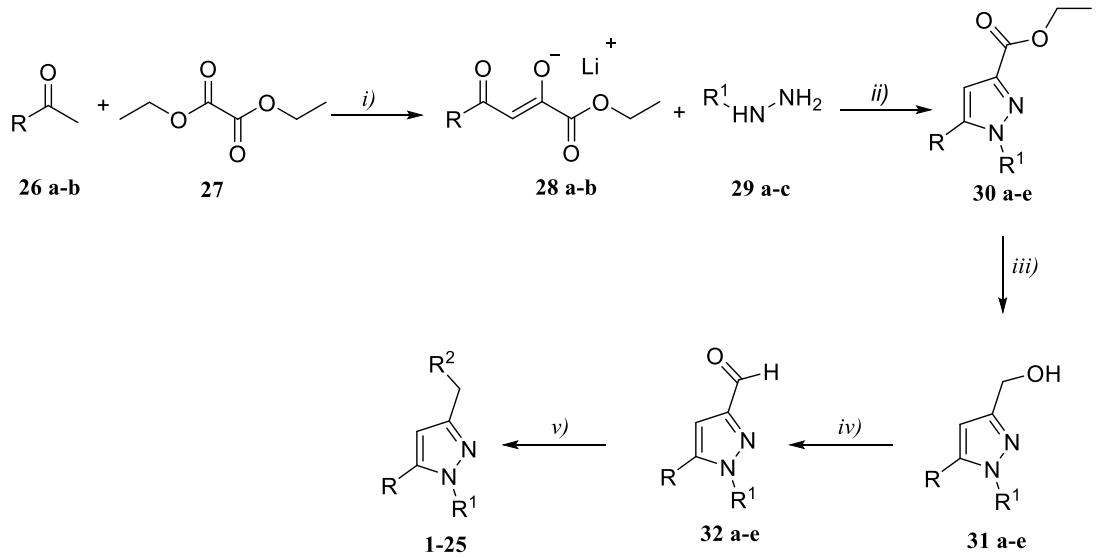

Reagents and conditions*: i)* $LiN(Si(CH_3)_3)_2$, THF, -78 °C and then rt, 25 h; *ii)* EtOH, 90 °C, 5h; *iii)* $LiAlH_4$, THF, 0 °C and then rt, 3h; *iv)* Dess-Martin periodinane, DCM, rt, 30 min; *v)* Ammine, CH_3COOH, $NaBH(CH_3COO)_3$, DCE, rt, 2 h.

2.5 *In vitro* assessment

Compounds **1-25** were evaluated *in vitro* to determine the Minimum Inhibitory Concentration (MIC) against MTB as well as cytotoxicity by measuring the concentration of compound resulting in 50% inhibition (TOX_{50}) of HepG2 cell line (Tab. 5). Among all synthetized compounds, those with MICs <1 μM and low cytotoxicity values, were evaluated for determining the drug-like properties (Chrom log $D_{pH7.4}$, artificial membrane permeability, percentage of binding to human serum albumin, the kinetic solubility *via* CLND and the human ether-a-go-go-related gene (hERG) binding (Tab. 6). *In vitro* activity against MTB was determined by Professor De Logu at the University of Cagliari, whereas the cytotoxicity assay as well as the experiments to assess the drug-like properties were performed by Doctor Fernandez-Menendez at the Disease of Developing World, Tres Cantos Medicine Development Campus. Compounds *in vitro* biological results are reported in **Table 5** and **Table 6**.

Table 5. MIC against *M. tuberculosis*, cytotoxicity (TOX_{50}) on HepG2 cell line and cytotoxicity/activity ratio (TOX_{50}/MIC) of compounds **1-25**, **BM635** and isoniazid.

Compound	MTB MIC (µM)[a]	TOX_{50} HepG2 (µM)[b]	TOX_{50}/MIC Ratio
1	20	12.60	0.63
2	2	80	40
3	0.5	64	128
4	0.00925	12.60	1362
5	>50	n.d[c]	n.d.[d]
6	1.3	40	30.76
7	21	10	0.48
8	1	40	40
9	20	n.d[c]	n.d.[d]
10	0.5	40	80
11	0.04	12.60	315
12	>50	n.d[c]	n.d[d]
13	4.7	80	17
14	0.3	32	106.66
15	2.5	40	16
16	4	>50	>12.5
17	2	32	16
18	0.02	16	800
19	1.2	63	52.50
20	1.2	32	26.66
21	2.5	50	20
22	2	>100	>50
23	1	50	50
24	0.07	12.60	180
25	2.5	40	16
BM635	0.12	40	333.33
Isoniazid	1.8	n.d[c]	n.d[d]

[a]activity against MTB *H37Rv*.
[b]cytotoxicity in HepG2 cells.
[c]not determined.
[d]not determined.

Table 6. Lipophilicity (Chrom log$D_{pH7.4}$), membrane permeability, percentage of binding to the HSA, water solubility (CLND), activity against hERG channels (IC_{50}) of compounds **3**, **4**, **10**, **11, 14**, **18** and **BM635**.

Compound	Chrom log$D_{pH7.4}$[a]	Membrane permeability cm/sec[b]	%HSA binding[c]	CLND (µM)[d]	hERG IC_{50} (µM)[e]
3	9.012	<0.30 x 10-5	n.d.[h]	6	25
4	11.01	4-Far	n.d.[h]	3.41	2
10	10.14	<0.03 x 10-5	n.d.[h]	15	>50
11	n.d.[f]	n.d.[g]	4-Far	n.d.[i]	8
14	7.31	1.70 x 10-5	96.47	258	3.2
18	10.04	4-Far	n.d.[h]	3.09	1.26
BM635	8.1	2.4 x 10-5	98.37	<1	10

[a]hydrophobicity by ChromLog$D_{pH=7.4.}$
[b]membrane permeability.
[c]percentage of binding to human serum albumin.
[d]water solubility via Chemi Luminescent Detection.
[e]activity against hERG channels.
[f]not determined.
[g]not determined.
[h]not determined.
[i]not determined.

Most of the newly synthetized pyrazoles retained the activity against MTB and among them, compounds **3**, **4**, **10**, **11**, **14**, **18**, and **24** provided remarkable MIC values (0.00925 µM <MIC< 0.5 µM) (Tab. 5). The C5 substitutions showed the same trend seen for the previous pyrrole series, confirming that both 4-isopropylphenyl and 4-trifluoromethylphenyl rings are well tolerated within the pyrazole scaffold. In contrast to pyrrole SARs [82], 4-F-phenyl and cyclohexyl rings at N1 seemed to work better than the isopropyl one. Moreover, the replacement of the 4-F-phenyl ring (**3,** CLND=

6 μM) with the cyclohexyl one (**10,** CLND= 15 μM) improves the solubility, reducing the high content of aromatic rings.

As observed in the pyrrole series, piperazinyl and *N*-methyl piperazinyl moieties (**1**, **7** and **9**) negatively affected the activity (MIC ≥ 20 μM), whereas the thiomorpholinyl (**6**, **13** and **19**) and piperidinyl (**15** and **21**) ones proved to be more tolerated (1.2 μM ≤ MIC ≤ 4.7 μM).

However, compared to pyrroles, the activity of pyrazoles seemed to be more influenced by the cyclic amine at position 3.

Consistent with the previous work by Ramesh and co-workers, pyrazoles incorporating silicon amines (**4**, **11**, **18** and **24**) provided outstanding activities against MTB (0.00925 μM ≤ MIC ≤ 0.07 μM) (Tab. 5), linked to an enhanced cell permeability [89]. Unfortunately, compounds **4**, **11**, **18** and **24** exhibited high HepG2 cytotoxicity (12.60 μM ≤ TOX_{50} ≤ 16 μM), marked hERG activities (hERG ≤ 2 μM) and low water solubility (CLND ≤ 3.41 μM) (Tab. 6) due to the high lipophilicity (10.4 ≤ ChromLog$D_{pH7.4}$ ≤ 11.01). Because of these liabilities, compounds **4**, **11**, **18** and **24** were not further progressed. Instead, 2-pyridyl piperazinyl analogues (**3** and **10)** exhibited good activities (MIC = 0.5 μM) combined with low HepG2 cytotoxicities (40 μM ≤ MIC ≤ 64 μM). Although the presence of an additional aromatic ring increases the lipophilicity of **3** and **10** (9.012 ≤ ChromLog$D_{pH7.4}$≤ 10. 04), they displayed an acceptable water solubility (6 μM ≤ CLND ≤ 15 μM) as a consequence of amine polarity. In addition, compounds **3** and **10** showed unexpected lower hERG activities (hERG ≥ 25 μM) compared to **BM635** (hERG = 10 μM) (Tab. 6). It was speculated that an aromatic substituent at C3 forces the molecule in a spatial arrangement that breaks hERG pharmacophore.

In general, the insertion of low nitrogen basicity amines didn't provide good results. The *tert*-butyl piperazin-1-carboxylate (**2**, **8**, **16** and **22**) partially retained the activity (1 μM ≤ MIC ≤ 4 μM), whereas the 2-oxa-7-azaspiro [3.5] nonanyl led to a complete loss of activity (MIC > 50 μM), presumably related to a less target binding affinity.

As observed for the first set of pyrazoles the 4-methoxypiperidinyl moiety seems to be a valid alternative to the morpholinyl one. Although there was no improvement in hERG activity, compound **14** displayed both good activity (MIC = 0.3 μM) and low HepG2 cytotoxicity (TOX_{50} = 30 μM), combined with a significant improvement in *in vitro* DMPK properties (Tab. 6). Consistent with previous studies, the huge increase of aqueous solubility could be explained by an unexpected consequence of the disruption of molecular symmetry and planarity [97]. Furthermore **14** exhibited good membrane permeability that suggests a presumable activity against intramacrophagic mycobacteria.

2.6 *In vivo* efficacy studies

Finally, *in vivo* efficacy of **14** was evaluated in a murine model of acute TB infection (n=3) at Tres Cantos laboratories. Compound **14** was administered at dose of 200 mg/Kg daily for eight days starting on day 1 after infection. Therapeutic efficacy was evaluated by the reduction of the mycobacteria log CFU (Colony Forming Unit) in the lungs of treated mice compared to untreated ones (Tab. 7). Compounds **14** proved to be effective in this model of acute infection, inducing a reduction of 2.0 log CFU in lung bacterial counts compared to untreated mice.

Table 7. Therapeutic efficacy of derivative **14** and moxifloxacin. Differences in the lung microorganism burden (log10 CFUs/lungs) with respect to untreated controls (Day 9 after infection).

Compound	Dose (mg/kg)[a]	Administration	Difference in logCFU/lungs	P[2]
14	200	Once a day	2.0	$p < 0.05$
moxifloxacin	30	Once a day	3.1	$p < 0.05$

[a]dose administered daily.

2.7 Target identification

To investigate whether pyrazoles were still on target, a complementary genetic approach was carried out by the research group of Professor Rubin at the Harvard School of Public Health. Spontaneous *M. tuberculosis* resistant mutants to compound **10,** as representative of its series**,** were generated in solid media containing 3 and 5 times the MIC. The resistors colonies were isolated, and their entire genomic DNA was sequenced. The resistors generated at the higher concentration of **10** showed no mutations, whereas the resistant colonies isolated at lower concentrations of **10** showed multiple mutations in the *mmpl3* coding sequence (i.e. A240V along with a missense mutation in ppsB, H239P along with a missense mutation in lprM and insertion mutation in fadD26), suggesting MmpL3 as the target of pyrazoles. All these mutations are placed in the fourth helix of MmpL3 transmembrane domain as well as the mutations of resistors to other known MmpL3 inhibitors.

2.8 Conclusions

In conclusion, the replacement of **BM635** pyrrole core with the pyrazole one led to an improvement of water solubility (3.09 μM ≤ CLND ≤ 258 μM) compared to **BM635** (CLND < 1 μM). Among the second series of pyrazoles, **3**, **10** and **14** showed promising *in vitro* biological profile, with anti-mycobacterial activity (0.3 μM ≤ MIC ≤ 0.5 μM) and cytotoxicity (32 μM ≤ TOX_{50} ≤ 64 μM) comparable to that of **BM635** (MIC = 0.12 μM, TOX_{50} = 40 μM). Furthermore, **3** and **10** presented lower activity values on hERG (IC_{50} ≥ 25 μM) (IC_{50} = 10 μM). Despite SAR differences between pyrroles an pyrazoles, target studies seem to confirm MmpL3 as target of pyrazoles.

Based on drug-like properties and *in vitro* activity, the best compound of the second pyrazole series that emerged from this study was **14**, displaying a good TOX_{50}/MIC ratio (106.66) as well as an outstanding improvement of water solubility (CLND = 258 μM) and a reduction of HSA binding percentage (HSA = 96.47%) compared to **BM 635** (CLND < 1 μM, HSA= 97.71%). Moreover, **14** proved to be effective in *in vivo* murine model of acute TB infection, statistically reducing the mycobacterial lung burden compared to untreated mice.

Further studies will be focused on evaluating the PK and *in vivo* toxicity of **14** and the *in vivo* efficacy of other promising pyrazoles **3** and **10.**

2.9 Materials and methods

2.9.1 Chemistry

All chemicals used were of reagent grade. Yields refer to purified products are not optimized. Melting points were determined in open capillaries on a Gallenkamp apparatus and are uncorrected. Sigma-Aldrich silica gel 60 (230−400 mesh) was used for column chromatography. Merck TLC plates (silica gel 60 F254) were used for thin-layer chromatography (TLC). Sigma-Aldrich aluminium oxide (activity II−III, according to Brockmann) was used for chromatographic purifications. Sigma-Aldrich Stratocrom aluminium oxide plates with a fluorescent indicator were used for TLC to check the purity of the compounds. ^{1}H NMR spectra were recorded with a Bruker AC 400 spectrometer in the indicated solvent (TMS as the internal standard). The values of the chemical shifts are expressed in ppm.

2.9.1.1 *General procedure for the preparation of lithium salts* ***28 a-b***

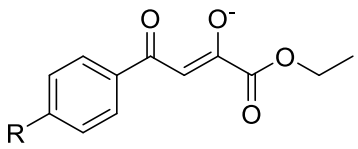

28 a-b

A solution of the appropriate acetophenone **26 a-b** in 3 mL of anhydrous tetrahydrofuran (THF) was added dropwise to a -70 °C cooled solution of lithium bis(trimethylsilyl)amide (12.3 mmol) in 30 mL of anhydrous THF, and the resulting solution was stirred for 1 h at -70 °C. Afterwards, diethyl oxalate (150 mmol) was added over 5 min and the resulting dark orange solution was warmed to room temperature over 4 h and then left stirring for 18 h. At the end, the precipitate was

filtered, washed with diethyl ether and petroleum ether and dried *in vacuo* to give lithium salts **28 a-b** in good yields (80-94%) [92].

Lithium (*Z*)-1-ethoxy-4-(4-isopropylphenyl)-1,4-dioxobut-2-en-2-olate (28 a). Pale yellow powder (yield 81%). ^{1}H NMR (400 MHz, $CDCl_3$): δ ppm=7.86 (d, 2H), 7.24 (d, 2H), 6.60 (s, 1H), 3.87 (s broad, 2H), 2.94 (sept, 1H), 1.265 (d, 6H), 0.98 (t, 3H).

Lithium (*Z*)-1-ethoxy-1,4-dioxo-4-(4-(trifluoromethyl)phenyl)but-2-en-2-olate (28 b). Pale yellow powder (yield 80%). ^{1}H NMR (400 MHz, $CDCl_3$): δ ppm=7.95 (d, 2H), 7.62 (d, 2H), 6.59 (s, 1H), 4.105 (m, 2H), 1.19 (m, 3H).

2.9.1.2 *General procedure for the preparation of carboxylates* ***30 a-e***

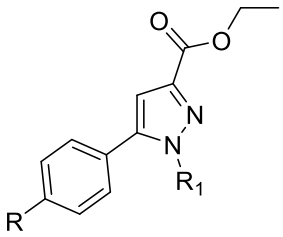

30 a-e

The appropriate hydrazine **29 a-c** was added (2.12 mmol) to solution of the appropriate lithium salt **28 a-b** (2.12 mmol) in 12 mL of ethanol, and the reaction mixture was heated at 90 °C for 5 h. At the end, the reaction mixture was cooled down to room temperature and the solvent was evaporated *in vacuo*. Water (10 mL) was added and the mixture was extracted with ethyl acetate. The organic layers were washed with brine, dried over Na_2SO_4 and evaporated *in vacuo*. The crude product was purified by column chromatography and a mixture of cyclohexane/ethyl acetate 10:1 (v/v) to give carboxylates **30 a-e** in good yields (35-90% yield) [93].

Ethyl 1-(4-fluorophenyl)-5-(4-isopropylphenyl)-1*H*-pyrazole-3-carboxylate (30 a). Pale yellow solid (yield 65%). ^{1}H NMR (400 MHz, $CDCl_3$): δ ppm=7.335 (m, 2H), 7.18 (d, 2H), 7.14 (d, 2H), 7.06 (t, 2H), 7.04 (s, 1H), 4.48 (q, 2H), 2.93 (sept, 1H), 1.45 (t, 3H), 1.27 (d, 6H).

Ethyl 1-cyclohexyl-5-(4-isopropylphenyl)-1*H*-pyrazole-3-carboxylate (30 b). Yellow oil (yield 85%). ^{1}H NMR (400 MHz, $CDCl_3$): δ ppm=7.36 (d, 2H), 7.30 (d, 2H), 6.76 (s, 1H), 4.39 (q, 2H), 4.15 (tt, 1H), 3.01 (sept,1H), 2.18 (m broad, 2H), 1.91 (m, 5H), 1.66 (m, 1H), 1.42 (t, 3H), 1.32 (m, 8H).

Ethyl 1-(4-fluorophenyl)-5-(4-(trifluoromethyl)phenyl)-1*H*-pyrazole-3-carboxylate (30 c). Yellow solid (yield 70%). ^{1}H NMR (400 MHz, $CDCl_3$): δ ppm=7.60 (d, 2H), 7.33 (m, 4H), 7.09 (m, 3H), 4.47 (q, 2H), 1.44 (t, 3H).

Ethyl 1-cyclohexyl-5-(4-(trifluoromethyl)phenyl)-1H-pyrazole-3-carboxylate (30 d). White solid (yield 74%). ^{1}H NMR (400 MHz, $CDCl_3$): δ ppm=7.76 (d, 2H), 7.50 (d, 2H), 6.81 (s, 1H), 4.43 (q, 2H), 4.09 (tt, 1H), 2.165 (q, 2H), 1.89 (m, 4H), 1.64 (m, 2H), 1.41 (t, 3H), 1.29 (q, 2H).

Ethyl 1-isopropyl-5-(4-(trifluoromethyl)phenyl)-1*H*-pyrazole-3-carboxylate (30 e). White solid (yield 63%). ^{1}H NMR (400 MHz, $CDCl_3$): δ ppm=7.75 (d, 2H), 7.51 (d, 2H), 6.81 (s, 1H), 4.55 (sept, 1H), 4.43 (q, 2H), 1.53 (d, 6H), 1.41 (t, 3H).

2.9.1.3 *General procedure for the preparation of alcohols* ***31 a-e***

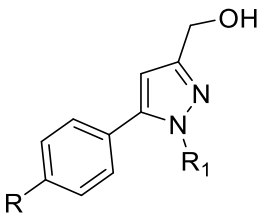

31 a-e

To an ice-cold solution of the appropriate carboxylate **30 a-e** (0.41 mmol) in anhydrous THF (5 mL), $LiAlH_4$ (0.49 ml, 1 M in THF) was added dropwise under N_2 atmosphere. The reaction mixture was stirred for 1 h at 0 °C and then for 2 h at room temperature. At the end, the reaction mixture was cooled down to 0 °C and diluted with 0.18 mL of ethyl acetate, 0.08 mL of H_2O and 0.1 mL of NaOH 2N and stirred for 30 min. The precipitate was filtered off and the filtrate was dried over Na_2SO_4, concentrated *in vacuo* and purified by column chromatography with a mixture of cyclohexane/ethyl acetate 6:1 (v/v) to give the products **31 a-e** in good yields (38-94% yield) [94].

(1-(4-Fluorophenyl)-5-(4-isopropylphenyl)-1*H*-pyrazol-3-yl)methanol (31 a). White solid (yield 91%). ^{1}H NMR (400 MHz, $CDCl_3$): δ ppm=7.28 (m, 2H), 7.17 (d, 2H), 7.12 (d, 2H), 7.04 (t, 2H), 6.49 (s, 1H), 4.79 (s, 2H), 2.90 (sept, 6H), 2.04 (s broad, 1H), 1.25 (d, 6H).

(1-Cyclohexyl-5-(4-isopropylphenyl)-1*H*-pyrazol-3-yl)methanol (31 b). Colourless oil (yield 57%). ^{1}H NMR (400 MHz, $CDCl_3$): δ ppm=7.32 (d, 2H), 7.275 (d, 2H), 6.21 (s, 1H), 4.73 (s, 2H), 4.08 (t, 1H), 3.485 (q, 1H), 2.98 (sept, 1H), 2.03 (s broad, 1H), 1.86 (q, 2H), 1.63 (m, 5H), 1.27 (m, 8 H).

(1-(4-Fluorophenyl)-5-(4-(trifluoromethyl)phenyl)-1*H*-pyrazol-3-yl)methanol (31 c). White solid (yield 63%). ^{1}H NMR (400 MHz, $CDCl_3$): δ ppm= 7.50 (d, 2H), 7.36 (d, 2H), 7.28 (m, 2H), 7.09 (t, 2H), 6.62 (s, 1H), 4.83 (s, 2H), 1.29 (s broad, 1H).

(1-Cyclohexyl-5-(4-(trifluoromethyl)phenyl)-1*H*-pyrazol-3-yl)methanol (31 d). White solid (yield 72%). ^{1}H NMR (400 MHz, $CDCl_3$): δ ppm= 7.87 (d, 2H, *J*= 8.06 Hz), 7.65 (d, 2H, *J*= 8.06 Hz), 6.69 (s, 1H), 4.77 (s, 2H), 4.18 (tt, 1H, *J*= 11.65, 3.91 Hz), 2.21 (m, 2H), 1.95 (m, 4H), 1.73 (m, 2H), 1.36 (m, 2H).

(1-Isopropyl-5-(4-(trifluoromethyl)phenyl)-1*H*-pyrazol-3-yl)methanol (31 e). White solid (yield 94%). ^{1}H NMR (400 MHz, $CDCl_3$): δ ppm=7.73 (d, 2H), 7.49 (d, 2H), 6.29 (s, 1H), 4.75 (s, 2H), 4.47 (sept, 1H), 2.18 (s broad, 1H), 1.475 (d, 6H).

2.9.1.4 *General procedure for the preparation of carbaldehydes* ***32 a-e***

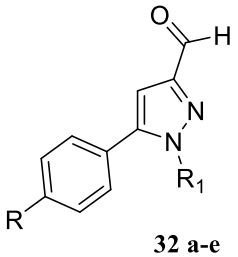

32 a-e

Dess-Martin periodinane (0.4 mmol) was added to a solution of the appropriate alcohol **31 a-e** (0.31 mmol) in anhydrous DCM (5 mL) under N_2 atmosphere. The reaction mixture was stirred for 30 min at room temperature, and at the end was diluted with 5.1 mL of sat $NaHCO_3$ and 5.1 mL of sat $Na_2S_2O_3$ and stirred for 30 min. The reaction mixture was extracted with DCM, the organic layers washed with sat $NaHCO_3$ and brine and dried over Na_2SO_4. After concentration *in vacuo* the crude product was purified by column chromatography (cyclohexane/ ethyl acetate 5:1 (v/v)) to give **32 a-e** in good yields (51-98% yield) [95].

1-(4-Fluorophenyl)-5-(4-isopropylphenyl)-1*H*-pyrazole-3-carbaldehyde (32 a). White solid (yield 73%). ^{1}H NMR (400 MHz, $CDCl_3$): δ ppm=10.09 (s, 1H), 7.36 (m, 2H), 7.22 (d, 2H), 7.12 (m, 4H), 7.01 (s, 1H), 2.94 (sept, 1H), 1.25 (d, 6H).

1-Cyclohexyl-5-(4-isopropylphenyl)-1*H*-pyrazole-3-carbaldehyde (32 b). White solid (yield 75%). ^{1}H NMR (400 MHz, $CDCl_3$): δ ppm=10.02 (s, 1H), 7.37 (d, 2H), 7.30 (d, 2H), 6.77 (s, 1H), 4.21 (tt, 1H), 3.02 (sept, 1H), 2.06 (q, 2H), 1.91 (m, 4H),1.72 (m, 1H), 1.64 (m, 1H), 1.31 (m, 8 H).

1-(4-Fluorophenyl)-5-(4-(trifluoromethyl)phenyl)-1*H*-pyrazole-3-carbaldehyde (32 c). White solid (yield 73%). ^{1}H NMR (400 MHz, $CDCl_3$): δ ppm=10.08 (s, 1H), 7.61 (d, 2H), 7.33 (m, 4H), 7.13 (t, 2H), 7.08 (s, 1H).

1-Cyclohexyl-5-(4-(trifluoromethyl)phenyl)-1*H*-pyrazole-3-carbaldehyde (32 d). White solid (yield 60%). ^{1}H NMR (400 MHz, $CDCl_3$): δ ppm= 10.03 (s, 1H), 7.79 (d, 2H), 7.52 (d, 2H), 6.83 (s, 1H), 4.15 (m, 1H), 2.09 (m, 2H), 1.97 (m, 4H), 1.86 (m, 1H), 1.30 (m, 3H).

1-Isopropyl-5-(4-(trifluoromethyl)phenyl)-1*H*-pyrazole-3-carbaldehyde (32 e). White solid (yield 91%). ^{1}H NMR (400 MHz, $CDCl_3$): δ ppm=10.01 (s, 1H), 7.75 (d, 2H), 7.50 (d, 2H), 6.82 (s, 1H), 4.565 (sept, 1H), 1.54 (d, 6H).

2.9.1.5 *General procedure for the preparation of compounds* ***1-25***

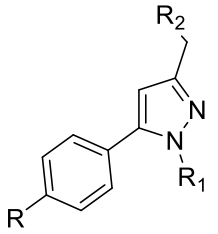

1-25

To a solution of the appropriate carbaldehyde (**32 a-e**) (0.26 mmol) in 5 mL of anhydrous dichloroethane a drop of glacial acetic acid was added, and the mixture was stirred for 10 min. Afterwards, the appropriate amine (0.26 mmol) and sodium triacetoxyborohydride (0.36 mmol) were added and the reaction mixture was stirred for 2 h. At the end, the mixture was quenched with sat $NaHCO_3$ (5 mL) and extracted with DCM. The organic layers were dried over Na_2SO_4, concentrated *in vacuo* and purified by column chromatography (DCM/ methanol 1% (v/v)) to yield compounds in good yields (34-94%) [96].

1-((1-(4-Fluorophenyl)-5-(4-isopropylphenyl)-1*H*-pyrazol-3-yl)methyl)-4-methylpiperazine (1). White solid (yield 58%). ^{1}H NMR (400 MHz, $CDCl_3$): δ ppm= 7.30 (m, 2H), 7.16 (m, 4H), 7.05 (m, 2H), 6.49 (s, 1H), 3.77 (s, 2H), 2.99-2.87 (m, 9 H), 2.52 (s, 3H), 1.27 (d, 6H). ^{13}C NMR (400 MHz, $CDCl_3$) δ ppm=161.76, 159.30, 148.19, 143.04, 135.26, 127.49, 126.59, 126.06, 125.98, 125.59, 114.86, 114.63,106.69, 57.96, 54.83, 51.82, 45.98, 32.81, 22.79.

***Tert*-butyl 4-((1-(4-fluorophenyl)-5-(4-isopropylphenyl)-1*H*-pyrazol-3-yl)methyl)piperazine-1-carboxylate (2).** White solid (yield 60%). ^{1}H NMR (400 MHz, $DMSOd_6$): δ ppm= 7.27 (m, 2H), 7.21 (m, 4H), 7.12 (d, 2H), 6.52 (s, 1H), 3.52 (s broad, 2H), 2.85 (sept, 1H), 2.49 (m, 4H), 2.40 (t, 4H), 1.37 (s, 9H), 1.16 (d, 6H).

^{13}C NMR (400 MHz, $CDCl_3$) δ ppm=161.76, 159.30, 153.77, 148.19, 143.04, 135.26, 127.49, 126.59, 126.06, 125.98, 125.59, 114.86, 114.63,106.69, 78.60, 57.96, 54.83, 51.82, 32.81, 28.68, 27.41, 22.79.

1-((1-(4-Fluorophenyl)-5-(4-isopropylphenyl)-1*H*-pyrazol-3-yl)methyl)-4-(pyridin-2-yl)piperazine (3). White solid (yield 44%). ^{1}H NMR (400 MHz, $CDCl_3$): δ ppm= 8.21 (dd, 1H), 7.50 (td, 1H), 7.31 (m, 2H), 7.175 (m, 4H), 7.06 (t, 2H), 6.66 (m, 2H), 6.57 (s broad, 1H), 3.80 (s broad, 2H), 3.67 (s broad, 4H), 2.92 (sept, 1H), 2.80 (s broad, 4H), 1.27 (d, 6H). ^{13}C NMR (400 MHz, $CDCl_3$): δ ppm= 162.73, 160.43, 159.37, 149.26, 147.98, 144.12, 137.51, 136.32, 128.56, 127.12, 127.03, 126.63, 115.91, 115.68, 113.40, 107.10, 55.67, 52.63, 44.93, 33.84, 23.75.

1-((1-(4-Fluorophenyl)-5-(4-isopropylphenyl)-1*H*-pyrazol-3-yl)methyl)-4,4-dimethyl-1,4-azasilinane (4). White solid (yield 70%). ^{1}H NMR (400 MHz, $CDCl_3$): δ ppm=7.20 (m, 2H), 7.08 (m, 4H), 6.96 (m, 2H), 6.45 (s, 1H), 4.63 (s, 2H), 2.815 (m, 5H), 1.19 (s, 6H), 0.78 (s, 4H), 0.01 (s, 6H). ^{13}C NMR (400 MHz, $CDCl_3$): δ ppm= 162.82, 160.36, 149.26, 144.24, 136.60, 128.56, 127.54, 127.09, 127.01, 126.61, 115.92, 115.69, 107.83, 55.69, 53.56, 33.84, 23.75.

7-((1-(4-Fluorophenyl)-5-(4-isopropylphenyl)-1H-pyrazol-3-yl)methyl)-2-oxa-7-azaspiro[3.5]nonane (5). White solid (yield 35%) ^{1}H NMR (400 MHz, $CDCl_3$): δ ppm= 7.26 (m, 4H), 7.135 (m, 4H), 7.03 (m, 2H), 6.49 (s, 1H), 4.42 (m, 4H), 3.62 (s, 2H), 2.89 (sept, 1H), 2.50 (m broad, 4H), 1.95 (m broad, 4H), 1.13 (d, 6H). ^{13}C NMR (400 MHz, $CDCl_3$) δ ppm= 162.13, 150.39, 148.23, 144.81, 135.28, 129.58, 128.82, 127.54, 124.23, 116.40, 103.87, 81.80, 56.96, 50.14, 38.75,34.20, 29.30, 23.37.

4-((1-Cyclohexyl-5-(4-isopropylphenyl)-1*H*-pyrazol-3-yl)methyl)thiomorpholine (6). Pale yellow oil (yield 54%). ^{1}H NMR (400 MHz, $CDCl_3$): δ ppm= 7.33 (m, 4H),

6.20 (s, 1H), 4.11 (tt, 1H), 3.70 (s broad, 2H), 3.00 (sep, 1H), 2.87 (s broad, 4H), 2.76 (s broad, 4H), 2.05 (m, 2H), 1.89 (m, 4H), 1.67 (m, 2H), 1.25-1.39 (m, 8H). ^{13}C NMR (400 MHz, $CDCl_3$) δ ppm=149.11, 143.45, 129.06, 128.41, 126.76, 105.88, 57.37, 56.25, 53.26, 33.75, 33.18, 27.00, 25.64, 25.09, 23.77.

1-((1-Cyclohexyl-5-(4-isopropylphenyl)-1*H*-pyrazol-3-yl)methyl)-4-methylpiperazine (7). White solid (yield 62%). ^{1}H NMR (400 MHz, $CDCl_3$): δ ppm= 7.34 (m, 4H), 6.18 (s, 1H), 4.09 (m, 1H), 3.67 (s, 2H), 3.12 (s broad, 2H), 2.99 (sep, 1H), 2.66 (m broad, 6H), 2.36 (s, 3H), 2.03 (m, 3H), 1.87 (m, 4H), 1.66 (m, 1H), 1.33 -1.29 (m, 8H). ^{13}C NMR (400 MHz, $CDCl_3$) δ ppm= 149.10, 147.73, 143.58, 128.86, 128.57, 126.76, 105.71, 57.50, 56.02, 52.67, 45.98, 33.93, 33.34, 27.57, 25.65, 25.09, 23.92.

***Tert*-butyl 4-((1-cyclohexyl-5-(4-isopropylphenyl)-1*H*-pyrazol-3-yl)methyl)piperazine-1-carboxylate (8).** White solid (yield 50%). ^{1}H NMR (400 MHz, $CDCl_3$): δ ppm= 7.32 (m, 4H), 6.20 (s, 1H), 4.10 (m, 1H), 3.65 (s, 2H), 3.49 (s broad 4H), 3.00 (sept, 1H), 2.53 (s broad, 4H), 2.05 (m, 2H), 1.99 (m 4H), 1.43 (s, 9H), 1.32 -1.32 (m, 10H). ^{13}C NMR (400 MHz, $CDCl_3$) δ ppm= 154.76, 149.10, 147.73, 143.58, 128.86, 128.57, 126.76, 105.71, 79.49, 57.50, 56.02, 52.67, 33.93, 33.34, 28.44, 27.57, 25.65, 25.09, 23.92.

1-((1-Cyclohexyl-5-(4-isopropylphenyl)-1*H*-pyrazol-3-yl)methyl)piperazine (9). White solid (yield 50%). ^{1}H NMR (400 MHz, $CDCl_3$): δ ppm= 7.28 (m, 4H), 6.18 (s, 1H), 4.09 (m, 1H), 3.67 (s, 2H), 2.98-2.91 (m, 5H), 2.50 (s broad, 3H), 2.20 (m, 1H), 2.03 (m, 2H), 1.88 (m, 4H), 1.21-1.40 (m, 10H). ^{13}C NMR (400 MHz, $CDCl_3$) δ ppm= 149.03, 147.45, 143.61, 128.81, 128.65, 126.82, 105.77, 57.69, 56.63, 53.64, 45.56, 34.02, 33.43, 25.73, 25.31, 23.91.

1-((1-Cyclohexyl-5-(4-isopropylphenyl)-1*H*-pyrazol-3-yl)methyl)-4-(pyridin-2-yl)piperazine (10). White solid (yield 70%). ^{1}H NMR (400 MHz, $CDCl_3$): δ ppm= 8.18 (dd, 1H), 7.46 (td, 1H), 7.29 (m, 4H), 6.60 (m, 2H), 6.20 (s, 1H), 4.08 (m, 1H), 3.68 (s, 2H), 3.58 (m, 4H), 2.96 (sept, 1H), 2.69 (m, 4H), 2.05 (m, 2H), 1.87 (m, 4H), 1.30 (m,10H). ^{13}C NMR (400 MHz, $CDCl_3$) δ ppm= 159.56, 149.06, 147.97, 147.26, 143.55, 137.41, 128.99, 128.99, 128.71, 126.84, 113.19, 107.16, 105.81, 57.50, 55.96, 52.65, 45.09, 33.88, 33.35, 25.66, 25.10, 23.92.

1-((1-Cyclohexyl-5-(4-isopropylphenyl)-1*H*-pyrazol-3-yl)methyl)-4,4-dimethyl-1,4-azasilinane (11). White solid (yield 60%). ^{1}H NMR (400 MHz, $CDCl_3$): δ ppm= 7.30 (s, 4H), 6.20 (s, 1H), 4.08 (tt, 1H), 3.68 (s, 2H), 2.97 (sept, 1H), 2.80 (t, 4H), 2.04 (qd, 2H), 1.86 (m, 4H), 1.30 (m, 10H), 0.80 (t, 4H), 0.04 (s, 6H). ^{13}C NMR (400 MHz, $CDCl_3$): δ ppm= 148.99, 143.49, 128.84, 128.58, 126.89, 126.69, 105.83, 57.42, 55.82, 52.19, 33.88, 33.31, 25.61, 25.08, 23.88, 13.17, 3.22.

7-((1-Cyclohexyl-5-(4-isopropylphenyl)-1H-pyrazol-3-yl)methyl)-2-oxa-7-azaspiro[3.5]nonane (12). White solid (yield 34%). ^{1}H NMR (400 MHz, $CDCl_3$): δ ppm= 7.31 (m, 4H), 6.18 (s, 1H), 4.43 (m, 4H), 4.10 (t, 1H), 3.57 (s, 2H), 2.98 (sept, 1H), 2.45 (m broad, 4H), 2.05 (q, 2H), 1.88 (m, 8H), 1.66 (m, 1H), 1.325 (m, 9H). ^{13}C NMR (400 MHz, $CDCl_3$) δ ppm= 150.45, 148.06, 141.78, 129.76, 129.29, 127.24, 103.92, 81.80, 61.77, 56.96, 50.14, 38.75, 34.20, 32.56, 29.30, 25.92, 24.75, 23.37.

4-((1-(4-Fluorophenyl)-5-(4-(trifluoromethyl)phenyl)-1*H*-pyrazol-3-yl)methyl)thiomorpholine (13). Yellow solid (yield 70%). ^{1}H NMR (400 MHz, $DMSOd_6$): δ ppm= 7.71 (d, 2H), 7.43 (d, 2H), 7.29 (m, 4H), 6.69 (s, 1H), 3.56 (s broad, 2H), 2.72 (m, 4H), 2.61 (m, 4H). ^{13}C NMR (400 MHz, $CDCl_3$): δ ppm= 160.4, 150.2, 143.5, 136.3, 135.3, 131.0, 126.1, 125.6, 124.1, 116.1, 115.6, 107.5, 60.2, 57.0, 28.3.

^{13}C NMR (400 MHz, $CDCl_3$) δ ppm= 162.96, 160.49, 142.39, 135.75, 133.69, 130.10, 128.77, 127.12, 127.04, 125.51, 125.16, 122.46, 116.22, 115.99, 108.59, 56.47, 54.82, 27.88.

1-((1-(4-Fluorophenyl)-5-(4-(trifluoromethyl)phenyl)-1*H*-pyrazol-3-yl)methyl)-4-methoxypiperidine (14). White solid (yield 63%). ^{1}H NMR (400 MHz, $CDCl_3$): δ ppm= 7.59 (d, 2H, *J*= 8.3 Hz), 7.36 (d, 2H, *J*= 8.3 Hz), 7.26 (m, 2H), 7.08 (m, 2H), 6.62 (s, 1H), 3.69 (s, 2H), 3.37 (s, 3H), 3.28 (m, 1H), 2.93 (m, 2H), 2.35 (m, 2H), 1.97 (m, 2H), 1.71 (m, 2H). ^{13}C NMR (400 MHz, $CDCl_3$) δ ppm= 163.16, 160.58, 149.94, 142.52, 135.82, 133.88, 130.78, 130.51, 130.21, 130.01, 128.74, 127.07, 125.58, 125.19, 122. 49, 116.28, 116.01, 108.81, 56.09, 53.58, 51.00, 30.63.

1-((1-(4-Fluorophenyl)-5-(4-(trifluoromethyl)phenyl)-1*H*-pyrazol-3-yl)methyl)piperidine (15). White solid (yield 70%). ^{1}H NMR (400 MHz, $CDCl_3$): δ ppm= 7.56 (d, 2H), 7.33 (d, 2H), 7.26 (m, 2H), 7.05 (m, 2H), 6.58 (s, 1H), 3.62 (s, 2H), 2.53 (s broad, 4H), 1.63 (m, 4H), 1.47 (m, 2H). ^{13}C NMR (400 MHz, $CDCl_3$) δ ppm= 163.15, 160.54, 142.53, 135.93, 133.85, 130.47, 130.03, 129.63, 128.80, 127.28, 127.16, 125.57, 125.22, 116.23, 115.96, 109.05, 108.79, 56.49, 54.53, 25.98, 24.09.

***Tert*-butyl 4-((1-(4-fluorophenyl)-5-(4-(trifluoromethyl)phenyl)-1*H*-pyrazol-3-yl)methyl)piperazine-1-carboxylate (16).** White solid (yield 71%). ^{1}H NMR (400 MHz, $CDCl_3$): δ ppm= 7.51 (d, 2H), 7.26 (d, 2H), 7.18 (m, 2H), 6.99 (m, 2H), 6.48 (s, 1H), 3.59 (s, 2H), 3.41 (t, 4H), 2.47 (t, 4H), 1.39 (s, 9H). ^{13}C NMR (400 MHz, $CDCl_3$) δ ppm= 162.14, 159.58, 153.71, 141.49, 134.76, 132.78, 129.54, 129.39, 129.19, 127.80, 126.20, 126.05, 124.52, 115.23, 115.06, 107.71, 78.68, 54.63, 51.90, 51.72, 27.46.

1-((1-(4-Fluorophenyl)-5-(4-(trifluoromethyl)phenyl)-1*H*-pyrazol-3-yl)methyl)-4-(pyridin-2-yl)piperazine (17). White solid (yield 61%). ^{1}H NMR (400 MHz, $CDCl_3$): δ ppm= 8.19 (m, 1H), 7.57 (d, 2H), 7.47 (td, 1H), 7.34 (d, 2H), 7.28 (m, 2H), 7.06 (m, 2H), 6.63 (m, 3H), 3.73 (s, 2H), 3.60 (t, 4H), 2.72 (t,4H). ^{13}C NMR (400 MHz, $CDCl_3$) δ ppm= 162.96, 160.49, 159.37, 149.26, 144.12, 142.39, 135.75, 133.69, 130.43, 130.10, 128.77, 127.12, 127.04, 125.51, 126.16, 122.46, 116.22, 115.99, 113.40, 108.59, 107.96, 56.47, 54.82, 44.93.

1-((1-(4-Fluorophenyl)-5-(4-(trifluoromethyl)phenyl)-1*H*-pyrazol-3-yl)methyl)-4,4-dimethyl-1,4-azasilinane (18). White solid (yield 65%). ^{1}H NMR (400 MHz, $CDCl_3$): δ ppm= 7.57 (d, 2H), 7.34 (d, 2H), 7.26 (m, 2H), 7.06 (t, 2H), 6.63 (s broad, 1H), 3.75 (s, 2H), 2.87 (m broad, 4H), 0.85 (m broad 4H), 0.08 (s, 6H). ^{13}C NMR (400 MHz, $CDCl_3$) δ ppm= 162.83, 160.61, 142.13, 133.89, 130.54, 130.23, 130.04, 129.76, 128.81, 127.14, 127.06, 125.59, 125.14, 116.07, 115.89, 108.72, 55.52, 52.43, 13.45, 3.07.

4-((1-Cyclohexyl-5-(4-(trifluoromethyl)phenyl)-1*H*-pyrazol-3-yl)methyl)thiomorpholine (19). Yellow solid (yield 53%). ^{1}H NMR (400 MHz, $CDCl_3$): δ ppm= 7.72 (d, 2H), 7.48 (d, 2H), 6.26 (s, 1H), 4.00 (t, 1H), 3.68 (s, 2H), 2.85 (m broad, 4H), 2.75 (m broad, 4H), 2.04 (q, 2H), 1.87 (d, 4H), 1.66 (m broad, 1H), 1.27 (d, 3H). ^{13}C NMR (400 MHz, $CDCl_3$): δ ppm= 141.93, 134.89, 129.30, 125.30, 125.64, 122.66, 120.49, 116.59, 106.56, 57.90, 56.55, 54.26, 33.32, 27.88, 25.56, 25.02.

1-((1-Cyclohexyl-5-(4-(trifluoromethyl)phenyl)-1*H*-pyrazol-3-yl)methyl)-4-methoxypiperidine (20). White solid (yield 75%). ^{1}H NMR (400 MHz, $CDCl_3$): δ ppm= 7.71 (d, 2H), 7.48 (d, 2H), 6.32 (s broad, 1H), 4.00 (tt, 1H), 3.66 (s , 2H), 3.27

(s, 3H), 3.14 (s broad, 1H), 2.88 (s broad 2H), 2.12 (s broad, 1H), 2.04 (m, 3H), 1.88 (m, 4H), 1.66 (m, 3H), 1.274 (m, 4H).^{13}C NMR (400 MHz, $CDCl_3$): δ ppm= 141.95, 134.90, 130.51, 130.18, 129.23, 125.65, 106.31, 57.91, 55.88, 55.53, 51.04, 33.31, 30.78, 29.71, 25.62, 25.02.

1-((1-Cyclohexyl-5-(4-(trifluoromethyl)phenyl)-1*H*-pyrazol-3-yl)methyl)piperidine (21). White solid (yield 70%). ^{1}H NMR (400 MHz, $DMSOd_6$): δ ppm= 7.84 (d, 2H), 7.63 (d, 2H), 6.27 (s, 1H), 4.02 (m, 1H), 2.49 (m, 4H), 2.35 (m broad, 3H), 1.85 (m broad, 4H), 1.74 (d, 2H), 1.58 (d, 1H), 1.46 (quin, 4H), 1.35 (m, 2H), 1.21 (m broad, 2H). ^{13}C NMR (400 MHz, $CDCl_3$): δ ppm= 141.93, 134.89, 129.30, 125.64, 122.66, 120.49, 116.59, 106.56, 57.90, 56.55, 54.26, 33.32, 25.73, 25.56, 25.02, 24.17

***Tert*-butyl 1-((1-cyclohexyl-5-(4-(trifluoromethyl)phenyl)-1*H*-pyrazol-3-yl)methyl)piperazine-4-carboxylate (22).** White solid (yield 86%). ^{1}H NMR (400 MHz, $CDCl_3$): δ ppm= 7.72 (d, 2H), 7.48 (d, 2H), 6.23 (s, 1H), 4.00 (m, 1H), 3.60 (s, 2H), 3.45 (t, 4H), 2.48 (t, 4H), 2.06 (m, 2H), 1.86 (m, 4H), 1.46 (s, 9H), 1.27 (m, 4H). ^{13}C NMR (400 MHz, $CDCl_3$): δ ppm= 154.82, 142.04, 134.79, 130.55, 130.22, 129.90, 129.23, 125.75, 125.72, 125.68, 125.64, 125.34, 122.63, 106.37, 57.96, 55.94, 52.76, 33.32, 29.72, 28.44, 25.60, 25.01.

2-(1-((1-Cyclohexyl-5-(4-(trifluoromethyl)phenyl)-1*H*-pyrazol-3-yl)methyl)piperazin-4-yl)pyridine (23). White solid (yield 87%). ^{1}H NMR (400 MHz, $CDCl_3$): δ ppm= 8.185 (dd, 1H), 7.72 (d, 2H), 7.47 (m, 3H), 6.62 (m, 2H), 6.27 (s, 1H), 4.00 (tt, 1H), 3.67 (s, 2H), 3.57 (t, 4H), 2.66 (t, 4H), 2.06 (dq, 2H), 1.885 (d, 4H), 1.27 (m, 4H). ^{13}C NMR (400 MHz, $CDCl_3$): δ ppm= 159.56, 149.06, 147.97,

147.26, 143.55, 137.41, 130.52, 130.41, 128.99, 128.71, 122.66, 113.19, 107.16, 105.81, 57.50, 55.96, 52.65, 45.09, 33.88, 33.35, 25.66, 25.10, 23.92.

1-((1-Cyclohexyl-5-(4-(trifluoromethyl)phenyl)-1*H*-pyrazol-3-yl)methyl)-4,4-dimethyl-1,4-azasilinane (24). White solid (yield 65%). ^{1}H NMR (400 MHz, $CDCl_3$): δ ppm= 7.66 (d, 2H, *J*= 8.07 Hz), 7.44 (d, 2H, *J*= 8.07 Hz), 6.24 (s, 1H), 3.95 (tt, 1H, *J*= 7.83, 3.67 Hz), 3.64 (s, 2H), 2.75 (m broad, 4H), 2.00 (m, 2H), 1.81 (m, 4H), 1.21 (m, 4H), 0.76 (m broad, 4H), 0.00 (s, 6H). ^{13}C NMR (400 MHz, $CDCl_3$): δ ppm=148.91, 141.84, 134.98, 130.52, 130.41, 129.96, 129.18, 125.58, 122.66, 106.25, 57.87, 55.81, 52.36, 33.31, 25.62, 25.03, 13.56, 3.09.

1-((1-Isopropyl-5-(4-(trifluoromethyl)phenyl)-1*H*-pyrazol-3-yl)methyl)-4-methoxypiperidine (25). White solid (yield 61%). ^{1}H NMR (400 MHz, $CDCl_3$): δ ppm= 7.70 (d, 2H), 7.49 (d, 2H), 6.26 (s, 1H), 4.46 (sept, 1H), 3.61 (s, 2H), 3.33 (s, 3H), 3.22 (m, 1H), 2.86 (m, 2H), 2.25 (m, 2H), 1.95 (m, 2H), 1.79 (m, 2H), 1.66 (d, 6H). ^{13}C NMR (400 MHz, $CDCl_3$): δ ppm= 148.01, 141.98, 134.81, 130.59, 130.27, 129.28, 125.72, 125.69, 125.65, 125.61, 125.31, 122.61, 106.40, 57.90, 56.33, 53.48, 50.18, 30.63, 22.92.

2.9.2 Mycobacterium tuberculosis H37Rv growth inhibition assay

The measurement of the minimum inhibitory concentration (MIC) against *M. tuberculosis* strains for each tested compound was performed in 96-well flat-bottom, polystyrene microtiter plates in a final volume of 100 mL. Then, two-fold drug dilutions in neat DMSO starting at 50 mM were performed. Drug solutions were added to Middlebrook 7H9 medium (Difco) and isoniazid (Sigma Aldrich) was used as a positive control with two-fold dilutions of isoniazid starting at 160 mg/mL. The inoculum was standardized to approximately 16 e^7 cfu/mL and diluted 1 in 100 in Middlebrook 7H9 broth (Difco). This inoculum (100 mL) was added to the entire plate but G-12 and H-12 wells were used as blank controls. All plates were placed in a sealed box to prevent drying out of the peripheral wells and incubated at 37 °C without shaking for six days. A Resazurin solution was prepared by dissolving one tablet of resazurin (Resazurin Tablets for Milk Testing; Ref 330884Y' VWR International Ltd) in 30 mL of sterile PBS (phosphate buffered saline). Of this solution, 25 mL were added to each well. Fluorescence was measured (Spectramax M5 Molecular Devices, Excitation 530 nm, Emission 590 nm) after 48 hours to determine the MIC value.

2.9.3 HepG2 cytotoxicity assay

HepG2 cells were cultured using Eagle's MEM supplemented with 10% heat-inactivated FBS, 1% NEAA and 1% penicillin/streptomycin. Prior to addition of the cell suspension, 250 nL of test compounds per well were pre-dispensed in TC-treated black clear-bottomed 384 well plates (Greiner, cat.# 781091) with an Echo 555 instrument. After that, 25 μL of HepG2 (ATCC HB-8065) cells (~3000 cells/well) grown to confluence in Eagle's MEM supplemented with 10% heat-inactivated FBS, 1% NEAA and 1% Penicillin/Streptomycin were added to each well with the reagent

dispenser. Plates were allowed to incubate at 37 °C with 20% O2 and 5% CO2 for 48 h. After the incubation period (48h), the plates were equilibrated to room temperature before proceeding to develop the luminescent signal. ATP levels measured with CellTiter Glo kit (Promega) were used as cell viability read-out. 25 µL of CellTiter Glo substrate dissolved in the buffer was added to each well. Plates were incubated at room temperature for 10 minutes for stabilization of luminescence signal and read on View Lux with excitation and emission filters of 613 and 655 nm, respectively.

2.9.4 Chrom log$D_{pH=7.4}$

The Chromatographic Hydrophobicity Index (CHI) values were measured as reported by Valko K. *et al.* and converted into Chrom log*D* using the following formula: Chrom log*D* = 0.0857CHI-2.00. The average error of the assay is 63 CHI unit or 60.25 Chrom log*D* [98].

2.9.5 Artificial membrane permeability assay

This experiment was carried out as previously described by Ward and co-workers [99].

2.9.6 CLND (Chemio Luminscent Nitrogen Detection)

5 mL of the stock solution in DMSO (10mM) were diluted to 100 mL using buffer phosphate solution at pH 7.4, then equilibrated for 1 hour at RT and filtrated through Millipore Multiscreen HTS-PCF (MSSL BPC). The volume of solvent necessary to dissolve the analysed compounds was measured through ChemioLuminescent Nitrogen Detection (CLND) [100].

2.9.7 %HSA (Percentage of Human Serum Albumin binding)

The assay uses an Agilent 1100 HPLC, a Chromtech HSA column 50x3.0 mm 5 micron, 50 mM ammonium acetate (pH7.4) as mobile phase A and 2-propanol as mobile phase B. 10 µL of 10mM DMSO stock solution of sample is diluted with 990 µL of 50:50 mobile phases A and B. The flow rate is 1.8mL/min at 30 °C with gradient of 0-3min 0-30%B, 3-5min 30%B, 5-5.1min 30-0% B, 5.1-6min 0% B. Injection volume 10 µL monitoring at 215 and 254nm. Retention time is then related to % HSA binding by relation to a set of 9 control standards with known binding affinities [101].

2.9.8 hERG activity assay

This experiment was carried out as previously described Chadwick and co-workers [102].

2.9.9 Dose-response studies in an acute murine infection TB model

This experiment was carried out as previously described by Rullas J. *et al*. Briefly, 8-10 week-old female C57BL/6 mice were intratracheally infected with 100.000 CFU/mouse (M. tuberculosis H37Rv strain). Products were administered for 4 consecutive days starting on day five after infection. Lungs were harvested on day nine (24 hours after the last administration). All lung lobes were aseptically removed, homogenized and frozen. Homogenates were plated in 10% OADC-7H11 medium for 14 days at 37 ºC [103].

Chapter 3. Novel inhibitors of tryptophan biosynthesis

3.1 State of the art

Several studies indicate that tryptophan (Trp) biosynthesis is crucial for mycobacteria survival during MTB infection. Inside the macrophage, the mycobacterial source of Trp is the cytoplasmic environment. When infected, macrophages are activated by T-cells and start to synthetize signalling molecules using the intracellular Trp. The intracellular depletion of Trp forces MTB to synthetize the amino acid, using the biosynthetic pathway reported in figure 29 [104, 105].

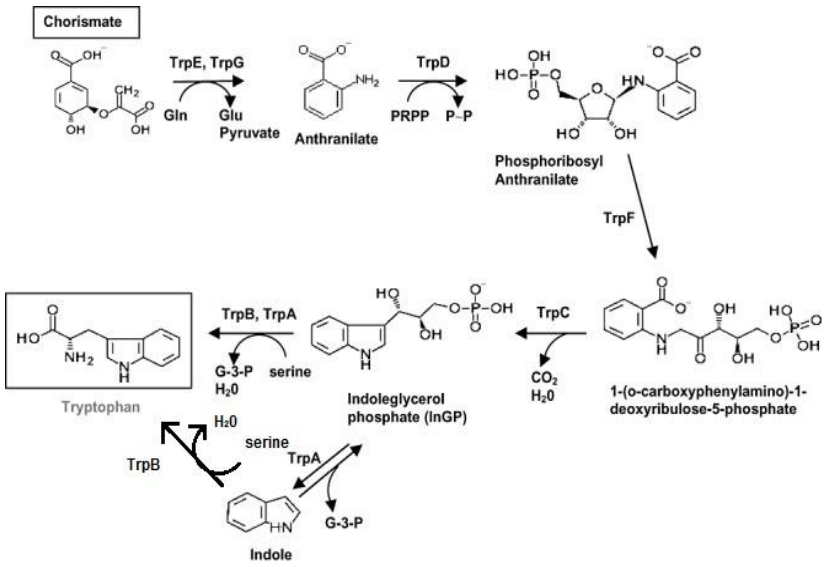

Figure 29. Adapted from *Microb Biotechnol*, **1**, 2009. Tryptophan biosynthetic pathway [106].

Therefore, the inhibition of Trp biosynthetic pathway could have a synergistic effect with the host immune response to eradicate MTB infection. Indeed, Trp auxotrophic

strains are unable to cause the disease both in immunocompetent and immunodeficient mice [104, 105]. Trp biosynthetic pathway is an interesting target for the development of anti-mycobacterial agents. Moreover, Trp biosynthesis inhibitors should have low toxicity, since Trp is an essential amino acid for humans.

In the past few years different research groups have identified inhibitors of Trp biosynthesis. Repurposing the chemical scaffold of the anti-arthritic lobenzarit, ACS172 (Fig. 30) was identified as the hit compound of a new class of anthranilate phosphor ribosyl transferase (AnPRT) inhibitors. The hit optimization led to the synthesis of the 2,6-bis-(2-carboxyphenylamino)-benzoate (Fig. 30), 40-fold more potent inhibitor than the original hit [107].

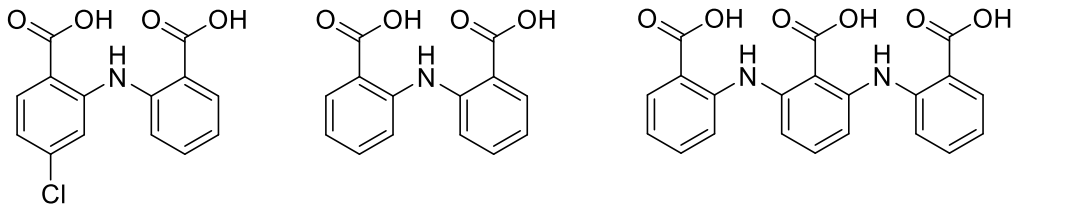

Figure 30. Chemical structures of lobenzarit, ACS172 and the 2,6-bis-(2-carboxyphenylamino)-benzoate.

A recent work by Abrahams and co-workers presented a series of sulfolanes and indoline-5-sulfonamides as promising *in vitro* anti-mycobacterial compounds (0.5 μM ≤ MIC ≤ 5.6 μM) [108]. Among them, compound 33 proved to be effective in reducing mycobacterial lung count in murine model of acute TB infection (Fig. 31) [108].

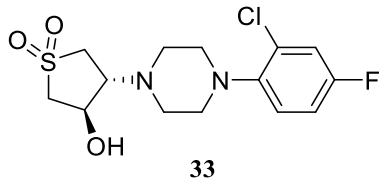

33

Figure 31. Chemical structures of sulfolane 33.

Target studies revealed tryptophan synthase (TrpAB) as the target of this class of compounds. TrpAB is a tetrameric enzyme (αββα) catalysing the last step of Trp biosynthesis.

Sulfolanes and indoline-5-sulfonamides inhibit TrpAB by targeting the interface between α and β subunits [108]. TrpAB is also the target of BRD4592 (2*R*,3*S*,4*R*)-3-(2′-fluoro-[1,1′-biphenyl]-4-yl)-4-(hydroxymethyl) azetidine-2-carbonitrile, a chiral azetidine derivative recently identified as antimycobacterial agent (Fig. 32) (MIC = 3 μM) [109].

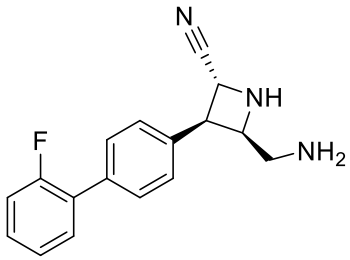

BRD4592

Figure 32. Chemical structure of BRD4592.

As well as the sulfolanes derivatives, BRD4592 is a TrpAB allosteric inhibitor, binding the subunits interface [109].

A 2-amino-6-fluoro benzoic acid (6-FABA) (Fig. 33) was identified by Zhang and co-workers as a new antimycobacterial agent (MIC= 5.0 μM), by screening of *P. aeruginosa* Trp biosynthesis inhibitors [104]. The loss of activity in the presence of Trp was consistent with the hypothesis that 6-FABA targets tryptophan biosynthesis in MTB (Fig. 34).

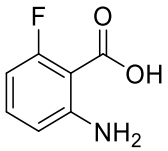

6-FABA

Figure 33. Chemical structure of 6-FABA.

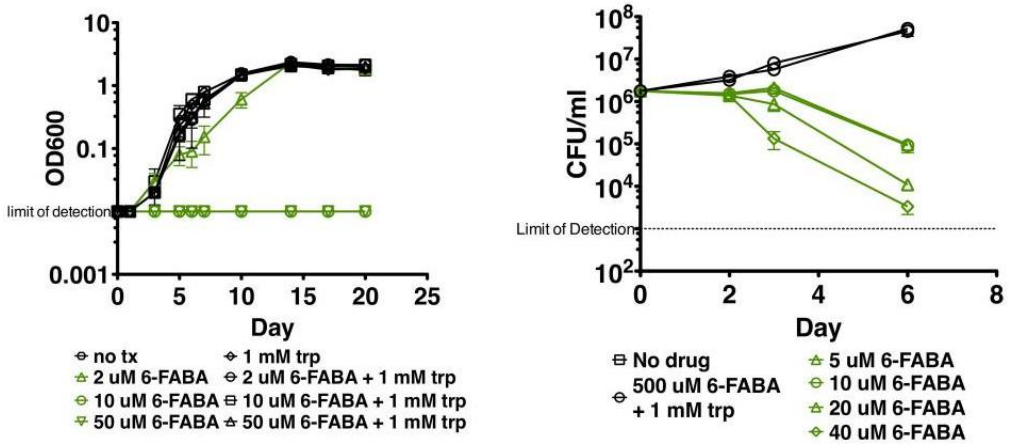

Figure 34. From *Cell*, **155**, 2013. 6-FABA inhibits the growth of MTB in 7H9 only in absence of tryptophan (left). To test the bactericidal potential of 6-FABA, wild type MTB was treated with 6-FABA in 7H9, and cultures were plated for CFU at various time points (right)[104].

Whole genome sequencing of *M. smegmatis* 6-FABA resistors revealed a mutation (F68I) in *trpE*, the gene encoding for Anthranilate Synthase (AnS). The mutation is located into the Trp binding pocket for the negative feedback regulation. The mutant AnS is a hypermorphic enzyme, less responsive to Trp allosteric inhibition. Zhang *et al.* speculated that 6-FABA activity is related to the formation of toxic metabolites that poisoned the biosynthetic pathway [104]. This hypothesis was supported by Cookson and co-workers with kinetic and molecular modelling studies about AnPRT[110]. AnPRT is the enzyme that catalyzes the second step of Trp biosynthesis: the reaction between 5′-phosphoribosyl-1′-pyrophosphate (PRPP) and anthranilate to obtain N-(5′-phosphoribosyl)-anthranilate (PRA) and pyrophosphate (PPi) (Fig. 35) [111].

Figure 35. From *Biochemistry*, **54**, 2015. Reaction catalyzed by AnPRT [111].

Anthranilate has three distinct binding sites in AnPRT, an inner catalytic one (S1) and an outer substrate-capture one (S3), and an intermediate binding site (S2) (Fig. 36) [110].

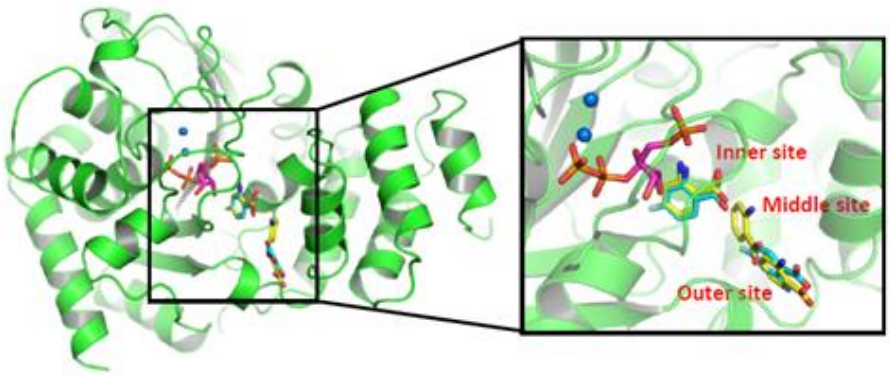

Figure 36. From *Biochem. J.*, **461**, 2014. The three anthranilate binding sites within *M. tuberculosis* AnPRT: wild-type AnPRT (green) with PRPP (magenta), Mg^{2+} (blue shere) and anthranilate (yellow) [110].

Because 6-FABA showed similar kinetic parameters to those of anthranilate, it was speculated that besides binding into S1, acting as substrate of AnPRT, it could also

bind S3 site miming the substrate inhibition. Thus, 6-FABA' anti-mycobacterial activity could be linked to toxicity of fluorinated intermediates generated by the turnover of MTB-AnPRT and the following pathway enzymes [110].

Furthermore, 6-FABA and 6-FABA ethyl ester showed to be effective against MTB in *in vivo* studies. After a preliminary 5 days *in vivo* tolerability trial, the efficacy of 6-FABA and its ethyl ester was evaluated in an *in vivo* murine model of acute TB infection. Unfortunately, 6-FABA caused death in 50% treated mice within 4 weeks probably due to a possible interaction between 6-FABA and the anaesthesia used during the experiment. On the contrary, the ester derivative of 6-FABA (Fig. 37) did not show toxicity, even though it releases the same amount of 6-FABA in mouse serum. After 2 weeks of treatment, 6-FABA and its ester showed to induce a significant reduction in the mycobacterial count in mouse spleens. The ester continued to decrease spleen and lungs mycobacterial growth in the following two weeks [104].

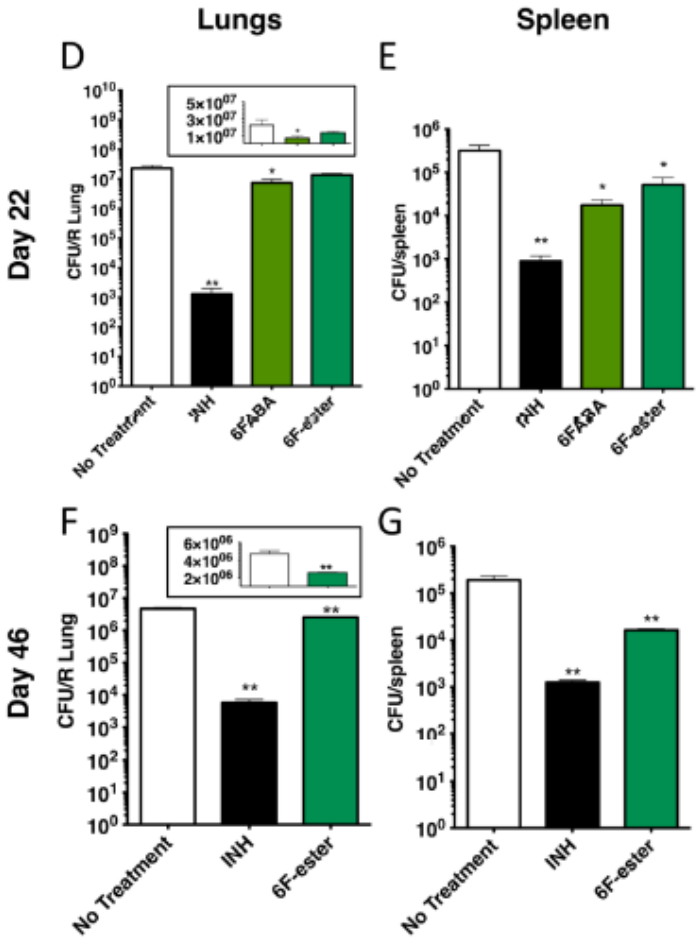

Figure 37. From *Cell*, 155, 2013. Mice were infected with 10^2 aerosolized MTB bacilli. After 8 days of infection, mice were treated with INH (25 mg/kg), 6-FABA (200 mg/kg) or with the ester derivative of 6-FABA (200 mg/kg). At 2 weeks (D and E) and 4 weeks (F and G) after infection, lungs and spleens were homogenized and plated for CFU [104].

3.2 Rationale and aims of the project

The second part of my PhD thesis concerned the development of new 6-FABA derivatives (**34-76**). Since 6-FABA and its ester exhibited good *in vitro* and *in vivo* activity against MTB, different sets of modifications were introduced, to meet the following goals:

- improve the safety profile of 6-FABA,
- improve drug-like properties of 6-FABA ethyl ester.

In detail, first we focused our attention on the carboxylic group. The carboxylic functional group is often associated to idiosyncratic drug toxicity. Carboxylate toxicity is related to the rearrangement of acyl glucuronide conjugates that could produce chemically reactive species *in vivo* [112]. Moreover, carboxylic acids can generate CoA esters, electrophilic species that could be a source of toxicity [113]. To avoid the *in vivo* toxicity caused by the metabolism of the carboxylic group, a series of new 6-FABA derivatives (**34-38**) were designed and synthetized. The carboxylic functional group was replaced with the following isosteric and bioisosteric groups (Fig. 38):

- *Hydroxamic acid and hydroxamic ester*: Barrett *et al.* identified benzohydroxamic acid and esters as excellent bioisosteres of anthranilic acids. Those substituents are more resistant to metabolic processes and can improve water solubility [114]. Therefore, 6-FABA hydroxamic acids and esters were synthetized (**34-35**).
- *Heterocycles.* The most common heterocycles used as carboxylate bioisosteres were incorporated: oxadiazoles and tetrazole (**36-38**) [115, 116]. Indeed, oxadiazoles and tetrazole display both acidity and planarity comparable to those of carboxylic acid, but they are metabolically stable. In contrast to carboxylic acid

metabolism, tetrazole undergoes *N*-glucuronidation, generating no reactive adducts [117].

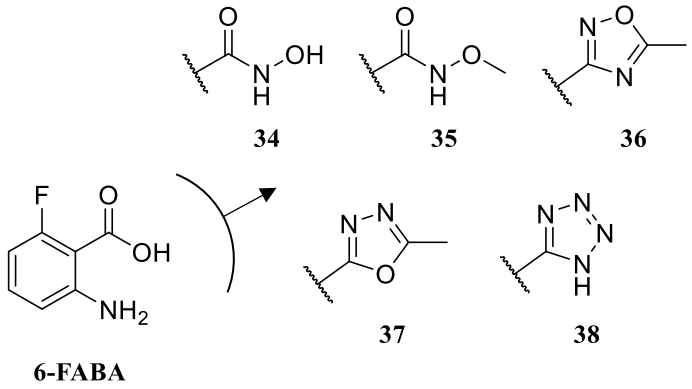

Figure 38. Chemical structures of compounds **34-38**.

The carboxylic acid esterification is a common strategy to prepare a prodrug, improving the physicochemical properties of the parent compound. However, the rapid ester hydrolysis operated by esterase could release an excessive amount of 6-FABA in the serum, causing toxic effects linked to the free acid functional group.

To avoid the rapid *in vivo* cleavage of 6-FABA ethyl ester and the resulting metabolic issues, the ester group was replaced with the following isosteres [118]:

- *Amides* (**39-50**) (Fig. 39). Amides are classical ester isosteres endowed with an enhanced stability to metabolic processes. In particular, amides are more resistant to hydrolysis than esters. Other than the primary amide **39**, isopropyl-, cyclopropyl-, cyclobutyl-, cyclohexyl-, pirrolidinyl-, piperidinyl- and *p*-fluorophenyl amides

(**40**, **42-44**, **46**, **47** and **50**) were prepared. Moreover, to maintain the right polarity/lipophilicity balance, amines containing additional heteroatoms (morpholine, *N*-methyl piperazine, 3-methoxypiperidine, ethanol amine) (**41**, **45**, **48** and **49**) were used.

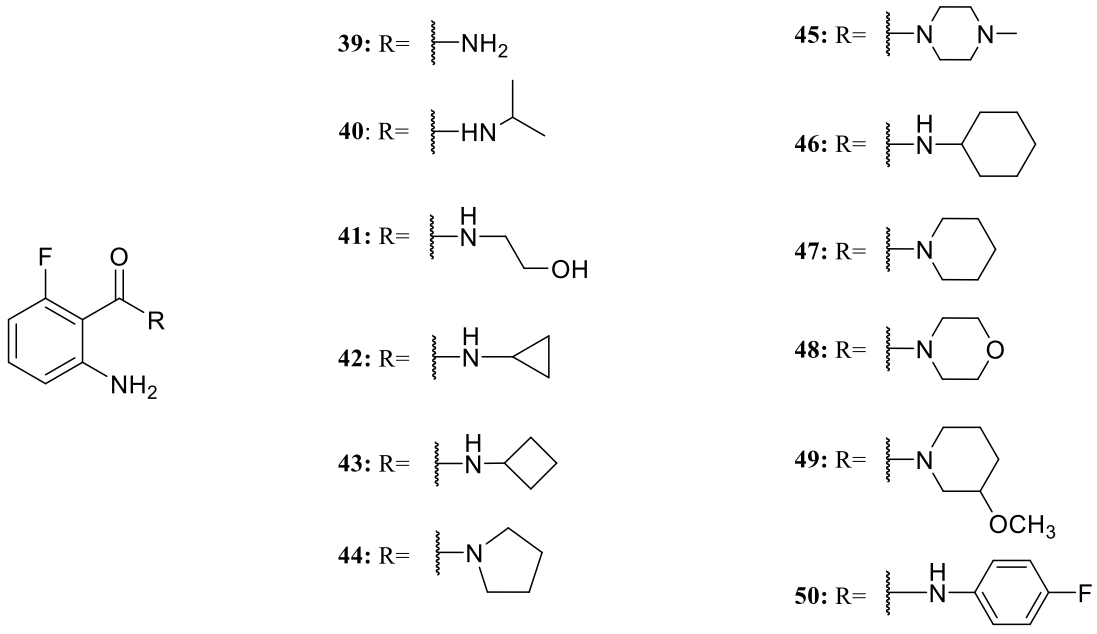

Figure 39. Chemical structures of amides **39-50.**

- *Hydrazides* (**51-73**) Hydrazides are amide bioisosteres characterized by a higher polarity than amides, due to the presence of an additional nitrogen atom (Fig. 40). Several hydrazides were synthetized, including the unsubstituted one (**51**). Derivatives **53-73** were obtained by decorating the nitrogen with either cycloalkyl groups (**53**) or aromatic rings decorated with both electron withdrawing substituents

(halogens, trifluoro methyl and nitro groups) (**55-59**, **68-71**) and electron donator substituents (methoxy group) (**67**). To investigate the influence of the substituent positions, multiple substituted aromatic hydrazides were synthetized (**60-65**, **71**). Moreover, some aryl hydrazide hydrochlorides were prepared, to obtain an improved aqueous solubility useful in biological assays (**72-73**).

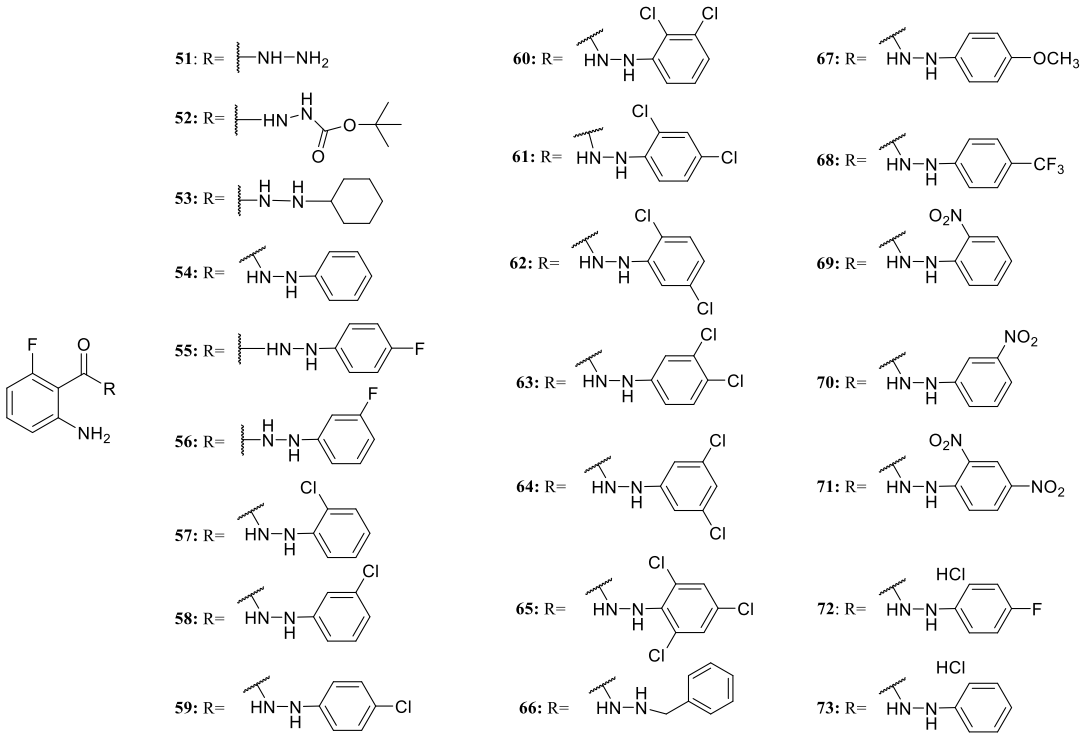

Figure 40. Chemical structures of hydrazides **51-73**.

- *Trifluoromethyl amines* (**74-76**). Black and co-workers showed that the carbonyl group of amides can be replaced by the trifluoromethyl one generating a metabolically stable, non-basic amine, maintaining the ability to form hydrogen bond (Fig. 41) [119].Therefore a small set of trifluoromethyl amines were prepared,

using amines having different basicity: the polar cycloalkyl amines morpholine and thiomorpholine (**74-75**), and the aryl amine *p*-fluorophenyl aniline (**76**).

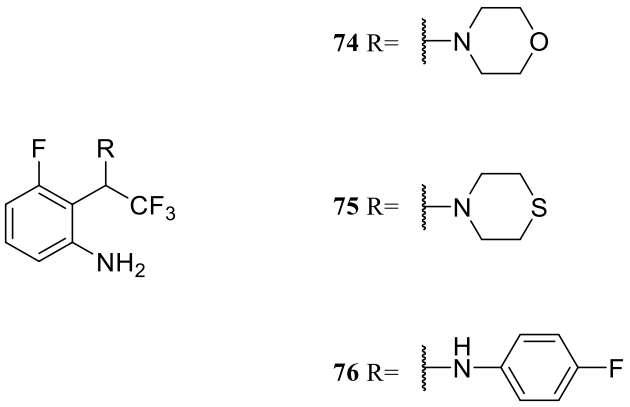

Figure 41. Chemical structures of trifluoromethyl amines **74-76**.

3.3 Chemistry

3.3.1 Preparation of hydroxamic acid and ester 34 and 35

Compounds **34** and **35** were prepared as shown in Scheme 2. 6-FABA was activated with 1,1'-carbonyldiimidazole (**77**) to achieve the isatoic anhydride **78** [120], which was in turn coupled with the suitable hydroxylamine to afford the corresponding final compounds **34** and **35**.

Scheme 2. Synthetic pathway for compounds **34** and **35.**

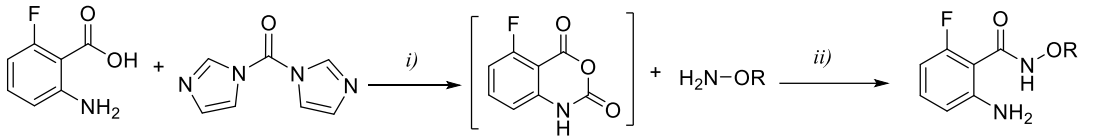

6-FABA **77** **78** **79 a-b** **34: R= H; 35: R= CH_3**

Reagents and conditions*: i)* THF, rt, 24 h; *ii)* THF, rt, 15h, yield 23-26%.

3.3.2 Preparation of 1,2,4-oxadiazole 36.

Compound **36** was obtained as reported in Scheme 3. Briefly, the reaction between the 2-amino-6-fluoro benzonitrile **80** and hydroxylamine hydrochloride (**81**) in basic conditions led to the formation of amidoxime **82.** The latter was then cyclized by using *tert*-butyl acetate (**83**) to afford compound **36** [121]**.**

Scheme 3. Synthetic pathway for compound **36.**

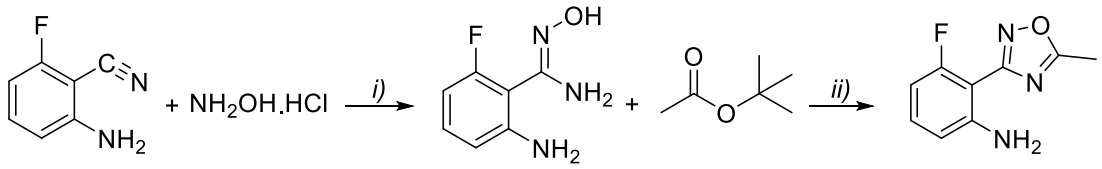

80 **81** **82** **83** **36**

Reagents and conditions: *i)* KOH, MeOH, 90 °C, 24 h, yield 68%; *ii)* *t*-BuOK, *t*-BuOH, 100 °C, 1.5 h, yield 55%.

3.3.3 Preparation of 1,3,4-oxadiazole 37.

Compounds **51, 52** and **37** were synthetized as reported in Scheme 4. Compound **52** was obtained by activating 6-FABA to isatoic anhydride **78** [120], which was then coupled with *t*-butyl carbazate. The deprotection of **52** with trifluoroacetic acid gave hydrazide **51,** which was then cyclized with triethyl orthoacetate (**84**) to achieve the oxadiazole derivative **37** [122].

Scheme 4. Synthetic pathway for compounds **51**, **52** and **37.**

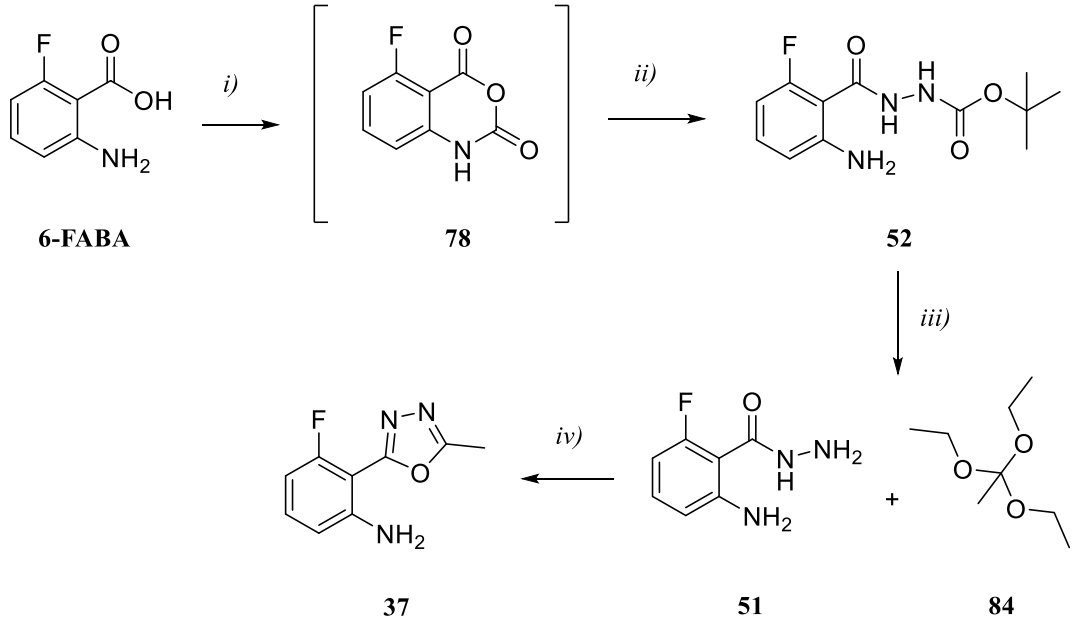

Reagents and conditions: *i)* 1,1'-carbonyldiimidazole, THF, rt, 24h; *ii*) *t*-butyl carbazate, THF, 80 °C, 15h, yield 64%; *iii)* TFA, DCM, rt, 30 min, yield >90%, *iv)* dioxane, 100 °C, 24 h, yield 24%.

3.3.4 Preparation of tetrazole 38.

Tetrazole **38** was obtained in one step from the cyclization of 2-amino-6-fluoro benzonitrile **80** with sodium azide (Scheme 5) [123].

Scheme 5. Synthetic pathway for compound **38.**

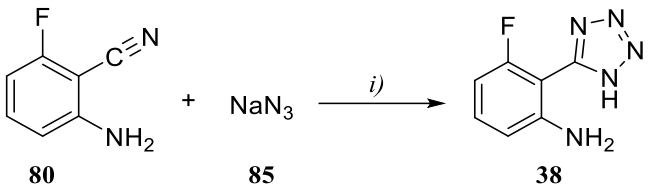

80 **85** **38**

Reagents and conditions: *i)* NH_4Cl, DMF, 120 °C, 24 h, yield 24%.

3.3.5 Preparation of amides and hydrazides 39-50, 53-73.

The general procedure for the preparation of derivatives **39-50, 53-73** is depicted in Scheme 6. Briefly, as previously reported for derivatives **34** and **35**, 6-FABA was activated with 1,1'-carbonyldiimidazole (**77**) to obtain the isatoic anhydride **78** [120]. The isatoic anhydride **78** was coupled with the suitable amine or hydrazine to give the corresponding amide or hydrazide **39-50, 53-71** [124]. The hydrochloride salts **72** and **73** were prepared from **54** and **55** by treatment with concentrated hydrochloric acid.

Scheme 6. Synthetic pathway for compounds **39-50, 53-73.**

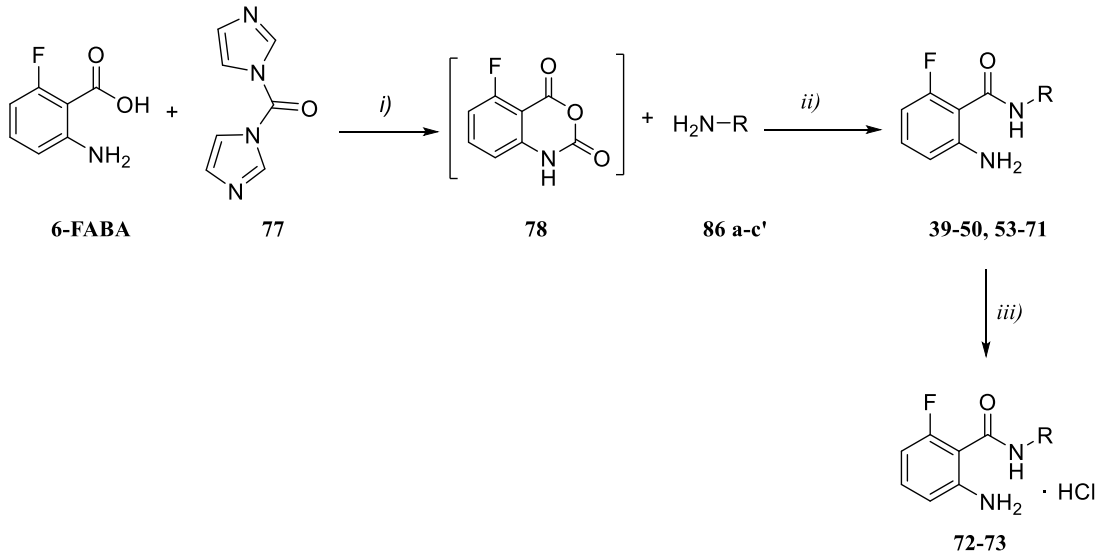

***Reagents and conditions**: i)* THF, rt, 24 h; *ii)* THF, rt, 15h, yield 13-70%; *iii)* HCl 37%, ethanol, rt, 30 min, yield 21-25%.

3.3.6 Preparation of trifluoromethyl amines 74-76

The trifluoromethyl amines **74-76** were obtained as shown in Scheme 7. Starting from the benzyl bromide **87**, the benzyl alcohol **88** was prepared by nucleophilic substitution in basic conditions [125]. Then, alcohol **88** was oxidized to the corresponding aldehyde **89**, which was used to synthetize the trifluoromethyl benzyl alcohol **90** [126]. The hydroxyl group was transformed into the correspondent trifluoromethyl sulphonate **91,** to promote the further reaction with the appropriate amine and formation of intermediates **92 a-c** [127]. Finally, the nitro group was reduced with nickel chloride and sodium borohydride to give the final compounds **74-76** [128].

Scheme 7. Synthetic pathway for compounds **74-76.**

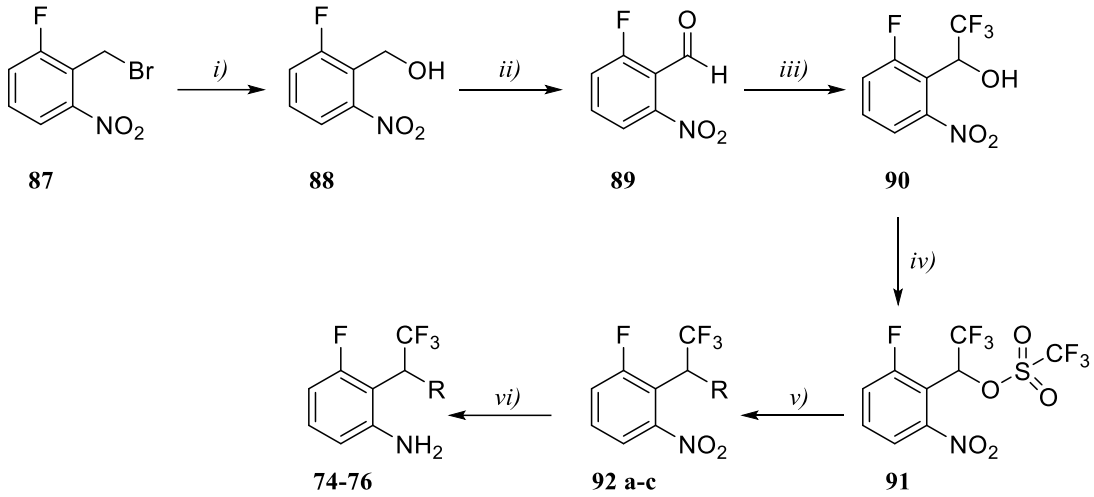

Reagents and conditions: *i)* $CaCO_3$, DCM, reflux, 16h, 75% yield; *ii*) Dess-Martin, DCM, 0 °C, 30 min, 55% yield*; iii)* $(CH_3)_3SiCF_3$, THF, 0 °C, 1h, 35% yield*; iv)* $(CF_3)(SO_2)_2O$, DCM, 0 °C, 3h, 30% yield; *v)* Amine, K_2CO_3, DCM, reflux, 16h, 43% yield*; vi)* $NiCl_2(6H_2O)$, $NaBH_4$, DCM, rt, 30 min, 60% yield.

3.4 *In vitro* assessment of derivatives 34-76.

MIC against MTB H37Rv of compounds **34-76** was evaluated *in vitro* by Doctor Helena Boshoff at the National Institute of Health, Bethesda. Three different media were used: Middlebrook 7H9/ADC/Tween 80, Gast Fe and Middlebrook 7H9/DPPC/casitone/ Tyloxapol (Tx) (Tab. 8). The main difference between the media is the presence of bovine serum albumin (BSA). Unlike the Middlebrook 7H9/ADC/Tw, Gast Fe and Middlebrook 7H9/DPPC/casitone/Tyloxapol media do not contain BSA. As reported in previous studies, BSA could have a negative effect on *in vitro* activity of drugs, due to a possible drug-BSA binding that could reduce the concentration of free drug in the medium [129]. Furthermore, Middlebrook 7H9/DPPC/casitone/Tx medium contains dipalmitoyl phosphatidyl choline as carbon source, whereas the other two media contain glucose.

Cytotoxicity against Vero cells was performed by Professor De Logu at the University of Cagliari. The cytotoxicity of derivatives **53**, **55-60**, **62, 65**, **70**, **73-76** was assessed by measuring the concentration of compound that causes a cytotoxic effect (CC_{50}) in 50% of treated Vero cells (Tab. 9).

Table 8. Minimum Inhibitory Concentration against 99% of MTB H37Rv in 7H9/ADC/Tween 80, GastFe, 7H9/ADC/casitone/ Tx after 1 week and 2 weeks of compounds **34-76** and 6-FABA**.**

Compound	MIC_{99} 7H9/ADC/Tw 1 week (µM)[a]	MIC_{99} 7H9/ADC/Tw 2 weeks (µM)[b]	MIC_{99} GastFe 1 week (µM)[c]	MIC_{99} GastFe 2 weeks (µM)[d]	MIC_{99} 7H9/DPPC/ casitone/Tx 1 week (µM)[e]	MIC_{99} 7H9/DPPC/ casitone/Tx 2 weeks (µM)[f]
34	>50	>50	>50	>50	n.t.[i]	n.t.[l]
35	>50	>50	>50	>50	n.t.[i]	n.t.[l]
36	>50	>50	>50	>50	n.t.[i]	n.t.[l]
37	>50	>50	>50	>50	n.t.[i]	n.t.[l]
38	>50	>50	>50	>50	n.t.[i]	n.t.[l]
39	>50	>50	>50	>50	n.t.[i]	n.t.[l]
40	>50	>50	>50	>50	n.t.[i]	n.t.[l]
41	>50	>50	>50	>50	n.t.[i]	n.t.[l]
42	>50	>50	>50	>50	n.t.[i]	n.t.[l]
43	>50	>50	>50	>50	n.t.[i]	n.t.[l]
44	>50	>50	>50	>50	n.t.[i]	n.t.[l]
45	>50	>50	>50	>50	n.t.[i]	n.t.[l]
46	>50	>50	>50	>50	n.t.[i]	n.t.[l]
47	>50	>50	>50	>50	n.t.[i]	n.t.[l]
48	>50	>50	>50	>50	n.t.[i]	n.t.[l]
49	>50	>50	>50	>50	n.t.[i]	n.t.[l]
50	>50	>50	>50	>50	n.t.[i]	n.t.[l]
51	>50	>50	>50	>50	n.t.[i]	n.t.[l]
52	>50	>50	>50	>50	n.t.[i]	n.t.[l]
53	37	50	9.4	9.4	9.4	12.5
54	45.45	22.72	11.36	11.36	1.42	0.71
55	12.5	9.4	1.56	2.3	1.56	2.3
56	12.5	6.25	1.56	0.78	1.56	0.78
57	25	6.25	3.125	3.125	3.125	0.78
58	25	6.25	6.25	3.125	1.56	0.39
59	12.5	6.25	3.125	1.56	0.78	0.19
60	>50	50	12.5	12.5	6.25	1.56

61	50	12.5	6.5	3.125	3.125	0.39
62	>50	>50	25	12.5	6.25	1.56
63	25	25	12.5	12.5	1.56	1.56
64	50	>50	25	25	6.25	6.25
65	5	5	1.25	1.25	0.625	0.3125
66	>50	>50	50	>50	50	25
67	12.5	3.125	0.78	0.39	1.56	0.19
68	45.45	22.72	11.36	11.36	1.42	0.71
69	>50	>50	>50	50	25	25
70	>50	>50	25	25	6.25	6.25
71	>50	>50	>50	>50	>50	>50
72	10.43	1.56	2.6	2.6	1.3	1.3
73	11	1.56	2.77	1.4	2.77	1.4
74	>50	n.t.[g]	>50	n.t.[h]	>50	n.t.[l]
75	>50	n.t.[g]	>50	n.t.[h]	>50	n.t.[l]
76	>50	n.t.[g]	>50	n.t.[h]	>50	n.t.[l]
6-FABA	5.0	n.t.[g]	5.0	n.t.[h]	n.t.[i]	n.t.[l]

[a]activity against MTB H37Rv in 7H9/ADC/Tween80 medium after 1 week.
[b]activity against MTB H37Rv in 7H9/ADC/Tween80 medium after 2 weeks.
[c]activity against MTB H37Rv in GastFe medium after 1 week.
[d]activity against MTB H37Rv in GastFe medium after 2 weeks.
[e]activity against MTB H37Rv in 7H9/DPPC/casitone/Tyloxapol medium after 1 week.
[f]activity against MTB H37Rv in 7H9/DPPC/casitone/Tyloxapol medium after 2 weeks.
[g]not tested.
[h]not tested.
[i]not tested.
[l]not tested.

Table 9. Cytotoxic Concentration in 50% of Vero Cells (CC_{50}) of compound **53-60**, **62**, **65**, **70**, **73-76**.

Compound	CC_{50} Vero cells (μM)[a]
53	909
54	2027
55	1360
56	1364
57	789
58	>1800
59	373
60	>1800
62	>1800
65	>1800
70	1304
73	>1800
74	769.5
75	178.6
76	155.5

[a]cytotoxicity in Vero cells.

3.5 Discussion

Among the 6-FABA derivatives, compounds **53-65**, **67**, **68**, **70**, **72** and **73** retained the antimycobacterial activity, providing good results especially in the Middlebrook 7H9/casitone/Tx medium (0.625 μM ≤ MIC ≤ 9.4 μM). The replacement of the carboxylic functional group with either the hydroxamic acid or the ester group (**34-35**, MIC > 50 μM) or the heterocyclic moieties (**36-38**, MIC > 50 μM) led to inactive compounds. A similar trend was observed when replacing the ester functional group with both amides (**39-50**) and trifluoromethyl amines (**74-76**) (MIC > 50 μM in all media), whereas several hydrazides (**54-63**, **67, 68, 72, 73**) provided good activities against MTB (Tab. 8). As expected, we obtained better results in cultures grown in both Middlebrook 7H9/DPPC/casitone/Tx and Gast Fe than those run in the Middlebrook 7H9/ADC/Tw one. This trend seems to confirm the negative impact of BSA on the hydrazides anti-mycobacterial activity. The significant lipophilicity of aryl hydrazides could promote the interaction with BSA, increasing the binding affinity [129]. Among the hydrazide derivatives **54-73**, the aromatic ones showed good activities (MIC ≤ 6.25 μM, 7H9/DPPC/casitone/Tx). To date, no significant correlation between electronic effects of substituents on hydrazide phenyl ring and activity was observed in Middlebrook 7H9/DPPC/casitone/Tx medium. Compounds substituted with electron withdrawing groups (**55, 5<9, 68**) and electron donating groups (**67**) at C4' showed the same range of MIC values (0.78 μM ≤MIC ≤1.56 μM). As general trend, *para*- (**55, 59, 67, 68**) and *meta*- (**56, 58**) (0.78 μM ≤MIC ≤1.56 μM, 7H9/DPPC/casitone/Tx) mono-substituted phenyl hydrazides proved to be more active than the o*rtho*-substituted one (**57**) (MIC = 3.125 μM, 7H9/DPPC/casitone/Tx). Moreover, multiple substitutions on the phenyl ring seem to affect negatively the activity (3.125 μM ≤ MIC≤ 6.25 μM, 7H9/DPPC/casitone/Tx μM, MIC≥ 6.5, GastFe),

except for **65** that display good MIC values in GastFe (MIC= 1.25 μM) and in 7H9/DPPC/casitone/Tx (MIC= 0.625 μM) media.

As documented for INH, the hydrazide moiety is often cause of toxicity, due to the production of radical species. Surprisingly, aryl hydrazides **54, 55, 65, 67, 72** and **73** provided outstanding values of cytotoxicity ($CC_{50} \geq$ 1360 μM) (Tab. 9). It could be explained because of an improved stability to oxidative process, due to the presence of a substituent linked to the hydrazide nitrogen.

3.6 Elimination of amino group: the 2-fluorobenzohydrazide series

3.6.1 Rationale

Considering the structural similarities between compounds **54, 5, 67, 68** and BRD4592 [109], the second step of this project was focused on evaluating the importance of the C2 amino group on the activity. Starting from the chemical scaffold of **53-55**, **67-68** hydrazides, a small set of 2-fluorobenzohydrazides were prepared and tested (**93-98**) (Fig. 42). Hydrazides **53-55**, **67**, **68** were selected based on the results of the previous series, to investigate differences in SARs.

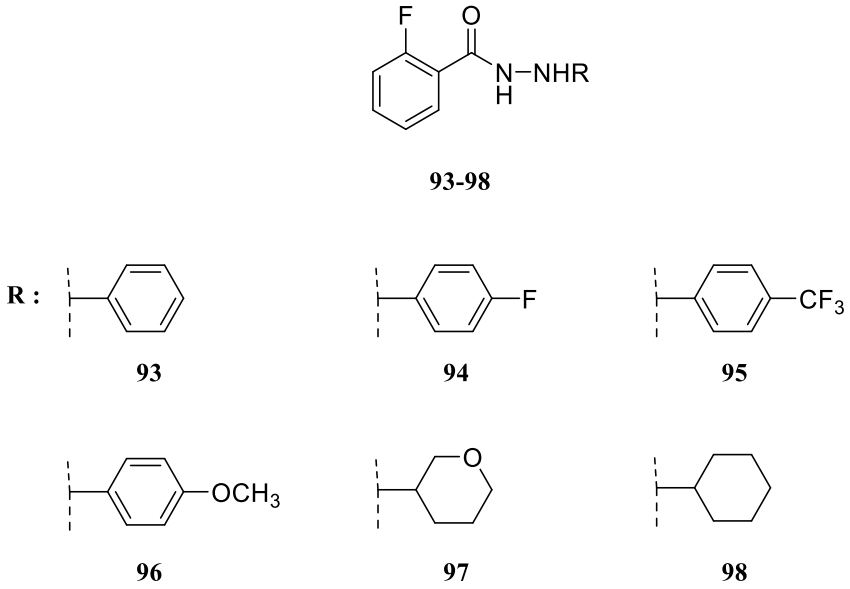

Figure 42. Chemical structures of 2-fluorobenzohydrazides **93-98**.

3.6.2 Chemistry

*3.6.2.1 Preparation of 2-fluorobenzohydrazides **93-98***

The procedure for the synthesis of derivatives **93-98** is reported in Scheme 8. Briefly, 2-fluorobenzaldehyde **99** was oxidized with Oxone [130] and the obtained acid **100** was activated by reaction with *N*-hydroxysuccinimide. Then, the activated acid **101** was coupled with the appropriate hydrazine to give the final 2-fluoro benzohydrazides **93-98**.

Scheme 8. Synthetic pathway for compounds **93-98.**

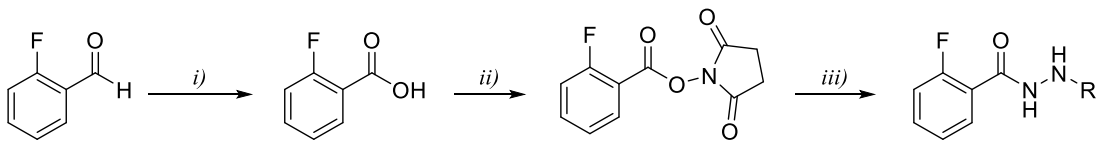

99 **100** **101** **93-98**

Reagents and conditions: *i)* Oxone, DMF, rt, 3h, yield 96%, *ii) N*-hydroxysuccinimide, THF, rt, 6h, 75% yield; *iii)* hydrazine, THF, rt, 16h, 17-25% yield.

3.6.3 In vitro assessment 2-fluorobenzohydrazides 93-98

Compounds **93-98** were evaluated *in vitro* to determine MIC against MTB H37Rv (Tab. 10) by the research group of Professor Rubin, using the same conditions seen for compounds **34-76.** In addition, Professor De Logu assessed the cytotoxicity (CC_{50}) against Vero cells (Tab. 11).

Table 10. Minimum Inhibitory Concentration against 99% of MTB H37Rv in 7H9/ADC/Tween 80, GastFe, 7H9/ADC/casitone/ Tyloxapol after 1 week of treatment of compounds **93-98** and 6-FABA**.**

Compound	MIC_{99} 7H9/ADC/Tw 1 week (µM)[a]	MIC_{99} GastFe 1 week (µM)[b]	MIC_{99} 7H9/DPPC/casitone/Tx 1 week (µM)[c]
93	>50	>50	8.7
94	>50	>50	2.0
95	>50	>50	1.68
96	>50	>50	8.5
97	>50	>50	>50
98	>50	>50	>50
6-FABA	5.0	5.0	n.t[d]

[a]activity against MTB H37Rv in 7H9/ADC/Tween80 medium after 1 week.
[b]activity against MTB H37Rv in GastFe medium after 1 week.
[c]activity against MTB H37Rv in 7H9/DPPC/casitone/Tyloxapol medium after 1 week.
[d]not tested.

Table 11. Cytotoxic Concentrations in 50% of Vero Cells (CC_{50}) of compounds **93-98**.

Compound	CC_{50} Vero cells (μM)[a]
93	2172
94	2014
95	1676
96	1002
97	2098
98	1398

[a]cytotoxicity in Vero cells.

3.6.4 Discussion

Compounds **93-98** retained the activity in Middlebrook 7H9/DPPC/casitone/Tw medium (1.68 μM ≤ MIC ≤ 8.7 μM), proving that the amino group at C2 is not essential for the activity. As observed in the previous series of hydrazides, aryl hydrazides (**93-96**) are more active than the cycloalkyl ones (**97** and **98)**. Moreover, the removal of the amino group at C2 did not affect the cytotoxicity (CC_{50} ≥1002 μM).

3.7 Preliminary target studies

Once the promising activity- toxicity profiles of this new class of anti-mycobacterial compounds were assessed, my PhD project turned on studying both the target and the mechanism of action of this new class of compounds and I moved to the research group of Prof Eric J. Rubin at the Harvard School of Public Health. Two different hypotheses of target were considered:

- *Trp biosynthetic pathway.* As speculated for 6-FABA, the aryl hydrazides could inhibit tryptophan biosynthesis. Therefore, hydrazide activities in the presence of Trp and its main biosynthesis precursors were determined. Then hydrazides resistant mutants were generated, to explore the resistance mechanism linked to target gene mutations.
- *Mycolic acid biosynthesis.* Because of the presence of the hydrazide moiety, the aryl hydrazides could have the same mechanism of action of INH. They could be activated by the catalase peroxidase KatG and inhibit the mycolic acid biosynthesis. Therefore, a preliminary synergy test was performed to assess the possible antagonism between INH and **54, 65** and **73**. In addition, the *in vitro* efficacy of **54** and **73** against BCG INH resistors was evaluated.

3.7.1 Compound 54, 65 and 73 susceptibility tests in presence of Trp and Trp biosynthesis intermediates.

To investigate the hypothesis of the inhibition of the Trp biosynthesis, the activity of 6-FABA and derivatives **54, 65** and **73** was evaluated in presence of Trp and its principal precursors: chorismate, anthranilate and indole (Tab. 12). A concentration 0.1 mM of each precursor was added to the Middlebrook 7H9/ADC/Tw medium. All the compounds proved to be inactive when Trp, anthranilate and indole were added to the medium. Since 6-FABA and the hydrazides retained the activity against BCG in presence of 0.1 mM chorismate, the susceptibility test was repeated increasing the concentration of chorismate (0.5 mM) in the medium (Tab. 13). Compounds **54, 65** and **73** and 6-FABA proved to be active.

Table 12. MICs of **54, 65** and **73** and 6-FABA against BCG in 7H9/ADC/Tw, in 7H9/ADC/Tw + chorismate 0.1 mM, in 7H9/ADC/Tw + sodium anthranilate 0.1 mM, in 7H9/ADC/Tw + indole 0.1 mM, in 7H9/ADC/Tw + Trp 0.1 mM.

	MIC BCG (µM) 1 week				
Comp	**7H9/ADC/Tw[a]**	**7H9/ADC/Tw + 0.1 mM chorismate[b]**	**7H9/ADC/Tw +0.1 mM sodium anthranilate[c]**	**7H9/ADC/Tw + 0.1 mM indole[d]**	**7H9/ADC/Tw + 0.1 mM Trp[e]**
54	2.0	8.15	> 50	> 50	>50
65	22.9	45.9	> 50	> 50	>50
73	3.5	7.1-14.2	> 50	> 50	>50
6-FABA	6.4	6.4	> 50	> 50	>50

[a]activity against *M. bovis* BCG in 7H9/ADC/Tween80 medium after 1week of treatment.
[b]activity against *M. bovis* BCG in 7H9/ADC/Tween80 medium added with chorismate 0.1 mM after 1week of treatment.
[c]activity against *M. bovis* BCG in 7H9/ADC/Tween80 medium added with anthranilate 0.1 mM after 1week of treatment.

[d]activity against *M. bovis* BCG in 7H9/ADC/Tween80 medium added with indole 0.1 mM after 1week of treatment.
[e]activity against *M. bovis* BCG in 7H9/ADC/Tween80 medium added with Trp 0.1 mM after 1week of treatment.

Table 13. MICs of **54**, **65**, **73** and 6-FABA MICs against BCG in 7H9/ADC/Tw and 7H9/ADC/Tw + chorismate 0.5 mM.

Compound	BCG MIC 7H9/ADC/Tw[a]	BCG MIC 7H9/ADC/Tw+ 0.5 mM chorismate[b]
54	1.0-2.0	8.15
65	22.9-45.9	45.9
73	3.5-7-1	14.2
6-FABA	6.4	6.4

[a]activity against *M. bovis* BCG in 7H9/ADC/Tween80 medium after 1week of treatment.
[b]activity against *M. bovis* BCG in 7H9/ADC/Tween80 medium added with chorismate 0.1 mM after 1week of treatment.

3.7.2 Compound 73 BCG resistant mutants

Compound **73** was chosen for the isolation and characterization of *M. bovis* BCG resistant mutants. Mycobacterial cultures (OD_{600}= 0.4-0.5) were plated onto solid media containing concentrations 3, 5, 10 times the MIC of compound **73** (Tab. 12). Different resistor colonies were isolated with a frequency approximately of $3x10^{-4}$. All the resistant mutants showed to lose susceptibility to **73**, with MICs 7-fold higher than to the wild type (Tab. 14). Moreover, 6-FABA exhibited a lower activity on **73** resistant compared to those of the wild type. The genomic DNA of each resistors was extracted and sent for the whole genome sequencing (WGS), but unfortunately the data are not available yet.

Table 14. Compound **73** BCG resistant mutants: colony number on the plate, **73** concentrations on the plate, **73** MIC (µM), 6-FABA MIC (µM) against the resistors and the wild type.

Colony n.[a]	**73 concentration**[b]	**73 MIC (µM)**[c]	**6-FABA MIC (µM)**[d]
1	x3 MIC	n.t.[e]	n.t.[f]
1	x5 MIC	>50	103
2	x5 MIC	56.7	25.8
3	x5 MIC	>50	51.5-103
4	x5 MIC	>50	103
1	x10 MIC	>50	51.5
2	x10 MIC	>50	103
Wt	-	7.1	6.4

[a]number of colony on the plate.
[b]concentration of compound 73 into the medium.
[c]activity of compound 73 against *M. bovis* BCG 73 resistant mutants.
[d]activity of 6-FABA against *M. bovis* BCG 73 resistant mutants.
[e]not tested.
[f]not tested.

3.7.3 6-FABA BCG resistant mutants

Based on the observation of a possible cross-resistance between **73** and 6-FABA, 6-FABA resistant mutants were generated to assess the activity of **73** against 6-FABA resistors. Mycobacterial cultures (OD_{600}= 0.4-0.5) were plated onto solid media containing concentrations 5, 10, 20 times the MIC of 6-FABA (Tab. 15). Resistors showing MICs 15-folds higher than the wild type strain were selected (Tab. 15). All the selected strains showed to be less sensitive to **73**, compared to the wild type, confirming the cross-resistance.

Table 15. 6-FABA BCG resistant mutants: colony number on the plate, 6-FABA concentrations in the medium, 6-FABA MIC (µM), **73** MIC (µM) against the resistors and the wild type.

Colony n.	6-FABA concentration	6-FABA MIC (µM)	73 MIC (µM)
1	x5 MIC	103	>50
1	x10 MIC	103	>50
1	x20 MIC	>103	>50
2	x20 MIC	>103	>50
Wt	-	6.4	7.10

[a]number of colony on the plate.
[b]concentration of 6-FABA into the medium.
[c]activity of 6-FABA against *M. bovis* BCG 6-FABA resistant mutants.
[d]activity of compound 73 against *M. bovis* BCG 6-FABA resistant mutants.

3.7.4 Synergy test by broth microdilution method

MICs of the single compound (**54, 65, 73** and INH) and of drugs combinations were determined using the broth microdilution technique. The fractional inhibitory concentration index (FICI) was calculated for each combination as the sum of the fractional inhibitory concentration of single agent (FIC), using the following formula: $FIC_A + FIC_B = FICI$. The FIC is the ratio between the MIC of drug in combination and the MIC of drug alone. FICI values less than 0.5 are interpreted as synergism, whereas antagonism is indicated by FICI >4. Instead, FICI values between 0.5 and 4 were interpreted as additivity. The combination of each hydrazide (**54**, **65** and **73**) with INH revealed an additive effect (Tab. 16).

Table 16. MIC values of single agent and in combination of compound **54, 65, 73** and isoniazid in 7H9/ADC/Tw, FIC and FICI values.

Compound	MIC 7H9/ADC/Tw alone (µM)[a]	MIC 7H9/ADC/Tw in combination (µM)[b]	FIC[c]	FICI[d]
INH	0.36	0.36	1	1.0625
40	14.2	0.25	0.0625	
INH	0.46	0.46	1	1.13
21	1.77	0.22	0.13	
INH	0.36	0.36	1	1.0157
32	22.9	0.36	0.0157	

[a]activity against *M. bovis* BCG of each single agent.
[b]activity against *M. bovis* BCG of each in combination.
[c]franctional inhibitory concentration.
[d]fractional inhibitory concentrations index.

3.7.5 INH resistant mutants

BCG resistant mutants were generated by plating and incubating the parent strain in presence of concentration of INH 3, 5 and 10 times the MIC. Among all the isolates, resistors 100- folds less sensitive to INH compared to the wild type were selected for the *katG* sequencing. Five INH resistors displayed a *katG* mutation (Tab. 17). Then, the activity of **54** and **73** against INH resistant mutants was assessed. Derivative **54** and **73** retained the activity against INH resistors, including the *katG* resistant mutants (Tab. 17).

Table 17. INH BCG resistant mutants: colony number on the plate, INH concentrations in the medium, *katG* mutations, INH MIC (µM), **54** and **73** MIC (µM) against the resistors and the wild type.

Colony n.[a]	INH conc[b]	*katG* mutation[c]	INH MIC (µM)[d]	54 MIC (µM)[e]	73 MIC (µM)[f]
1	x3 MIC	1080^1081insA	>100	4.0-2.0	14.2
2	x3 MIC	Δ405_414CCGACAACG (ΔD137_A139)	>100	8.1	1.77
3	x3 MIC	1080^1081insA	>100	0.1	28.4
4	x3 MIC	n.d.[g]	>100	0.1-0.5	n.t.[i]
1	x5 MIC	n.d.[g]	>100	n.t.[h]	7.1
2	x5 MIC	1080^1081insA	>100	n.t.[h]	7.1
1	x10 MIC	n.d.[g]	>100	0.1	n.t.[i]
2	x10 MIC	1080^1081insA	>100	n.t.[h]	28.4-14.2
Wt	none	None	0.9	2.0	7.1

[a]number of colony on the plate.
[b]concentration of INH into the medium.
[c]mutation of *katG* gene.
[d]activity of INH against *M. bovis* BCG INH resistant mutants.
[e]activity of compound 54 against *M. bovis* BCG INH resistant mutants.
[f]activity of compound 54 against *M. bovis* BCG INH resistant mutants.
[g]not determined.
[h]not tested.
[i]not tested.

3.7.6 Discussion

The target preliminary studies seem to confirm the hypothesis that this new class of compounds inhibit Trp biosynthesis. Compounds **54, 65** and **73** and 6-FABA are inactive in the presence of both Trp and the precursors anthranilate and indole. Instead, they retained the activity when chorismate is added to the medium (Tab. 12, 13). Unlike anthranilate and indole, chorismate is also a precursor of phenylalanine and tyrosine biosynthesis. Therefore, the chorismate addition to the medium could not affect Trp biosynthesis but other pathways.

The evidence of a cross-resistance between 6-FABA and derivative **73** suggested that the two compounds act by inhibiting the same target (Tab. 14, 15). It is not clear if hydrazides are prodrug of 6-FABA or act by inhibiting a specific enzyme. The WGS results of **73** resistors will be crucial to clarify this aspect.

Regarding the possibility that the hydrazide derivatives inhibit mycolic acid biosynthesis, the experimental results seem to deny this hypothesis. No antagonism between INH and aryl hydrazides was observed (Tab. 16). Instead, the additive effect of INH-aryl hydrazides combination indicates a different mechanism of action. Furthermore, analogues **54** and **73** are active against INH resistant mutants, including *katG* mutants (Tab. 17). About katG, further studies will be carried out to verify the possibility that KatG activates hydrazides. The activity of **54, 65** and **73** will be evaluated against BCG *katG*-knockout strain.

3.8 Conclusions

In conclusion, among the newly synthetized compounds only hydrazides proved to be active against MTB. Aryl hydrazides **54, 55, 65, 67, 72** and **73** displayed a significant improved activity ($MIC_{GastFe} \leq 1.56$ μM) compare to 6-FABA (MIC_{GastFe}= 5.0 μM) and promising values of cytotoxicity ($CC_{50} \geq 1360$ μM). The preliminary SAR analysis about the aryl hydrazide chemical scaffolds revealed that the 2-amino group is not relevant for the activity. The 2-fluorobenzohydrazides **94** and **95** showed a comparable activity to the parent amino-derivatives **55** and **68**. Although the amino group is not essential for the activity, probably it could be important for drug-like properties, in particular the aqueous solubility.

Preliminary target studies suggest aryl hydrazides acting by inhibiting Trp biosynthetic pathway. The mechanism of action is not clear. They could be 6-FABA prodrugs or act by binding directly one of Trp biosynthetic enzymes. More information about the mechanism of action will be soon available from WGS data of **73** resistant mutants.

Interestingly, derivatives **54** and **73** are effective *in vitro* against INH resistors. Since the INH resistance is the most commonly found in MDR clinical isolates, this result highlights the potentiality of the aryl hydrazide as antitubercular agents.

Further studies will concern the evaluation of drug-like properties of **54, 55, 65, 67, 72,** and **73** and *in vivo* efficacy of the best derivatives.

3.9 Materials and methods

3.9.1 Chemistry

All chemicals used were of reagent grade. Yields refer to purified products are not optimized. Melting points were determined in open capillaries on a Gallenkamp

apparatus and are uncorrected. Sigma-Aldrich silica gel 60 (230−400 mesh) was used for column chromatography. Merck TLC plates (silica gel 60 F254) were used for thin-layer chromatography (TLC). Sigma-Aldrich aluminum oxide (activity II−III, according to Brockmann) was used for chromatographic purifications. Sigma-Aldrich Stratocrom aluminum oxide plates with a fluorescent indicator were used for TLC to check the purity of the compounds. ^{1}H NMR spectra were recorded with a Bruker AC 400 spectrometer in the indicated solvent (TMS as the internal standard). The values of the chemical shifts are expressed in ppm.

*3.9.1.1 General procedure for the preparation of **34, 35,39-50, 53-71**.*

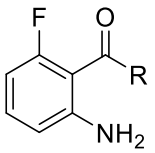

34, 35, 39-50, 53-71

1-1`- Carbonyl diimidazole (0,97 mmol; 1,5 eq) was added at room temperature to a solution of 2-amino- 6-fluoro benzoic acid (0,65 mmol; 1,0 eq) in tetrahydrofuran (7 mL) in a round-bottom flask equipped with a stirring bar in dry conditions [120]. After 24 hours the appropriate amine, hydrazine or hydroxylamine was added (0,65 mmol; 1,0 eq) and then the reaction mixture was stirred at room temperature for 16 hours. The reaction was quenched with aqueous sodium bicarbonate and the organic solution was extracted with ethyl acetate, washed with brine and dried over Na_2SO_4.

After filtration and concentration, the crude material was purified by column chromatography on silica gel with a mixture of dichloromethane/ ethyl acetate in the opportune volumes to give the expected products **34, 35,39-50, 53-71**.[124]**.**

2-Amino-6-fluoro-*N*-hydroxybenzamide (34). White solid (26% yield). ^{1}H NMR (400MHz, $CDCl_3$), δ ppm= 7.11 (m, 1H), 6.61 (s broad, 1H), 6.46-6.32 (m, 1H), 6.37-6.32 (m, 1H), 6.06 (s broad, 2H), 5.65 (s broad, 1H). ^{13}C NMR (400 MHz, $CDCl_3$), δ ppm= 168.06, 160.24, 154.93, 131.81, 116.59, 107.09, 97.17.

2-Amino-6-fluoro-*N*-methoxybenzamide (35). White solid (23% yield). ^{1}H NMR (400MHz, $CDCl_3$), δ ppm= 9.19 (d, 1H), 7.28-7.12 (m, 1H), 6.50-6.47 (m, 1H), 6.40-6.32 (m, 1H), 3.90 (s, 3H). ^{13}C NMR (400 MHz, $CDCl_3$), δ ppm= 167.16, 160.24, 154.93, 131.81, 116.59, 107.09, 97.17.

2-Amino-6-fluorobenzamide (39). White solid (73% yield).^{1}H NMR (400MHz, DMSO-d_6), δ (ppm): 7.47 (s broad, 2H), 7.06-7.04 (m, 1H), 6.49-6.47 (m, 1H), 6.30-6.26 (m, 1H), 6.12 (s broad, 2H). ^{13}C NMR (400 MHz, $CDCl_3$), δ ppm= 171.23, 159.09, 150.09, 131.33, 115.02, 106.35, 101.31.

2-Amino-6-fluoro-*N*'-isopropylbenzamide (40). White-grey solid (67% yield). ^{1}H NMR (400MHz, $CDCl_3$), δ ppm= 7.10-7.04 (m, 1H), 6.44-6.43 (m, 2H), 6.36-6.31 (m, 1H), 5.87 (s broad, 2H), 4.27 (m, 1H), 1.25 (d, 6H). ^{13}C NMR (400 MHz, $CDCl_3$), δ ppm= 169.63, 159.65, 151.62, 131.61, 115.55, 105.77, 100.91, 43.20, 22.66.

2-Amino-6-fluoro-*N*-(2-hydroxyethyl) benzamide (41). Yellowish oil (15% yield). ^{1}H NMR (400MHz, $CDCl_3$) δ ppm= 7.12-7.07 (m, 2H), 6.46-6.44 (m, 1H), 6.38-6.34 (m, 1H), 5.90 (s broad, 2H), 3.83-3.81 (m, 2H), 3.63-3.58 (m, 2H), 2.66 (s broad, 1H).

^{13}C NMR (400 MHz, $CDCl_3$) δ ppm=169.27, 159.36, 151.32, 131.54, 115.69, 105.93, 100.96, 60.68, 42.65.

2-Amino-*N*-cyclopropyl-6-fluorobenzamide (42). White solid (25% yield). ^{1}H NMR (400MHz, $CDCl_3$), δ ppm= 7.10-7.04 (m, 1H), 6.79 (s broad, 1H), 6.44-6.42 (m, 1H), 6.34-6.29 (m, 1H), 5.98 (s broad, 2H), 2.87 (m, 1H), 0.86-0.83 (m, 2H), 0.63-0.57 (m, 2H). ^{13}C NMR (400 MHz, $CDCl_3$), δ ppm= 172.88, 159.65, 151.62, 131.61, 115.55, 105.77, 100.91, 26.11, 8.92.

2-Amino-*N*-cyclobuthyl-6-fluorobenzamide (43). White solid (25% yield). ^{1}H NMR (400MHz, $CDCl_3$), δ ppm= 7.13-7.06 (m, 1H), 6.79 (s broad, 1H), 6.47-6.44 (m, 1H), 6.37-6.32 (m, 1H), 4.58-4.53(m, 1H), 2.49-2.39 (m, 2H), 2.01-1.94 (m, 2H), 1.83-1.80 (m, 2H). ^{13}C NMR (400 MHz, $CDCl_3$), δ ppm= 169.18, 159.65, 151.62, 131.61, 115.55, 105.77, 100.91, 46.10, 31.54, 13.80.

2-Amino-6-fluorophenyl(pyrrolidin-1-yl) methanone (44). White solid (30% yield). ^{1}H NMR (400MHz, $CDCl_3$), δ ppm= 7.15-7.07 (m, 1H), 6.49-6.38 (m, 2H), 3.65 (t, 2H), 3.39 (s broad, 2H), 2.05-1.86 (m, 6H). ^{13}C NMR (400 MHz, $CDCl_3$), δ ppm= 161.91, 158.56, 151.47, 130.03, 115.07, 104.45, 103.93, 47.91, 25.16.

(2-Amino-6-fluorophenyl) (4-methylpiperazin-1-yl) methanone (45). White solid (53% yield). ^{1}H NMR (400MHz, $CDCl_3$), δ ppm= 7.13-7.06 (m, 1H), 6.50-6.39 (m, 2H), 4.29 (s broad, 2H), 3.87-3.77 (m, 2H), 3.44-3.39 (m, 2H), 2.53-2.43 (m, 3H), 2.32 (s, 3 H). ^{13}C NMR (400 MHz, $CDCl_3$), δ ppm= 165.35, 158.56, 151.47, 130.03, 115.07, 104.45, 103.93, 52.66, 46.04, 44.61.

2-Amino-*N*-cyclohexyl-6-fluorobenzamide (46). White solid (80% yield). ^{1}H NMR (400MHz, DMSO-d_6), δ ppm= 8.04 (d, 1H), 7.08-7.03 (m, 1H), 6.50-6.48 (m, 1H), 6.33-6.29 (m, 1H), 5.72 (s broad, 2H), 3.75-3.70 (m, 1H), 1.83-1.80 (m, 2H), 1.72-1.69 (m, 2H), 1.56-1.54 (m, 1H), 1.32-1.24 (m, 4H), 1.20-1.10 (m, 1H). ^{13}C NMR (400 MHz, $CDCl_3$), δ ppm= 169.51, 159.65, 151.62, 131.61, 115.55, 105.77, 100.91, 51.20, 33.51, 25.92, 21.72.

(2-Amino-6-fluorophenyl) (piperidin-1-yl)methanone (47). Grey solid (42% yield). ^{1}H NMR (400MHz, DMSO-d_6), δ ppm= 7.06-7.00 (m, 1H), 6.49-6.47 (m, 1H), 6.34-6.29 (m, 1H), 5.22 (s broad, 2H), 3.58 (s broad, 2H), 3.17 (s broad, 2H), 1.57-1.42 (m, 6H). ^{13}C NMR (400 MHz, $CDCl_3$), δ ppm= 169.25, 159.82, 153.01, 133.21, 115.62, 106.58, 100.82, 61.45, 32.81, 25.92, 24.72.

(2-Amino-6-fluorophenyl) (morpholino)methanone (48) White oil (42% yield). ^{1}H NMR (400MHz, $CDCl_3$), δ ppm= 7.13-7.07 (m, 1H), 6.50-6.48 (m, 1H), 6.44-6.40 (m, 1H), 4.32 (s broad, 2H), 3.85-3.71 (m, 5H), 3.63-3.57 (m, 1H), 3.50-3.46 (m, 1H), 3.35-3.30 (m, 1H). ^{13}C NMR (400 MHz, $CDCl_3$), δ ppm= 165.35, 158.56, 151.47, 130.03, 115.07, 104.45, 103.93, 66.10, 44.61

(2-Amino-6-fluorophenyl) (3-methoxy-piperidin-1-yl)methanone (49). Yellowish oil (35% yield). ^{1}H NMR (400MHz, $CDCl_3$), δ ppm= 7.11-7.06 (m, 1H), 6.52-6.41 (m, 2H), 3.81-3.78 (m, 1H), 3.72-3.67 (m, 1H), 3.34 (s, 3H). ^{13}C NMR (400 MHz, $CDCl_3$), δ ppm= 166.37, 158.56, 151.47, 130.03, 115.07, 104.15, 103.93, 75.20, 56.13, 48.99, 45.45, 29.58, 23.15.

2-Amino-6-fluoro-*N*-(4-fluorophenyl) benzamide (50). White solid (12% yield). ^{1}H NMR (400MHz, $CDCl_3$), δ ppm= 8.29 (d, 1H), 7.58-7.52 (m, 2H), 7.18-7.09 (m, 1H),

7.08-7.03 (m, 2H), 6.50-6.48 (m, 1H), 6.44-6.39 (m, 1H), 5.98 (s broad, 2H). ^{13}C NMR (400 MHz, $CDCl_3$), δ ppm= 170.40, 160.07, 159.98, 151.96, 134.31, 131.75, 123.31, 126.19, 125.45, 105.66, 100.87.

2-Amino-*N*'-cyclohexyl-6-fluorobenzohydrazide (53). White solid (33% yield). ^{1}H NMR (400MHz, $CDCl_3$), δ ppm= 7.13-7.08 (m, 1H), 6.76 (s broad, 1H), 6.47-6.44 (m, 1H), 6.35-6.30 (m, 1H), 2.91-2.86 (m, 1H), 1.82-1.69 (m, 4H), 1.40-1.35 (m, 1H), 1.31-1.20 (m, 4H), 1.12-1.06 (m, 1H). ^{13}C NMR (400 MHz, $CDCl_3$), δ ppm= 169.25, 159.82, 153.01, 133.21, 115.62, 106.58, 100.82, 61.45, 32.81, 25.92, 24.72.

2-Amino-6-fluoro-*N'*-phenylbenzohydrazide (54). White solid (yield 25%). ^{1}H NMR (400MHz, $CDCl_3$), δ ppm= 8.29 (d, 1H), 7.19 (t, 2H), 7.08 (q, 1H), 6.87 (m, 3H), 6.40 (m, 2H), 6.00 (s brood, 2H). ^{13}C NMR (400 MHz, $CDCl_3$), δ ppm=170.02, 159.82, 153.02, 148.78, 133.21, 128.85, 119.39, 115.62, 113.12, 106.58, 100.78.

2-Amino-6-fluoro-*N*'-(4-fluorophenyl) benzohydrazide (55). White solid (17% yield). ^{1}H NMR (400MHz, $CDCl_3$), δ ppm= 8.29 (d, 1H), 7.09-7.06 (m, 1H), 6.89-6.81 (m, 4H), 6.41-6.39 (m, 1H), 6.37-6.31 (m, 1H), 5.92 (s broad, 2H). ^{13}C NMR (400 MHz, $CDCl_3$), δ ppm=165.05, 150.25, 150.18, 148.23, 132.16, 132.05, 115.77, 115.55, 113.94, 111.95, 102.62, 102.39.

2-Amino-6-fluoro-*N'*-(3-fluorophenyl) benzohydrazide (56). White solid (20% yield). ^{1}H NMR (400 MHz, DMSO-d_6), δ ppm= 10.10 (s, 1H), 8.23 (s, 1H), 7.16 (m, 2H), 6.62 (d, 1H), 6.54 (3H, m), 6.41 (dd, 1H), 5.80 (s 2H). ^{13}C NMR (400 MHz, $CDCl_3$), δ ppm= 170.02, 162.58, 159.82, 153.01, 150.57, 133.21, 129.66, 115.62, 108.86, 106.63, 106.58, 101.00, 100.82.

2-Amino-*N'*-(2-chlorophenyl)-6-fluorobenzohydrazide (57). Brownish solid (yield 18%). ^{1}H NMR (400 MHz, $CDCl_3$), δ ppm= 8.29 (d, 1H), 7.24 (dd, 1H), 7.09 (dd, 2H), 6.93 (d t, 1H), 6.56 (s broad, 1H), 6.41 (d, 1H), 6.355 (dd, 1H). ^{13}C NMR (400 MHz, $CDCl_3$), δ ppm= 170.02, 159.82, 153.01, 143.49, 133.21, 130.33, 126.63, 121.08, 119.70, 115.62, 114.98, 106.58, 100.82.

2-Amino-*N'*-(3-chlorophenyl)-6-fluorobenzohydrazide (58). White solid (yield 35%). ^{1}H NMR (400 MHz, $CDCl_3$), δ ppm= 8.28 (d, 1H), 7.10 (tt, 2H), 6.86 (t, 1H), 6.82 (dd, 1 H), 6.74 (dd, 1H), 6.41 (d, 1H), 6.34 (dd, 1H). ^{13}C NMR (400 MHz, $CDCl_3$), δ ppm= 170.02, 159.82, 153.01, 147.91, 133.21, 132.31, 129.35, 119.36, 115.62, 113.88, 112.20, 106.58, 100.82.

2-Amino-*N'*-(4-chlorophenyl)-6-fluorobenzohydrazide (59). Brownish solid (yield 70%). ^{1}H-NMR (400 MHz, $CDCl_3$), δ ppm= 8.28 (d, 1H), 7.14 (d, 1H), 7.09 (q, 1H), 6.81 (d, 2H), 6.40 (d, 1H), 6.34 (dd, 1H), 6.19 (s broad, 1H), 5.88 (s broad, 2H). ^{13}C NMR (400 MHz, $CDCl_3$), δ ppm=166.85, 163.59, 161.16, 152.06, 152.00, 146.92, 133.27, 133.14, 129.21, 126.11, 114.92, 113.27, 103.12, 102.86.

2-Amino-*N'*-(2,3-dichlorophenyl)-6-fluorobenzohydrazide (60). Brownish solid (yield 13%). ^{1}H NMR (400 MHz, $CDCl_3$), δ ppm= 8.39 (d, 1H), 7.18 (q, 1H), 7.11 (t, 1H), 7.02 (d, 1H), 6.92 (d, 1H), 6.72 (s broad, 1H), 6.50 (d, 1H), 6.43 (dd, 1H). ^{13}C NMR (400 MHz, $CDCl_3$), δ ppm= 170.02, 159.82, 153.01,144.09, 133.21, 132.77, 127.12, 122.54, 120.58, 115.62, 112.89, 106.58, 100.78.

2-Amino-*N'*-(2,4-dichlorophenyl)-6-fluorobenzohydrazide (61). Grey solid (yield 28%); ^{1}H NMR (400 MHz, $CDCl_3$), δ ppm= 8.28 (d, 1 H), 7.25 (d, 1H), 7.09 (m, 2H), 6.86 (d, 1H), 6.52 (s, 1H), 6.41 (d, 1H), 6.34 (dd, 1H). ^{13}C NMR (400 MHz, $CDCl_3$),

δ ppm= 170.02, 159.82, 153.01, 141.57, 133.21, 130.47, 127.21, 124.97, 121.68, 115.62, 115.07, 106.58, 100.82.

2-Amino-*N'*-(2,5-dichlorophenyl)-6-fluorobenzohydrazide (62). Brownish solid (yield 29%). ^{1}H NMR (400 MHz, $CDCl_3$) δ ppm= 8.36 (d, 1H), 7.24 (d, 1H), 7.19 (q, 1H), 6.98 (d, 1H), 6.83 (dd, 1H), 6.63 (s,1 H), 6.49 (d, 1H), 6.43 (dd, 1H). ^{13}C NMR (400 MHz, $CDCl_3$), δ ppm= 164.91, 149.91, 146.28, 133.01, 132.14, 132.09, 131.06, 119.32, 116.09, 112.73, 111.74, 106.39, 102.30, 102.12.

2-Amino-*N'*-(3,4-dichlorophenyl)-6-fluorobenzohydrazide (63). Grey solid (yield 18%). ^{1}H NMR (400 MHz, $CDCl_3$), δ ppm= 8.28 (d, 1H), 7.22 (d, 1H), 7.10 (q, 1H), 6.95 (d, 1H), 6.71 (dd, 1H), 6.42 (d, 1H), 6.35 (dd, 1H), 6.21 (s broad, 1H). ^{13}C NMR (400 MHz, $CDCl_3$), δ ppm=166.97, 161.20, 152.12, 152.06, 148.01, 133.45, 133.32, 133.12, 130.81, 124.17, 115.29, 113.35, 113.33, 113.22, 103.15, 102.99.

2-Amino-*N*'-(3,5-dichlorophenyl)-6-fluorobenzohydrazide (64). Brownish solid (yield 20%). ^{1}H NMR (400 MHz, $CDCl_3$), δ ppm= 7.16 (q, 1H), 6.82 (s, 2H), 6.80 (s, 1H), 6.58 (d, 1H), 6.42 (t, 1H). ^{13}C NMR (400 MHz, $CDCl_3$), δ ppm= 170.02, 159.82, 153.01, 147.13, 133.21, 132.91, 129.27, 115.62, 113.02, 106.58, 100.80.

2-Amino-6-fluoro-*N*'-(2,4,6-trichlorophenyl) benzohydrazide (65). White solid (yield 63%). ^{1}H NMR (400 MHz, DMSO), δ ppm= 10.27 (s, 1H), 7.53 (s, 2H), 7.08 (q,1H), 6.48 (d, 1H), 6.30 (t, 1H), 5.84 (s, 2H). ^{13}C NMR (400 MHz, $CDCl_3$), δ ppm= 170.02, 159.82, 153.01, 143.62, 133.21, 129.31, 127.41, 126.47, 115.62, 106.58, 100.82.

2-Amino-*N*'-benzyl-6-fluorobenzohydrazide (66). White solid (yield 35%). ^{1}H NMR (400 MHz, $CDCl_3$), δ ppm= 7.97 (s, 1H), 7.29 (m, 5H), 7.03 (q, 1H), 6.38 (d, 1H), 6.25 (dd, 1H), 5.75 (s brood, 2H), 4.00 (s, 2H). ^{13}C NMR (400 MHz, $CDCl_3$), δ ppm=168.63, 159.78, 153.01, 137.83, 133.21, 128.50, 127.70, 126.11, 115.62, 106.58, 100.82, 57.43.

2-Amino-6-fluoro-*N*'-(4-methoxyphenyl) benzohydrazide (67). White solid (yield 35%); ^{1}H NMR (400 MHz, $CDCl_3$), δ ppm= 8.37 (s, 1H), 7.08 (q, 1H), 6.83 (d, 2H), 6.74 (d, 2H), 6.46 (d, 1H), 6.38 (d d, 1H), 3.68 (s, 3H). ^{13}C NMR (400 MHz, $CDCl_3$), δ ppm=170.02, 159.82, 153.01, 152.85, 140.93, 133.21, 115.62, 114.62, 113.21, 106.58, 100.80, 56.01.

2-Amino-6-fluoro-*N'*-(4-(trifluoromethyl) phenyl) benzohydrazide (68). Brownish solid (yield 18%). ^{1}H NMR (400 MHz, $CDCl_3$), δ ppm= 8.3 (d, 1H), 7.43 (d, 2H), 7.10 (q, 1H), 6.91 (d, 2H), 6.41 (d, 1H), 6.35 (dd, 1H), 5.80 (s broad, 2H). ^{13}C NMR (400 MHz, $CDCl_3$), δ ppm= 170.00, 159.82, 153.1, 152.22, 133.21, 125.21, 121.76, 121.47, 115.62, 113.14, 106.58, 100.81.

2-Amino-6-fluoro-*N'*-(2-nitrophenyl) benzohydrazide (69). Yellow solid (yield 30%). ^{1}H NMR (400 MHz, DMSO-d_6), δ ppm= 10.55 (s, 1H), 9.48 (s, 1H), 8.13 (dd, 1H), 7.64 (t, 1H), 7.18 (d, 1H), 7014 (q, 1H), 6.89 (dt, 1H), 6.53 (d, 1H), 6.38 (dt, 1H), 5.91 (s, 2H). ^{13}C NMR (400 MHz, $CDCl_3$), δ ppm= 164.63, 162.13, 159.76, 149.78, 145.87, 136.97, 126.34, 118.47, 114.92, 111.82, 106.28, 102.17, 101.74.

2-Amino-6-fluoro-*N'*-(3-nitrophenyl) benzohydrazide (70). Yellow solid (yield 25%). ^{1}H NMR (400 MHz, DMSO-d_6), δ ppm= 10.26 (s, 1H), 8.61 (s, 1H), 7.59 (d, 2H), 7.46 (t, 1H), 7.18 (m, 2H), 6.58 (d, 1H), 6.43 (t, 1H), 5.84 (s, 2H). ^{13}C NMR (400

MHz, $CDCl_3$), δ ppm= 165.19, 162.23, 159.81, 150.97, 150.44, 149.20, 132.41, 130.61, 118.96, 113.40, 112.01, 106.14, 102.54, 102.54, 102.31.

2-Amino-*N'*-(2,4-dinitrophenyl)-6-fluorobenzohydrazide (71). Orange solid (yield 15%), ^1H NMR (400 MHz, DMSO-d_6), δ ppm= 10.51 (s broad, 1H), 9.01 (s broad, 1H), 8.50 (s, 1H), 8.38 (dd, 1H), 7.41 (m, 2H), 6.48 (m, 1H), 6.50 (dd, 1H), 5.90 (s broad, 2H). ^{13}C NMR (400 MHz, $CDCl_3$), δ ppm= 164.8, 158.7, 154, 150, 139.2, 134.9, 130.5, 120.5, 115, 112, 107.1, 105.6.

*3.9.1.2 Preparation of 2-amino-6-fluoro-N'-(4-fluorophenyl) benzohydrazide hydrochloride **72** and 2-amino-6-fluoro-N'-phenylbenzohydrazide hydrochloride* **73**.

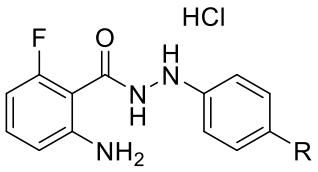

72-73

To a solution of the 2-amino-6-fluoro-*N*'-(4-fluorophenyl) benzohydrazide **72** or 2-amino-6-fluoro-*N'*-phenylbenzohydrazide **73** (0.08 mmol, 1 eq) in ethanol (0.5 mL), aqueous HCl 37% was added dropwise. The mixture was stirred for 30 minutes at room temperature and then the white precipitate was separated by filtration and washed with cold ethanol to obtain the desired product.

2-Amino-6-fluoro-*N'*-(4-fluorophenyl) benzohydrazide hydrochloride (72). White solid 25% yield. ^{1}H NMR (400MHz, DMSO-d_6), δ ppm= 10.08 (s, 1H), 7.16 (q, 1H), 7.02 (t, 2H), 6.81 (m, 2H), 6.59 (d, 1H), 6.44 (t, 1H), 5.40 (s broad, 2H). ^{13}C NMR (400 MHz, $CDCl_3$), δ ppm= 169.99, 159.80, 153.01, 148.78, 133.21, 128.85, 119.39, 115.62, 113.12, 106.58, 100.82.

2-Amino-6-fluoro-*N'*-phenylbenzohydrazide hydrochloride (73). White solid (21% yield). ^{1}H-NMR (400MHz, DMSO-d_6), δ ppm= 10.05 (s, 1H), 7.17 (m, 3H), 6.81 (d, 2H), 6.73 (t, 1H), 6.59 (d, 1H), 6.44 (t, 1H), 5.01 (s broad, 2H). ^{13}C NMR (400 MHz, $CDCl_3$), δ ppm= 170.00, 159.79, 152.99, 148.78, 133.21, 128.85, 119.39, 115.62, 113.12, 106.58, 100.80.

3.6.1.3 Preparation of (Z)-2-Amino-6-fluoro-N'-hydroxybenzimidamide ***82***

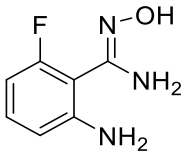

82

In a round bottom flask equipped with a stirring bar, hydroxylamine hydrochloride (1,53 mmol; 2,1 eq) and potassium hydroxide (2,2 mmol; 3,0 eq) were add to a solution of 2-amino-6-fluorobenzonitrile **80** (0,73 mmol; 1,0 eq) in dry methanol (1 mL) at room temperature. After 24 hours, the reaction mixture was concentrated, dissolved in water and extracted with ethyl acetate. Then the organic layer was washed with brine, dried over Na_2SO_4 and concentrated *in vacuo*. The crude material was purified by column chromatography on silica gel and a mixture of dichloromethane/ ethyl acetate (10:1, v/v), and crystallized with diethyl ether to give **82** as a brownish powder [121].

2-Amino-6-fluoro-*N*'-hydroxybenzimidamide (82). Brownish solid (68% yield). ^{1}H NMR (400MHz, DMSO-d_6), δ ppm= 9.46 (s, 1H), 7.06-7.00 (m, 1H), 6.50-6.48 (m, 1H), 6.35-6.30 (m, 1H), 5.78 (s, 2H), 5.50 (s, 2H).

*3.9.1.3 Preparation of 3-Fluoro-2-(5-methyl-1,2,4-oxadiazol-3-yl) aniline **36**.*

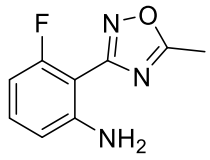

36

In a round flask bottom equipped with a stirring bar, potassium *tert*-butoxide (0.57 mmol; 1,9 eq) and *tert*-butyl acetate (15 mL) were added to a solution of **47** (0,3 mmol; 1,0 eq) in 5 mL of dry *tert*-butanol. The reaction mixture was heated to reflux of solvent and stirred for 2,5 hours.

Then the reaction was concentrated under *vacuum*, and the residue was diluted in water, extracted with ethyl acetate and dried over Na_2SO_4. The crude material obtained after filtration and solvent evaporation was purified by column chromatography on silica gel and a mixture of cyclohexane/ ethyl acetate (6:1, v/v) to give the desired product **36** as a white powder [121].

3-Fluoro-2-(5-methyl-1,2,4-ossadiazol-3-yl) aniline (36). White solid (55% yield). ^{1}H NMR (400MHz, DMSO-d_6), δ ppm= 7.20-7.17 (m, 1H), 6.65-6.63 (m, 1H), 6.44-6.41 (m, 1H), 6.25 (s broad, 2H), 2.68 (s, 3H). ^{13}C NMR (400 MHz, $CDCl_3$), δ ppm= 176.74, 164.21, 163.09, 160.60, 150.17, 132.73, 132.62, 111.99, 102.50, 102.28, 98.04, 97.87, 12.43.

*3.9.1.4 Preparation of hydrazide **52***

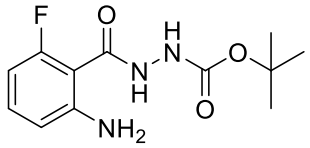

52

1-1'- Carbonyl diimidazole (0,97 mmol; 1,5 eq) was added at room temperature to a solution of 2-amino- 6-fluoro benzoic acid (0,65 mmol; 1,0 eq) in tetrahydrofuran (7 mL) in a round-bottom flask equipped with a stirring bar in dry conditions [120]. After 24 hours the *t*-butyl carbazate was added (0,65 mmol; 1,0 eq) and then the reaction mixture was stirred at reflux temperature for 16 hours. The reaction was quenched with aqueous sodium bicarbonate and the organic solution was extracted with ethyl acetate, washed with brine and dried over Na_2SO_4.

After filtration and concentration, the crude material was purified by column chromatography on silica gel with a mixture of dichloromethane/ ethyl acetate in the opportune volumes to give the expected product **52** [124].

***Tert*-butyl 2-(2-amino-6-fluorobenzoyl) hydrazine-1-carboxylate (52).** Oil (60% yield). ^{1}H NMR (400MHz, $CDCl_3$), δ ppm= 8.30 (d, 1H), 7.14-7.11 (m, 1H), 6.66 (s broad, 1H), 6.49-6.47 (m, 1H), 6.40-6.35 (m, 1H), 1.50 (s, 9H). ^{13}C NMR (400 MHz, $CDCl_3$), δ ppm= 164.70, 161.86, 159.44, 156.20, 149.49, 131.88, 131.78, 111.44, 107.18, 106.98, 102.08, 101.86, 28.56.

*3.9.1.5 Preparation of hydrazide **51***

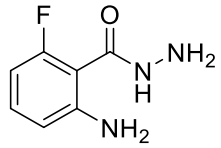

51

Trifluoro acetic acid (5 mL) was added to a solution of **52** (0.07 mmol, 1 eq) in DCM (5 mL) and the reaction mixture was stirred for 30 minutes at room temperature. Then the solvent was evaporated and the product **51** was precipitated as white powder.

2-Amino-6-fluorobenzohydrazide (51). White solid (> 90% yield). ^{1}H NMR (400MHz, DMSO-d_6), δ ppm= 9.38 (s broad, 1H), 7.09-7.04 (m, 1H), 6.51-6.48 (m, 1H), 6.33-6.29 (m, 1H), 5.78 (s broad, 2H), 4.48 (s broad, 2H). ^{13}C NMR (400 MHz, $CDCl_3$), δ ppm= 170.61, 159.31, 152.61, 133.12, 115.78, 106.88, 101.03.

*3.9.1.6 Preparation of 3-Fluoro-2-(5-methyl-1,3,4-oxadiazol-2-yl) aniline **37**.*

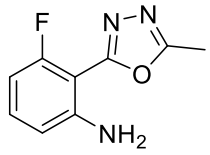

37

In a round bottom flask, triethyl orthoacetate (0,3 mmol; 1,0 eq) was added to a solution of **37** (0,3 mmol; 1,0 eq) in dioxane (2 mL). The reaction mixture was stirred in reflux condition for 24 hours, then diluted with water and extracted with dichloromethane. The organic layer was washed with brine, dried over Na_2SO_4 and concentrated to give the crude material, that was then purified by column chromatography on silica gel and a mixture of cyclohexane/ ethyl acetate (10:1, v/v) to achieve the desired product **37** as a white powder [122].

3-Fluoro-2-(5-methyl-1,3,4-oxadiazol-2-yl) aniline (37). White solid (24% yield).^{1}H NMR (400MHz, DMSO-d_6), δ ppm= 7.26-7.22 (m, 1H), 6.98 (s broad, 2H), 6.72-6.70 (m, 2H), 6.48-6.43 (m, 1H), 2.58 (s, 3H). ^{13}C NMR (400 MHz, $CDCl_3$), δ ppm= 163.13, 162.20, 161.64, 161.61, 159.70, 150.12, 150.07, 133.22, 133.11, 112.07, 102.09, 101.87, 94.51, 94.35, 10.96.

*3.9.1.7 Preparation of 3-Fluoro-2-(1H-tetrazol-5-yl) aniline **38**.*

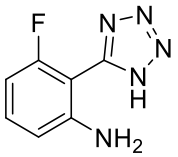

38

To a solution of 2-amino-6-fluoro benzonitrile **80** (0,73 mmol; 1,0 eq) in 1 mL of dry dimethylformamide, ammonium chloride (4,8 mmol; 13 eq) and sodium azide (4,8 mmol, 13 eq) were added and the reaction mixture was stirred for 24 hours at solvent reflux temperature. After solvent evaporation, water was added, and the brownish precipitate was filtered off. The liquid layer was extract with ethyl acetate, washed with a solution of 2N HCl and brine and dried over Na_2SO_4. After filtration and evaporation of solvent, the residue was purified by column chromatography on silica gel and a mixture of dichloromethane/ methanol 1% (v/v), to obtain the product **38** as a white powder [123].

3-Fluoro-2-(1H-tetrazol-5-yl) aniline (38). White solid (24% yield).^{1}H NMR (400MHz, DMSO-d_6), δ ppm= 7.27-7.21 (m, 1H), 6.72-6.70 (m, 1H), 6.52-6.49 (m, 1H). ^{13}C NMR (400 MHz, $CDCl_3$), δ ppm= 160.65, 151.83, 144.78, 131.72, 116.71, 109.85, 95.99.

*3.9.1.8 Preparation of (2-fluoro-6-nitrophenyl) methanol **88**.*

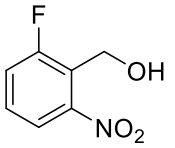

88

Water (1.24 mL) and $CaCO_3$ (2.215 mmol, 5.15 eq) were added to a solution of 2-(bromomethyl)-1-fluoro-3-nitrobenzene (0.43 mmol, 1 eq) in dioxane (1.24 mL), the reaction mixture was refluxed for 8 hours. The solution was cooled down to rt and dioxane was removed under reduced pressure. The solid residue was diluted in dichloromethane and dissolved with 1N HCl at 0 °C. The mixture was extracted with dichloromethane and washed with $NaHCO_3$ aqueous solution and brine, dried over Na_2SO_4 and filtered. After solvent evaporation, the crude material was purified by column chromatography on silica gel and a mixture of petroleum ether/ ethyl acetate (10:1) to give the (2-fluoro-6-nitrophenyl) methanol as a white powder [125].

(2-Fluoro-6-nitrophenyl) methanol (88). White solid (74% yield). ^{1}H NMR (400 MHz, $CDCl_3$), δ ppm= 7.84 (d, 1H), 7.46 (m, 2H), 4.90 (s, 2 H).

*3.9.1.9 Preparation of 2-fluoro-6-nitrobenzaldehyde **89**.*

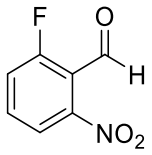

89

To a solution of (2-fluoro-6-nitrophenyl) methanol **88** (1.6 mmol, 1 eq) in anhydrous dichloromethane (10 mL), the Dess-Martin reagent periodinane (2.5 mmol, 1.5 eq) was added at 0 °C. The reaction was stirred for 1 hour at room temperature and then quenched with aqueous Na_2HCO_3 and solid $Na_2S_2O_3$. The mixture was extracted with dichloromethane, washed with brine and dried over anhydrous sodium sulfate. After filtration and concentration under *vacuum* the solid yellowish residue was purified by column chromatography on silica gel and a mixture of petroleum ether/ ethyl acetate (10:1) to give the 2-fluoro-6-nitrobenzaldehyde as a white solid [95].

2-Fluoro-6-nitrobenzaldehyde (89). White solid (70% yield). ^{1}H NMR (400 MHz, $CDCl_3$), δ ppm= 10.83 (s, 1H), 7.90 (d, 1H), 7.71 (q, 1H), 7.52 (t, 1H).

*3.9.1.10 Preparation of 2,2,2-trifluoro-1-(2-fluoro-6-nitrophenyl) ethan-1-ol **90**.*

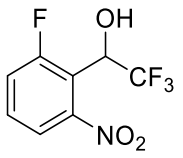

90

To a solution of 2-fluoro-6-nitrobenzaldehyde **89** (0.42 mmol, 1 eq) in anhydrous tetrahydrofuran (1 mL), trifluoromethyltrimethyl silane (0.2 mmol, 2M in THF, 1.2 eq) and TBAF (1.0 M in THF, 3 µL) were added at 0 °C with stirring. After 15 minutes, methanol (3 mL) and aqueous 2M HCl (1 mL) were added and the whole mixture was stirred for additional 15 minutes. Then the solvents were removed under reduced pressure and the aqueous mixture was extracted with dichloromethane, washed with brine and dried over Na_2SO_4. The filtered organic layer was concentrated *in vacuo* and the final residue **90** was purified by column chromatography on silica gel and a mixture of petroleum ether/ ethyl acetate (15:1) [126].

2,2,2-Trifluoro-1-(2-fluoro-6-nitrophenyl) ethan-1-ol (90). Brownish oil (50% yield). ^{1}H NMR (400 MHz, $CDCl_3$), δ ppm= 7.81 (d, 1H), 7.62 (q, 1H), 7.48 (t, 1H), 5.83 (m, 1H), 3.99 (s, 1H).

*3.9.1.11 Preparation of 2,2,2-trifluoro-1-(2-fluoro-6-nitrophenyl) ethyl trifluoro methane sulfonate **91**.*

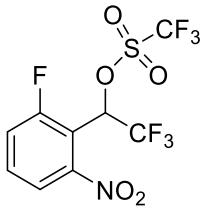

91

In a round bottom flask, 2,2,2-trifluoro-1-(2-fluoro-6-nitrophenyl) ethan-1-ol **90** (1.13 mmol, 1 eq), 2,6-lutidine (1.36 mmol, 1.2 eq), were dissolved in anhydrous dichloromethane (5 mL). The resulting solution was cooled in an ice bath, and trifluoromethanesulfonic anhydride (2.83 mmol, 2.5 eq) was added portion wise. The reaction was stirred at 0-4 °C for 2 hours and then quenched by addition of water. The mixture was extracted with dichloromethane, the combined organic layers were washed with brine and dried over Na_2SO_4 and filtered. The filtrate was concentrated *in vacuo* to give the crude material purified by column chromatography on silica gel and a mixture of petroleum ether/ ethyl acetate (15:1) [127].

2,2,2-trifluoro-1-(2-fluoro-6-nitrophenyl) ethyl trifluoromethanesulfonate (91). Brown oil (70% yield). ^{1}H NMR (400 MHz, $CDCl_3$), δ ppm= 8.00 (d, 1H), 7.79 (q, 1H), 7.59 (t, 1H), 7.04 (q, 1H).

*3.9.1.12 Preparation of 2,2,2-trifluoro-1-(2-fluoro-6-nitrophenyl) ethan-1-amine N-substituted **92 a-c**.*

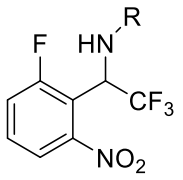

92 a-c

To a solution of **91** (0.95 mmol, 1 eq) in anhydrous dichloromethane, potassium carbonate (1.85 mmol, 1.95 eq) and the appropriate amine were added (1.55 mmol, 1.63 eq). The mixture was stirred at 75 °C for 16 hours then cooled to room temperature, diluted with aqueous 2N HCl, extracted with dichloromethane and washed with brine. The organic layer was dried over Na_2SO_4, filtered and concentrated *in vacuo*. The brownish liquid residue was purified by column chromatography on silica gel and a mixture of petroleum ether/ ethyl acetate (15:1) [127].

4-(2,2,2-Trifluoro-1-(2-fluoro-6-nitrophenyl) ethyl) morpholine (92 a). Yellow oil (51% yield). ^{1}H NMR (400 MHz, $CDCl_3$), δ ppm= 7.55 (m, 2H), 7.39 (m, 1H), 4.89 (q, 1H), 3.65 (m, 4H), 2.69 (m, 2H), 2.59 (m, 2H).

4-(2,2,2-trifluoro-1-(2-fluoro-6-nitrophenyl) ethyl) thiomorpholine (92 b). Yellow oil (49% yield).^{1}H NMR (400 MHz, $CDCl_3$), δ ppm= 7.53 (m, 2H), 7.35 (t, 1H), 5.03 (q, 1H), 3.02 (t, 2H), 2.91 (t, 2H)**,** 2.53 (m, 4H).

4-Fluoro-N-(2,2,2-trifluoro-1-(2-fluoro-6-nitrophenyl) ethyl) aniline (**92 c).** Brown oil (47% yield). ^{1}H NMR (400 MHz, $CDCl_3$), δ ppm= 7.77 (m, 1H), 7.56 (m, 1H), 7.42 (t, 1H), 6.91 (t, 2H), 6.73 (m, 2H), 6.09 (m, 1H), 4.71 (dd, 1H).

*3.9.1.13 Preparation of 2-(1-amino-2,2,2-trifluoroethyl)-3-fluoroaniline N-substituted **74-76**.*

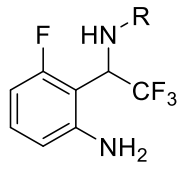

74-76

To a solution of *2*,2,2-trifluoro-1-(2-fluoro-6-nitrophenyl) ethan-1-amine *N*-substituted **92 a-c** (0.28 mmol, 1 eq) in acetonitrile/ water (1: 0.1 mL) $NiCl_2$ $6H_2O$ (0.056 mmol, 0.2 eq) was added and the mixture was then stirred for 5 minutes. Afterwards, sodium borohydride (1.4 mmol, 5 eq) as a fine powder was added to the reaction mixture at 0 °C and a black solid immediately precipitated. The reaction continued to be stirred for 30 minutes and then quenched by addition of water. The mixture was extracted with dichloromethane and the organic layer was dried over sodium sulfate. Filtration and evaporation of the solvent gave the crude material that was purified by column chromatography on silica gel with the opportune mixture of cyclohexane/ ethyl acetate [128].

3-Fluoro-2-(2,2,2-trifluoro-1-morpholinoethyl) aniline (74). White solid (64% yield). ^{1}H NMR (400 MHz, $CDCl_3$), δ ppm= 7.07 (q, 1H), 6.40 (m, 2H), 5.25 (s broad, 2H), 4.37 (q, 1H), 3.76 (m, 4 H), 2.68 (s broad, 2H), 2.60 (m, 2H). ^{13}C NMR (400 MHz, $CDCl_3$), δ ppm= 164.06, 153.42, 131.44, 126.10, 115.01, 104.66, 101.94, 67.36, 67.22, 50.47.

3-Fluoro-2-(2,2,2-trifluoro-1-thiomorpholinoethyl) aniline (75). Yellow oil (47% yield). ^{1}HNMR (400 MHz, $CDCl_3$), δ ppm= 7.07 (q, 1H), 6.41 (m, 2H), 5.04 (s broad,

2H), 4.49 (q, 1H), 2.97 (m, 4H), 2.72 (m, 4H). ^{13}C NMR (400 MHz, $CDCl_3$), δ ppm= 164.06, 153.42, 131.40, 126.10, 115.01, 104.65, 101.94, 67.36, 48.70, 29.13.

N-(1-(2-amino-6-fluorophenyl)-2,2,2-trifluoroethyl)-4-fluoroaniline (76). Brown oil (77% yield). ^{1}H-NMR (400 MHz, $CDCl_3$) δ ppm= 7.12 (q, 1H), 6.90 (t, 2H), 6.69 (m, 2H), 6.54 (m, 2H), 5.32 (q, 1H), 4.57 (s broad, 2H). ^{13}C NMR (400 MHz, $CDCl_3$) δ ppm= 162.57, 157.69, 153.16, 143.15, 131.81, 125.91, 117.34, 117.01, 113.30, 103.48, 103.36, 54.20.

*3.9.1.14 Preparation of 2-fluorobenzoic acid **100***

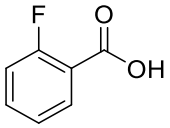

100

The 2-fluorobenzahldeyde **99** (2.014 mmol, 1 eq) was dissolved in anhydrous dimethylformamide (12 mL). Oxone (4.03 mmol, 2 eq) was added in one portion and the mixture was stirred at room temperature for 3 hours. Aqueous 1N HCl was added to dissolve the solid and the mixture was extracted with ethyl acetate and washed with brine. The organic layer was dried over Na_2SO_4, filtered and concentrated *in vacuo.* The crude product was purified by column chromatography on silica gel and the mixture of petroleum ether /ethyl acetate (2:1) to obtain the 2-fluorobenzoic acid **100** as white solid [130].

2-Fluorobenzoic acid (100). White solid (96% yield). ^{1}H NMR (400 MHz, $CDCl_3$), δ ppm= 13.25 (s broad, 1H), 7.86 (t, 1H), 7.61 (m, 1H), 7.29 (m, 2H).

*3.9.1.15 Preparation of 2,5-dioxopyrrolidin-1-yl 2-fluorobenzoate **101***

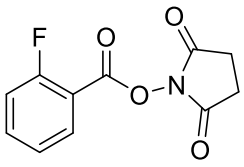

101

To a solution of 2-fluorobenzoic acid **100** (0.71 mmol, 1 eq) in anhydrous dimethylformamide (10 mL), dicyclohexyl carbodiimide (0.71 mmol, 1 eq) and *N*-hydroxysuccinimide (0.71 mmol, 1 eq) were added at 0 °C. After 16 hours the reaction mixture was filtered, and the liquid was concentrated *in vacuo* to give the crude product that was purified by column chromatography on silica gel and a mixture of petroleum ether /ethyl acetate (2:1).

2,5-Dioxopyrrolidin-1-yl 2-fluorobenzoate (101). White solid (77% yield). ^{1}H NMR (400 MHz, $CDCl_3$), δ ppm= 8.06 (td, 1H), 7.89 (m, 1H), 7.5 (m, 2H), 2.89 (s, 4H).

3.9.1.16 Preparation of 2-fluorobenzohydrazide N-substituted **93-98**

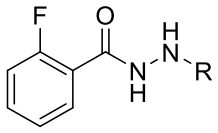

93-98

To a solution of the appropriate hydrazine hydrochloride (0.4 mmol, 1 eq) in anhydrous dichloromethane (5 mL), triethylamine (0.8 mmol, 2 eq) and 2,5-dioxopyrrolidin-1-yl 2-fluorobenzoate **101** (0.4 mmol, 1 eq) were added. The reaction mixture was stirred at room temperature for 2 hours and then quenched by the addition of 5 mL of aqueous 10% acetic acid. The mixture was extracted with dichloromethane, washed with brine, dried over sodium sulfate. After filtration and evaporation of the solvent, the solid residue was purified by column chromatography on silica gel and the appropriate volumes mixture of cyclohexane/ethyl acetate.

2-Fluoro-*N'*-phenylbenzohydrazide (93). White solid (17 % yield). ^{1}H NMR (400 MHz, $CDCl_3$), δ ppm= 8.36 (d, 1H), 8.04 (qd, 1H), 7.47 (m, 1H), 7.21 (m, 5H), 6.86 (t, 3H). ^{13}C NMR (400 MHz, $CDCl_3$), δ ppm=163.65, 161.95, 159.58, 147.88, 134.05, 132.25, 129.26, 125.09, 121.55, 119.23, 116.27, 116.03, 113.90.

2-Fluoro-*N'*-(4-fluorophenyl) benzohydrazide (94). White solid (14% yield). ^{1}H NMR (400 MHz, $CDCl_3$), δ ppm= 8.35 (d; 1H), 8.03 (td, 1H), 7.48 (qd, 1H), 7.19 (m, 4H), 6.86 (m, 3H). ^{13}C NMR (400 MHz, $CDCl_3$), δ ppm= 164.55, 160.88, 158.40, 157.58, 146.12, 133.23, 133.15, 130.47, 130.44, 125.11, 125.09, 123.43, 123.43, 123.28, 116.77, 116.55, 115.81, 115.59, 113.98, 113.90.

2-Fluoro-*N′*-(4-(trifluoromethyl) phenyl) benzohydrazide (95). White solid (8% yield). ^{1}H NMR (400 MHz, $CDCl_3$), δ ppm= 8.37 (d, 1H), 8.12 (td, 1H), 7.58 (qd, 1H), 7.51 (d, 2H), 7.33 (t, 1H), 7.25 (m, 1H), 6.98 (d, 2H), 6.54 (s broad, 1H). ^{13}C NMR (400 MHz, $CDCl_3$), δ ppm= 164.09, 164.04, 161.98, 159.52, 150.77, 134.46, 132.22, 126.70, 126.67, 125.25, 125.15, 118.73, 116.37, 113.11, 100.00.

2-Fluoro-*N′*-(p-tolyl)benzohydrazide (96). Yellowish solid. (17% yield). ^{1}H-NMR (400 MHz, $CDCl_3$) δ ppm= 8.44 (d, 1H), 8.12 (td, 1H), 7.54 (qd, 1H), 7.31 (t, 2H), 7.20 (dd,1H), 6.93 (d, 2H), 6.84 (d, 2H), 3.77 (s, 3H). ^{13}C NMR (400 MHz, $CDCl_3$) δ ppm= 161.20, 160.71, 152.85, 140.93, 133.70, 128.40, 124.00, 120.86, 117.24, 114.62, 113.21, 56.04.

2-Fluoro-*N′*-(tetrahydro-2H-pyran-3-yl) benzohydrazide (97). White solid (25% yield). ^{1}HNMR (400 MHz, $CDCl_3$), δ ppm= 8.09 (td, 1H), 7,51 (qd, 1H), 7.29 (t, 2H), 7.16 (dd, 1H), 3.9 (dd, 1H), 3.75 (m, 1H), 3.55 (m, 1H), 3.45 (dd, 1H), 3.12 (quin, 1H), 2.00 (m,1 H), 1.82 (m, 1H), 1.58 (m, 2H). ^{13}C NMR (400 MHz, $CDCl_3$), δ ppm= 163.54, 161.78, 159.30, 133.84, 133.74, 124.95, 119.29, 116.25, 115.97, 70.34, 68.21, 55.94, 27.63, 23.83.

***N′*-cyclohexyl-2-fluorobenzohydrazide (98).** White solid (17% yield). ^{1}H NMR (400 MHz, $CDCl_3$), δ (ppm): 8.02 (t, 1H), 7.42 (q, 1H), 7.21 (t, 1H), 7.06 (t, 1H), 2.84 (s broad, 1H), 1.86 (d, 2H), 1.69 (m broad, 2H), 1.56 (d, 1H), 1.16 (m, 6H). ^{13}C NMR (400 MHz, DMSO), δ ppm= 161.77, 159.30, 133.62, 133.53, 131.88, 124.93, 116.19, 115.94, 59.22, 31.14, 25.91, 24.47.

3.9.2 Mycobacterium tuberculosis H37Rv growth inhibition assay.

The anti-mycobacterial activity was determined using the serial dilution method in liquid medium culture. 10 mL of MTB (ATCC27294) was grown up to an OD_{600} of 0.6-0.7, followed by dilution 1: 500 with 7H9 or 1: 100 with GAST-Fe. 50 μL of culture medium were added in rows 2-12 of a 96-well plate. The compounds (previously dissolved in DMSO) were added in line 1 in duplicate, to obtain a final concentration of 640 μM. A double dilution was then carried out by transferring 50 μL of liquid from line 1 to line 2.50 μL of liquid from line 2 to line 3, and so on to line 12. Three controls were used: 5% DMSO, rifampicin and Kanamycin. Finally, 50 μL of the culture of MTB (1: 500 for 7H9 or 1: 100 for GAST-Fe) were added to all rows 2-12. The plate was sealed to prevent the wells on the margins being dry and then incubated at 37 ° C, and the MIC_{99} readings were performed for one week and two weeks.

Finally, Sauton's medium was added with dipalmitoyl phosphatidylcholine (DPPC) (0.1 mM) and used to determine the MIC_{99} of the derivatives as before.

3.9.3 Vero cells cytotoxicity assay.

This experiment was carried out as previously described[131]. Briefly, Vero cells were grown and maintained in RPMI 1640 medium supplemented with 2 mM of L-glutamine and 10% FCS. Cells were seeded in 96-well plates at a density of $1x10^4$ cells/well. After 24 h, medium was replaced with fresh medium containing decreasing concentrations of the tested compound and incubated at 37°C in 5% CO_2. Morphological changes were observed at 24, 48 and 72 h of incubation. The effects on the proliferation of Vero cells were determined after 72 h by tetrazolium-based

colorimetric MTT assay. The 50% cell-inhibitory concentration (CC_{50}) reduced by 50% the optical density values ($OD_{540,690}$) with respect to control no-drug treated cells.

3.9.4 Isolation of M. bovis BCG mutants resistant to 40 and INH.

Mycobacterial strains were grown in Middlebrook 7H9 broth (Becton Dickinson) supplemented with 0.05% Tween 80 and 10% (vol/vol) albumin-dextrose-catalase (ADC) enrichment (Becton Dickinson). Mycobacterial cultures were grown at 37 °C with shaking for about one week, until reached exponential growth phase (OD_{600}= 0.4-0.5). Compounds **73** and INH were dissolved in dimethyl sulfoxide. Cultures were diluted to the final concentration of about 10^7 CFU/mL and 1 µL of dilutions and then streaked onto plates containing 2-fold scalar dilutions of compounds **73** and INH. The MIC was defined as the lowest concentration of drug preventing bacterial growth. All experiments were repeated three times.

M. tuberculosis and *M. bovis* mutants resistant to compounds **73** and INH were isolated by plating about 10^{10} cells from wild-type cultures (OD_{600}= 0.5-0.6) onto solid media containing different concentrations of each compound, ranging from 3 to 10-fold MIC for the wild-type strain. Plates were incubated at 37 °C for 4 weeks. The MIC of compounds **73** and INH for the isolated resistant mutants was evaluated three times.

3.9.5 Broth Microdilution Checkerboard Method

The MICs of the individual compounds **73** (0.063 to 8 µg/mL), **65** (0.125 to 16 µg/mL), **54** (0.063 to 8 µg/mL), and isoniazid (0.025 to 0.4 µg/mL) and of the combinations were determined using the broth microdilution technique as described in the literature[132]. Briefly, the broth microdilution plates were inoculated with BCG colture (OD_{600}= 0.3-0.5) in 100 µL 7H9/ADC/Tween broth (OD_{600}= 0.006) and

incubated for 4 days at 37 °C. Column 11 with no antibiotic was used as a positive growth control on each plate. After 4 days of incubation 20 µL of Resazurin (Sigma-Aldrich) aqueous solution (0.02%) were added to each well. Plates were read for visual change of colour, and results were recorded after 24 h of incubation at 37 °C. The MIC was determined as the well in the microtiter plate with the lowest drug concentration at which there was blue colour of no growth. The MICs of single drugs A and B (MIC_A and MIC_B) and in combination (MIC_{AB} and MIC_{BA}) were determined after 4 days of incubation at 37°C. MIC_{AB} was defined as the MIC of drug A in the presence of drug B; MIC_{BA} was defined as the MIC of drug B in the presence of drug A. The fractional inhibitory concentration index (FICI) was calculated for each compound in each combination by using the following formula: $FIC_A + FIC_B = FICI$, where FIC_A equals the MIC of drug A in combination divided by the MIC of drug A alone and FIC_B equals the MIC of drug B in combination divided by the MIC of drug B alone. The FICIs were interpreted as follows: synergy, FICI of ≤ 0.5; additivity, FICI of >0.5 to ≤ 1; no interaction (indifference), FICI of >1 to ≤ 4; antagonism, FICI of >4.

Concluding Remarks

The research reported in this thesis investigated two novel approaches to eradicate MTB infection, developing new chemical entities.

With the optimization of Mmpl3 inhibitor **BM635** we obtained a new potent antimycobacterial pyrazole, effective in a murine model of TB infection and promising candidate for pre-clinical trials.

Carrying out the SAR analyses on the MTB Trp biosynthesis inhibitor 6-FABA, we identified a new class of aryl hydrazides as antimycobacterial agents with an outstanding *in vitro* safety/activity profile.

These results highlighted as MmpL3 and Trp biosynthetic pathway are an attractive druggable targets for the further perspectives in the anti-TB research field and valuable strategies to overcome the drug-resistance.

Chapter 5. References

1 WHO. (2017) Global tuberculosis report.

2 Hingley-Wilson, S.M., Sambandamurthy, V.K. and Jacobs, W.R., Jr. (2003) Survival perspectives from the world's most successful pathogen, Mycobacterium tuberculosis. *Nat Immunol*, **4**, 949-955.

3 Paulson, T. (2013) Epidemiology: A mortal foe. *Nature*, **502**, S2-3.

4 Katalinic Jankovic V., F.L., Cirillo D.M. (2015) Microbiology of Mycobacterium tuberculosis and a new diagnostic test for TB. *Eur Res Monog*, 1-13.

5 Abrahams, K.A. and Besra, G.S. (2018) Mycobacterial cell wall biosynthesis: a multifaceted antibiotic target. *Parasitology*, **145**, 116-133.

6 Gordon, S.V. and Parish, T. (2018) Microbe Profile: Mycobacterium tuberculosis: Humanity's deadly microbial foe. *Microbiology*, **164**, 437-439.

7 Pai, M., Behr, M.A., Dowdy, D., Dheda, K., Divangahi, M., Boehme, C.C., Ginsberg, A., Swaminathan, S., Spigelman, M., Getahun, H. *et al.* (2016) Tuberculosis. *Nat rev Dis primers*, **2**, 16076.

8 Garcia-Aguilar, T., Espinosa-Cueto, P., Magallanes-Puebla, A., Mancilla, R. (2016) The Mannose Receptor Is Involved in the Phagocytosis of Mycobacteria-Induced Apoptotic Cells. *J Immunol Res*, **2016**, 1-14.

9 Lugo-Villarino, G., Troegeler, A., Balboa, L., Lastrucci, C., Duval, C., Mercier, I., Benard, A., Capilla, F., Al Saati, T., Poincloux, R. *et al.* (2018) The C-Type Lectin Receptor DC-SIGN Has an Anti-Inflammatory Role in Human M(IL-4)

Macrophages in Response to Mycobacterium tuberculosis. *Front Immunol*, **9**, 1123-1138.

10 Lang, R. (2013) Recognition of the mycobacterial cord factor by Mincle: relevance for granuloma formation and resistance to tuberculosis. *Front Immunol*, **4**, 5-12.

11 Kang, B.K. and Schlesinger, L.S. (1998) Characterization of mannose receptor-dependent phagocytosis mediated by Mycobacterium tuberculosis lipoarabinomannan. *Infect Immun*, **66**, 2769-2777.

12 Pradhan, G., Shrivastva, R. and Mukhopadhyay, S. (2018) Mycobacterial PknG Targets the Rab7l1 Signaling Pathway To Inhibit Phagosome-Lysosome Fusion. *J Immunol*, **201**, 1421-1433.

13 Jamwal, S.V., Mehrotra, P., Singh, A., Siddiqui, Z., Basu, A. and Rao, K.V. (2016) Mycobacterial escape from macrophage phagosomes to the cytoplasm represents an alternate adaptation mechanism. *Sci Rep*, **6**, 23089-23098.

14 Romagnoli, A., Etna, M.P., Giacomini, E., Pardini, M., Remoli, M.E., Corazzari, M., Falasca, L., Goletti, D., Gafa, V., Simeone, R. *et al.* (2012) ESX-1 dependent impairment of autophagic flux by Mycobacterium tuberculosis in human dendritic cells. *Autophagy*, **8**, 1357-1370.

15 Cooper, A.M. (2009) Cell-mediated immune responses in tuberculosis. *Annu Rev Immunol*, **27**, 393-422.

16 Chai, Q., Zhang, Y. and Liu, C.H. (2018) Mycobacterium tuberculosis: An Adaptable Pathogen Associated With Multiple Human Diseases. *Front Cell Infect Mi*, **8**, 158-173.

17 Yuan, T. and Sampson, N.S. (2018) Hit Generation in TB Drug Discovery: From Genome to Granuloma. *Chem Rev*, **118**, 1887-1916.

18 Al Shammari, B., Shiomi, T., Tezera, L., Bielecka, M.K., Workman, V., Sathyamoorthy, T., Mauri, F., Jayasinghe, S.N., Robertson, B.D., D'Armiento, J. *et al.* (2015) The Extracellular Matrix Regulates Granuloma Necrosis in Tuberculosis. *J Infect Dis*, **212**, 463-473.

19 Rittershaus, E.S., Baek, S.H. and Sassetti, C.M. (2013) The normalcy of dormancy: common themes in microbial quiescence. *Cell Host Microbe*, **13**, 643-651.

20 Dutta, N.K. and Karakousis, P.C. (2014) Latent tuberculosis infection: myths, models, and molecular mechanisms. *Microbiol Mol Bio R*, **78**, 343-371.

21 WHO. (2009) Guidelines for treatment of tuberculosis 4th edition.

22 WHO. (2016) WHO treatment guideline for drug-resistant tuberculosis.

23 WHO. (2016) The shorter MDR-TB regimen.

24 WHO. (2014) World Health Organization. Guidelines on the Management of Latent Tuberculosis Infection.

25 Bruchfeld, J., Correia-Neves, M. and Kallenius, G. (2015) Tuberculosis and HIV Coinfection. *CSH Perspec Med*, **5**, a017871.

26 Poce, G., Cocozza, M., Consalvi, S. and Biava, M. (2014) SAR analysis of new anti-TB drugs currently in pre-clinical and clinical development. *Eur J Med Chem*, **86**, 335-351.

27 Fox, G.J. and Menzies, D. (2013) A Review of the Evidence for Using Bedaquiline (TMC207) to Treat Multi-Drug Resistant Tuberculosis. *Infec Dis T*, **2**, 123-144.

28 Prevention, C.f.D.C.a. (2013) Provisional CDC guidelines for the use and safety monitoring of bedaquiline fumarate (Sirturo) for the treatment of multidrug-resistant tuberculosis. *MMWR* **62**, 1-16.

29 Gler, M.T., Skripconoka, V., Sanchez-Garavito, E., Xiao, H., Cabrera-Rivero, J.L., Vargas-Vasquez, D.E., Gao, M., Awad, M., Park, S.K., Shim, T.S. *et al.* (2012)

Delamanid for multidrug-resistant pulmonary tuberculosis. *New Engl J Med*, **366**, 2151-2160.

30 Andries, K., Verhasselt, P., Guillemont, J., Gohlmann, H.W., Neefs, J.M., Winkler, H., Van Gestel, J., Timmerman, P., Zhu, M., Lee, E. *et al.* (2005) A diarylquinoline drug active on the ATP synthase of Mycobacterium tuberculosis. *Science*, **307**, 223-227.

31 Huitric, E., Verhasselt, P., Andries, K. and Hoffner, S.E. (2007) In vitro antimycobacterial spectrum of a diarylquinoline ATP synthase inhibitor. *Antimicrob Agents Ch*, **51**, 4202-4204.

32 Koul, A., Dendouga, N., Vergauwen, K., Molenberghs, B., Vranckx, L., Willebrords, R., Ristic, Z., Lill, H., Dorange, I., Guillemont, J. *et al.* (2007) Diarylquinolines target subunit c of mycobacterial ATP synthase. *Nat Chem Bio*, **3**, 323-324.

33 Haagsma, A.C., Podasca, I., Koul, A., Andries, K., Guillemont, J., Lill, H. and Bald, D. (2011) Probing the interaction of the diarylquinoline TMC207 with its target mycobacterial ATP synthase. *PloS one*, **6**, e23575.

34 Matsumoto, M., Hashizume, H., Tomishige, T., Kawasaki, M., Tsubouchi, H., Sasaki, H., Shimokawa, Y. and Komatsu, M. (2006) OPC-67683, a nitro-dihydro-imidazooxazole derivative with promising action against tuberculosis in vitro and in mice. *PloS Med*, **3**, e466.

35 Chen, X., Hashizume, H., Tomishige, T., Nakamura, I., Matsuba, M., Fujiwara, M., Kitamoto, R., Hanaki, E., Ohba, Y. and Matsumoto, M. (2017) Delamanid Kills Dormant Mycobacteria In Vitro and in a Guinea Pig Model of Tuberculosis. *Antimicrob Agents Ch*, **61**, e02402-02416.

36 Stover, C.K., Warrener, P., VanDevanter, D.R., Sherman, D.R., Arain, T.M., Langhorne, M.H., Anderson, S.W., Towell, J.A., Yuan, Y., McMurray, D.N. *et al.*

(2000) A small-molecule nitroimidazopyran drug candidate for the treatment of tuberculosis. *Nature*, **405**, 962-966.

37 Lenaerts, A.J., Gruppo, V., Marietta, K.S., Johnson, C.M., Driscoll, D.K., Tompkins, N.M., Rose, J.D., Reynolds, R.C. and Orme, I.M. (2005) Preclinical testing of the nitroimidazopyran PA-824 for activity against Mycobacterium tuberculosis in a series of in vitro and in vivo models. *Antimicrob Agents Ch*, **49**, 2294-2301.

38 Singh, R., Manjunatha, U., Boshoff, H.I., Ha, Y.H., Niyomrattanakit, P., Ledwidge, R., Dowd, C.S., Lee, I.Y., Kim, P., Zhang, L. *et al.* (2008) PA-824 kills nonreplicating Mycobacterium tuberculosis by intracellular NO release. *Science*, **322**, 1392-1395.

39 Swaney, S.M., Aoki, H., Ganoza, M.C. and Shinabarger, D.L. (1998) The oxazolidinone linezolid inhibits initiation of protein synthesis in bacteria. *Antimicrob Agents Ch*, **42**, 3251-3255.

40 Barbachyn, M.R., Hutchinson, D.K., Brickner, S.J., Cynamon, M.H., Kilburn, J.O., Klemens, S.P., Glickman, S.E., Grega, K.C., Hendges, S.K., Toops, D.S. *et al.* (1996) Identification of a novel oxazolidinone (U-100480) with potent antimycobacterial activity. *J Med Chem*, **39**, 680-685.

41 Cynamon, M.H., Klemens, S.P., Sharpe, C.A. and Chase, S. (1999) Activities of several novel oxazolidinones against Mycobacterium tuberculosis in a murine model. *Antimicrob Agents Ch*, **43**, 1189-1191.

42 Wallis, R.S., Jakubiec, W., Kumar, V., Bedarida, G., Silvia, A., Paige, D., Zhu, T., Mitton-Fry, M., Ladutko, L., Campbell, S. *et al.* (2011) Biomarker-assisted dose selection for safety and efficacy in early development of PNU-100480 for tuberculosis. *Antimicrob Agents Ch*, **55**, 567-574.

43 Wallis, R.S., Jakubiec, W.M., Kumar, V., Silvia, A.M., Paige, D., Dimitrova, D., Li, X., Ladutko, L., Campbell, S., Friedland, G. *et al.* (2010) Pharmacokinetics and whole-blood bactericidal activity against Mycobacterium tuberculosis of single doses of PNU-100480 in healthy volunteers. *J Infect Dis*, **202**, 745-751.

44 Jeong, J.W., Jung, S.J., Lee, H.H., Kim, Y.Z., Park, T.K., Cho, Y.L., Chae, S.E., Baek, S.Y., Woo, S.H., Lee, H.S. *et al.* (2010) In vitro and in vivo activities of LCB01-0371, a new oxazolidinone. *Antimicrob Agents Ch*, **54**, 5359-5362.

45 Zong, Z., Jing, W., Shi, J., Wen, S., Zhang, T., Huo, F., Shang, Y., Liang, Q., Huang, H. and Pang, Y. (2018) Comparison of In Vitro Activity and MIC Distributions between the Novel Oxazolidinone Delpazolid and Linezolid against Multidrug-Resistant and Extensively Drug-Resistant Mycobacterium tuberculosis in China. *Antimicrob Agents Ch*, **62**, e00165-00118.

46 Choi, Y., Lee, S.W., Kim, A., Jang, K., Nam, H., Cho, Y.L., Yu, K.S., Jang, I.J. and Chung, J.Y. (2018) Safety, tolerability and pharmacokinetics of 21 day multiple oral administration of a new oxazolidinone antibiotic, LCB01-0371, in healthy male subjects. *J Antimicrob Chemot*, **73**, 183-190.

47 Shoen, C., DeStefano, M., Hafkin, B. and Cynamon, M. (2018) In Vitro and In Vivo Activities of Contezolid (MRX-I) against Mycobacterium tuberculosis. *Antimicrob Agents Ch*, **62**, e00493-00418.

48 Makarov, V., Manina, G., Mikusova, K., Mollmann, U., Ryabova, O., Saint-Joanis, B., Dhar, N., Pasca, M.R., Buroni, S., Lucarelli, A.P. *et al.* (2009) Benzothiazinones kill Mycobacterium tuberculosis by blocking arabinan synthesis. *Science*, **324**, 801-804.

49 Trefzer, C., Skovierova, H., Buroni, S., Bobovska, A., Nenci, S., Molteni, E., Pojer, F., Pasca, M.R., Makarov, V., Cole, S.T. *et al.* (2012) Benzothiazinones are suicide

inhibitors of mycobacterial decaprenylphosphoryl-beta-D-ribofuranose 2'-oxidase DprE1. *J Am Chem Soc*, **134**, 912-915.

50 Tiwari, R., Moraski, G.C., Krchnak, V., Miller, P.A., Colon-Martinez, M., Herrero, E., Oliver, A.G. and Miller, M.J. (2013) Thiolates chemically induce redox activation of BTZ043 and related potent nitroaromatic anti-tuberculosis agents. *J Am Chem Soc*, **135**, 3539-3549.

51 Piton, J., Foo, C.S. and Cole, S.T. (2017) Structural studies of Mycobacterium tuberculosis DprE1 interacting with its inhibitors. *Drug Discov Today*, **22**, 526-533.

52 Makarov, V., Lechartier, B., Zhang, M., Neres, J., van der Sar, A.M., Raadsen, S.A., Hartkoorn, R.C., Ryabova, O.B., Vocat, A., Decosterd, L.A. *et al.* (2014) Towards a new combination therapy for tuberculosis with next generation benzothiazinones. *EMBO Mol Med*, **6**, 372-383.

53 http://im4tb.org/news/.

54 Lee, R.E., Protopopova, M., Crooks, E., Slayden, R.A., Terrot, M. and Barry, C.E., 3rd. (2003) Combinatorial lead optimization of [1,2]-diamines based on ethambutol as potential antituberculosis preclinical candidates. *J Comb Chem*, **5**, 172-187.

55 Protopopova, M., Hanrahan, C., Nikonenko, B., Samala, R., Chen, P., Gearhart, J., Einck, L. and Nacy, C.A. (2005) Identification of a new antitubercular drug candidate, SQ109, from a combinatorial library of 1,2-ethylenediamines. *J Antimicrob Chemoth*, **56**, 968-974.

56 Jia, L., Tomaszewski, J.E., Hanrahan, C., Coward, L., Noker, P., Gorman, G., Nikonenko, B. and Protopopova, M. (2005) Pharmacodynamics and pharmacokinetics of SQ109, a new diamine-based antitubercular drug. *Brit J Pharmacol*, **144**, 80-87.

57 Sacksteder, K.A., Protopopova, M., Barry, C.E., 3rd, Andries, K. and Nacy, C.A. (2012) Discovery and development of SQ109: a new antitubercular drug with a novel mechanism of action. *Future Microbiol*, **7**, 823-837.

58 Tullius, M.V., Harmston, C.A., Owens, C.P., Chim, N., Morse, R.P., McMath, L.M., Iniguez, A., Kimmey, J.M., Sawaya, M.R., Whitelegge, J.P. *et al.* (2011) Discovery and characterization of a unique mycobacterial heme acquisition system. *P Natl Acad Sci USA*, **108**, 5051-5056.

59 Tahlan, K., Wilson, R., Kastrinsky, D.B., Arora, K., Nair, V., Fischer, E., Barnes, S.W., Walker, J.R., Alland, D., Barry, C.E., 3rd *et al.* (2012) SQ109 targets MmpL3, a membrane transporter of trehalose monomycolate involved in mycolic acid donation to the cell wall core of Mycobacterium tuberculosis. *Antimicrob Agents Ch*, **56**, 1797-1809.

60 Barry, V.C., Belton, J.G., Conalty, M.L., Denneny, J.M., Edward, D.W., O'Sullivan, J.F., Twomey, D. and Winder, F. (1957) A new series of phenazines (rimino-compounds) with high antituberculosis activity. *Nature*, **179**, 1013-1015.

61 O'Connor, R., O'Sullivan, J.F. and O'Kennedy, R. (1995) The pharmacology, metabolism, and chemistry of clofazimine. *Drug Metab Rev*, **27**, 591-614.

62 Kasim, N.A., Whitehouse, M., Ramachandran, C., Bermejo, M., Lennernas, H., Hussain, A.S., Junginger, H.E., Stavchansky, S.A., Midha, K.K., Shah, V.P. *et al.* (2004) Molecular properties of WHO essential drugs and provisional biopharmaceutical classification. *Mol Pharm*, **1**, 85-96.

63 Zhang, D., Liu, Y., Zhang, C., Zhang, H., Wang, B., Xu, J., Fu, L., Yin, D., Cooper, C.B., Ma, Z. *et al.* (2014) Synthesis and biological evaluation of novel 2-methoxypyridylamino-substituted riminophenazine derivatives as antituberculosis agents. *Molecules*, **19**, 4380-4394.

64 Morrison, N.E. and Marley, G.M. (1976) The mode of action of clofazimine DNA binding studies. *Int J Lepr Other Mycobact Dis*, **44**, 133-134.

65 Morrison, N.E. and Marley, G.M. (1976) Clofazimine binding studies with deoxyribonucleic acid. *Int J Lepr Other Mycobact Dis*, **44**, 475-481.

66 Krajewska, M.M. and Anderson, R. (1993) An in vitro comparison of the effects of the prooxidative riminophenazines clofazimine and B669 on neutrophil phospholipase A2 activity and superoxide generation. *J Infect Dis*, **167**, 899-904.

67 Steel, H.C., Matlola, N.M. and Anderson, R. (1999) Inhibition of potassium transport and growth of mycobacteria exposed to clofazimine and B669 is associated with a calcium-independent increase in microbial phospholipase A2 activity. *J Antimicrob Chemother*, **44**, 209-216.

68 Yano, T., Kassovska-Bratinova, S., Teh, J.S., Winkler, J., Sullivan, K., Isaacs, A., Schechter, N.M. and Rubin, H. (2011) Reduction of clofazimine by mycobacterial type 2 NADH:quinone oxidoreductase: a pathway for the generation of bactericidal levels of reactive oxygen species. *J Biol Chem*, **286**, 10276-10287.

69 Kang, S., Kim, R.Y., Seo, M.J., Lee, S., Kim, Y.M., Seo, M., Seo, J.J., Ko, Y., Choi, I., Jang, J. *et al.* (2014) Lead optimization of a novel series of imidazo[1,2-a]pyridine amides leading to a clinical candidate (Q203) as a multi- and extensively-drug-resistant anti-tuberculosis agent.*J Med Chem*, **57**, 5293-5305.

70 Pethe, K., Bifani, P., Jang, J., Kang, S., Park, S., Ahn, S., Jiricek, J., Jung, J., Jeon, H.K., Cechetto, J. *et al.* (2013) Discovery of Q203, a potent clinical candidate for the treatment of tuberculosis. *Nat Med*, **19**, 1157-1160.

71 Kalia, N.P., Hasenoehrl, E.J., Ab Rahman, N.B., Koh, V.H., Ang, M.L.T., Sajorda, D.R., Hards, K., Gruber, G., Alonso, S., Cook, G.M. *et al.* (2017) Exploiting the

synthetic lethality between terminal respiratory oxidases to kill Mycobacterium tuberculosis and clear host infection. *PNAS*, **114**, 7426-7431.

72 Vondenhoff, G.H. and Van Aerschot, A. (2011) Aminoacyl-tRNA synthetase inhibitors as potential antibiotics. *Eur J Med Chem*, **46**, 5227-5236.

73 Rock, F.L., Mao, W., Yaremchuk, A., Tukalo, M., Crepin, T., Zhou, H., Zhang, Y.K., Hernandez, V., Akama, T., Baker, S.J. *et al.* (2007) An antifungal agent inhibits an aminoacyl-tRNA synthetase by trapping tRNA in the editing site. *Science*, **316**, 1759-1761.

74 Palencia, A., Li, X., Bu, W., Choi, W., Ding, C.Z., Easom, E.E., Feng, L., Hernandez, V., Houston, P., Liu, L. *et al.* (2016) Discovery of Novel Oral Protein Synthesis Inhibitors of Mycobacterium tuberculosis That Target Leucyl-tRNA Synthetase. *Antimicrob Agents Chemother*, **60**, 6271-6280.

75 Li, X., Hernandez, V., Rock, F.L., Choi, W., Mak, Y.S.L., Mohan, M., Mao, W., Zhou, Y., Easom, E.E., Plattner, J.J. *et al.* (2017) Discovery of a Potent and Specific M. tuberculosis Leucyl-tRNA Synthetase Inhibitor: (S)-3-(Aminomethyl)-4-chloro-7-(2-hydroxyethoxy)benzo[c][1,2]oxaborol-1(3H)-ol (GSK656). *J Med Chem*, **60**, 8011-8026.

76 Shirude, P.S., Shandil, R., Sadler, C., Naik, M., Hosagrahara, V., Hameed, S., Shinde, V., Bathula, C., Humnabadkar, V., Kumar, N. *et al.* (2013) Azaindoles: noncovalent DprE1 inhibitors from scaffold morphing efforts, kill Mycobacterium tuberculosis and are efficacious in vivo. *J Med Chem*, **56**, 9701-9708.

77 Shirude, P.S., Shandil, R.K., Manjunatha, M.R., Sadler, C., Panda, M., Panduga, V., Reddy, J., Saralaya, R., Nanduri, R., Ambady, A. *et al.* (2014) Lead optimization of 1,4-azaindoles as antimycobacterial agents. *J Med Chem*, **57**, 5728-5737.

78 Chatterji, M., Shandil, R., Manjunatha, M.R., Solapure, S., Ramachandran, V., Kumar, N., Saralaya, R., Panduga, V., Reddy, J., Prabhakar, K.R. *et al.* (2014) 1,4-azaindole, a potential drug candidate for treatment of tuberculosis. *Antimicrob Agents Chemother*, **58**, 5325-5331.

79 Deidda, D., Lampis, G., Fioravanti, R., Biava, M., Porretta, G.C., Zanetti, S. and Pompei, R. (1998) Bactericidal activities of the pyrrole derivative BM212 against multidrug-resistant and intramacrophagic Mycobacterium tuberculosis strains. *Antimicrob Agents Chemother*, **42**, 3035-3037.

80 Poce, G., Bates, R.H., Alfonso, S., Cocozza, M., Porretta, G.C., Ballell, L., Rullas, J., Ortega, F., De Logu, A., Agus, E. *et al.* (2013) Improved BM212 MmpL3 inhibitor analogue shows efficacy in acute murine model of tuberculosis infection. *PLoS One*, **8**, e56980.

81 Poce, G., Consalvi, S., Cocozza, M., Fernandez-Menendez, R., Bates, R.H., Ortega Muro, F., Barros Aguirre, D., Ballell, L. and Biava, M. (2017) Pharmaceutical salt of BM635 with improved bioavailability. *Eur J Pharma Sci*, **99**, 17-23.

82 Poce, G., Cocozza, M., Alfonso, S., Consalvi, S., Venditti, G., Fernandez-Menendez, R., Bates, R.H., Barros Aguirre, D., Ballell, L., De Logu, A. *et al.* (2018) In vivo potent BM635 analogue with improved drug-like properties. *Eur J Med Chem*, **145**, 539-550.

83 La Rosa, V., Poce, G., Canseco, J.O., Buroni, S., Pasca, M.R., Biava, M., Raju, R.M., Porretta, G.C., Alfonso, S., Battilocchio, C. *et al.* (2012) MmpL3 is the cellular target of the antitubercular pyrrole derivative BM212. *Antimicrob Agents Chemother*, **56**, 324-331.

84 Grzegorzewicz, A.E., Pham, H., Gundi, V.A., Scherman, M.S., North, E.J., Hess, T., Jones, V., Gruppo, V., Born, S.E., Kordulakova, J. *et al.* (2012) Inhibition of mycolic

acid transport across the Mycobacterium tuberculosis plasma membrane. *Nat Chemi Bio*, **8**, 334-341.

85 Poce, G., Consalvi, S. and Biava, M. (2016) MmpL3 Inhibitors: Diverse Chemical Scaffolds Inhibit the Same Target. *Mini Rev Med Chem*, **16**, 1274-1283.

86 Campanico, A., Moreira, R. and Lopes, F. (2018) Drug discovery in tuberculosis. New drug targets and antimycobacterial agents. *Eur J Med Chem*, **150**, 525-545.

87 Li, W., Upadhyay, A., Fontes, F.L., North, E.J., Wang, Y., Crans, D.C., Grzegorzewicz, A.E., Jones, V., Franzblau, S.G., Lee, R.E. *et al.* (2014) Novel insights into the mechanism of inhibition of MmpL3, a target of multiple pharmacophores in Mycobacterium tuberculosis. *Antimicrob Agents Chemother*, **58**, 6413-6423.

88 Xu, Z., Meshcheryakov, V.A., Poce, G. and Chng, S.S. (2017) MmpL3 is the flippase for mycolic acids in mycobacteria. *PNAS*, **114**, 7993-7998.

89 Ramesh, R., Shingare, R.D., Kumar, V., Anand, A., B, S., Veeraraghavan, S., Viswanadha, S., Ummanni, R., Gokhale, R. and Srinivasa Reddy, D. (2016) Repurposing of a drug scaffold: Identification of novel sila analogues of rimonabant as potent antitubercular agents. *Eur J Med Chem*, **122**, 723-730.

90 Wuitschik, G., Rogers-Evans, M., Buckl, A., Bernasconi, M., Marki, M., Godel, T., Fischer, H., Wagner, B., Parrilla, I., Schuler, F. *et al.* (2008) Spirocyclic oxetanes: synthesis and properties. *Angew Chem*, **47**, 4512-4515.

91 Wuitschik, G., Carreira, E.M., Wagner, B., Fischer, H., Parrilla, I., Schuler, F., Rogers-Evans, M. and Muller, K. (2010) Oxetanes in drug discovery: structural and synthetic insights. *J Med Chem*, **53**, 3227-3246.

92 Brandt, T. A. (2006) Process for preparing bicyclic pyrazolyl compounds. WO 035310.

93 Pommery, N., Taverne, T., Telliez, A., Goossens, L., Charlier, C., Pommery, J., Goossens, J.F., Houssin, R., Durant, F. and Henichart, J.P. (2004) New COX-2/5-LOX inhibitors: apoptosis-inducing agents potentially useful in prostate cancer chemotherapy. *J Med Chem*, **47**, 6195-6206.

94 Kobayashi, K., Tsujita, T., Ito, H., Ozaki, S., Tani, T., Ishii, Y., Okuda, S., Tadano, K., Fukuroda, T., Ohta, H. *et al.* (2009) Identification of MK-1925: a selective, orally active and brain-penetrable opioid receptor-like 1 (ORL1) antagonist. *Bioorganic Med Chem Lett*, **19**, 4729-4732.

95 Dess B D, Martin, .J.C. (1983) Readily accessible 12-I-5 oxidant for the conversion of primary and secondary alcohols to aldehydes and ketones. *J Org Chem*, **48**, 4155-4156.

96 Abdel-Magid, A. F., Harris, B. D., Maryanoff, C. A., Shah, R. D. (1996) Reductive Amination of Aldehydes and Ketones with Sodium Triacetoxyborohydride. Studies on Direct and Indirect Reductive Amination Procedures. *J Org Chem*, **61**, 3849–3862.

97 Ishikawa, M. and Hashimoto, Y. (2011) Improvement in aqueous solubility in small molecule drug discovery programs by disruption of molecular planarity and symmetry. *J Med Chem*, **54**, 1539-1554.

98 Valko K, B.C., Reynolds D (1997) Chromatographic hydrophobicity index by fast-gradient RP-HPLC: A high-throughput alternative to log P/log D. *Anal Chem*, **69**, 2022–2029.

99 Ward, S.E., Harries, M., Aldegheri, L., Austin, N.E., Ballantine, S., Ballini, E., Bradley, D.M., Bax, B.D., Clarke, B.P., Harris, A.J. *et al.* (2011) Integration of lead optimization with crystallography for a membrane-bound ion channel target:

discovery of a new class of AMPA receptor positive allosteric modulators. *J Med Chem*, **54**, 78-94.

100 Kestranek, A., Chervenak, A., Longenberger, J. and Placko, S. (2013) Chemiluminescent nitrogen detection (CLND) to measure kinetic aqueous solubility. *Curr Protoc Chem Bio*, **5**, 269-280.

101 Valko, K., Nunhuck, S., Bevan, C., Abraham, M.H. and Reynolds, D.P. (2003) Fast gradient HPLC method to determine compounds binding to human serum albumin. Relationships with octanol/water and immobilized artificial membrane lipophilicity. *J Pharm Sci*, **92**, 2236-2248.

102 Chadwick, C.C., Ezrin, A.M., O'Connor, B., Volberg, W.A., Smith, D.I., Wedge, K.J., Hill, R.J., Briggs, G.M., Pagani, E.D., Silver, P.J. *et al.* (1993) Identification of a specific radioligand for the cardiac rapidly activating delayed rectifier K+ channel. *Circ Res*, **72**, 707-714.

103 Rullas, J., Garcia, J.I., Beltran, M., Cardona, P.J., Caceres, N., Garcia-Bustos, J.F. and Angulo-Barturen, I. (2010) Fast standardized therapeutic-efficacy assay for drug discovery against tuberculosis. *Antimicrob Agents Chemother*, **54**, 2262-2264.

104 Zhang, Y.J., Reddy, M.C., Ioerger, T.R., Rothchild, A.C., Dartois, V., Schuster, B.M., Trauner, A., Wallis, D., Galaviz, S., Huttenhower, C. *et al.* (2013) Tryptophan biosynthesis protects mycobacteria from CD4 T-cell-mediated killing. *Cell*, **155**, 1296-1308.

105 Parish, T. (2003) Starvation survival response of Mycobacterium tuberculosis. *J Bacteriol*, **185**, 6702-6706.

106 Molina-Henares, M.A., Garcia-Salamanca, A., Molina-Henares, A.J., de la Torre, J., Herrera, M.C., Ramos, J.L. and Duque, E. (2009) Functional analysis of aromatic

biosynthetic pathways in Pseudomonas putida KT2440. *Microb Biotechnol*, **2**, 91-100.

107 Evans, G.L., Gamage, S.A., Bulloch, E.M., Baker, E.N., Denny, W.A. and Lott, J.S. (2014) Repurposing the chemical scaffold of the anti-arthritic drug Lobenzarit to target tryptophan biosynthesis in Mycobacterium tuberculosis. *Chem Bio Chem*, **15**, 852-864.

108 Abrahams, K.A., Cox, J.A.G., Futterer, K., Rullas, J., Ortega-Muro, F., Loman, N.J., Moynihan, P.J., Perez-Herran, E., Jimenez, E., Esquivias, J. *et al.* (2017) Inhibiting mycobacterial tryptophan synthase by targeting the inter-subunit interface. *Sci Rep*, **7**, 9430-9445.

109 Wellington, S., Nag, P.P., Michalska, K., Johnston, S.E., Jedrzejczak, R.P., Kaushik, V.K., Clatworthy, A.E., Siddiqi, N., McCarren, P., Bajrami, B. *et al.* (2017) A small-molecule allosteric inhibitor of Mycobacterium tuberculosis tryptophan synthase. *Nat Chem Biol*, **13**, 943-950.

110 Cookson, T.V., Castell, A., Bulloch, E.M., Evans, G.L., Short, F.L., Baker, E.N., Lott, J.S. and Parker, E.J. (2014) Alternative substrates reveal catalytic cycle and key binding events in the reaction catalysed by anthranilate phosphoribosyltransferase from Mycobacterium tuberculosis. *Biochem J*, **461**, 87-98.

111 Cookson, T.V., Evans, G.L., Castell, A., Baker, E.N., Lott, J.S. and Parker, E.J. (2015) Structures of Mycobacterium tuberculosis Anthranilate Phosphoribosyltransferase Variants Reveal the Conformational Changes That Facilitate Delivery of the Substrate to the Active Site. *Biochemistry*, **54**, 6082-6092.

112 Lassila, T., Hokkanen, J., Aatsinki, S.M., Mattila, S., Turpeinen, M. and Tolonen, A. (2015) Toxicity of Carboxylic Acid-Containing Drugs: The Role of Acyl Migration and CoA Conjugation Investigated. *Chem Res Toxicol*, **28**, 2292-2303.

113 Li, C., Benet, L.Z. and Grillo, M.P. (2002) Studies on the chemical reactivity of 2-phenylpropionic acid 1-O-acyl glucuronide and S-acyl-CoA thioester metabolites. *Chem Res Toxicol*, **15**, 1309-1317.

114 Barrett, S.D., Bridges, A.J., Dudley, D.T., Saltiel, A.R., Fergus, J.H., Flamme, C.M., Delaney, A.M., Kaufman, M., LePage, S., Leopold, W.R. *et al.* (2008) The discovery of the benzhydroxamate MEK inhibitors CI-1040 and PD 0325901. *Bioorganic Med Chem Lett*, **18**, 6501-6504.

115 Herr, R.J. (2002) 5-Substituted-1H-tetrazoles as carboxylic acid isosteres: medicinal chemistry and synthetic methods. *Bioorganic Med Chem Lett*, **10**, 3379-3393.

116 Ballatore, C., Huryn, D.M. and Smith, A.B. (2013) Carboxylic acid (bio)isosteres in drug design. *ChemMedChem*, **8**, 385-395.

117 Gardner I, O.R., Smith DA, Miao Z, Alex AA, Beaumont K, Kalgutkar A, Walker D, Dalvie D, Prakash C, Alf V. (2010) Metabolism, Pharmacokinetics and Toxicity of Functional Groups, Impact of Chemical Building Blocks on ADMET. **9**, 390-459.

118 Priyanka, L.G., Priyanka S. G., Deepali M. J., Vilasrao J. K. (2012) The Use of Bioisosterism in Drug Design and Molecular Modification. *Int J PharmTech Res*, **2**, 1-23.

119 Black, W.C., Bayly, C.I., Davis, D.E., Desmarais, S., Falgueyret, J.P., Leger, S., Li, C.S., Masse, F., McKay, D.J., Palmer, J.T. *et al.* (2005) Trifluoroethylamines as amide isosteres in inhibitors of cathepsin K. *Bioorganic Med Chem Lett*, **15**, 4741-4744.

120 Tedesco, R., Shaw, A.N., Bambal, R., Chai, D., Concha, N.O., Darcy, M.G., Dhanak, D., Fitch, D.M., Gates, A., Gerhardt, W.G. *et al.* (2006) 3-(1,1-dioxo-2H-(1,2,4)-benzothiadiazin-3-yl)-4-hydroxy-2(1H)-quinolinones, potent inhibitors of hepatitis C virus RNA-dependent RNA polymerase. *J Med Chem*, **49**, 971-983.

121 Chandrappa, S., Chandru, H., Sharada, A. C., Vinaya,K., Ananda Kumar,C. S., Thimmegowda, N. R., Nagegowda, P., Karuna Kumar, M., Rangappa, K. S. (2010) Synthesis and in vivo anticancer and antiangiogenic effects of novel thioxothiazolidin-4-one derivatives against transplantable mouse tumor. *Med Chem Res*, **18**, 236-249.

122 Peet, N.P., Sunder, S. (1984) Factors which influence the formation of oxadiazoles from anthranilhydrazides and other benzoylhydrazides. *J Heterocyclic Chem*, **21**, 1807-1816.

123 Dahl, B. H., Christophersen, P. (2002) Substituted phenyl derivatives, their preparation and use. US 6706749B2.

124 Yang, W., Qiao, R., Chen, J., Huang, X., Liu, M., Gao, W., Ding, J. and Wu, H. (2015) Palladium-Catalyzed Cascade Reaction of 2-Amino-N'-arylbenzohydrazides with Triethyl Orthobenzoates To Construct Indazolo[3,2-b]quinazolinones. *J Org Chem*, **80**, 482-489.

125 Meddour, A., Courtieu, J. (2000) Achiral deuterated derivatizing agent for enantiomeric analysis of carboxylic acids by NMR in a chiral liquid crystalline solvent. *Tetrahedron: Asimmetry*, **11**, 3635-3644.

126 Fang K., H.M., Jockusch S., Turro N. J., Nakanishi K. (1998) A Bifunctional Photoaffinity Probe for Ligand/Receptor Interaction Studies. *J Am Chem Soc*, **120**, 8543-8544.

127 Dinsmore, C., Fuller, P., Guerin, D., Katz, J. D., Thompson, C. F., Falcone, D., Deng, W., Torres, L., Zeng, H., Bai, Y. (2014) Acicyl cyanoethylpyrazole pyridones as janus kinase inhibitors. WO 146493.

128 Setamdideh, D., Khezri, B., Mollapour, M. (2011) Convenient reduction of nitro compounds to their corresponding amines with promotion of $NaBH_4/Ni(OAc)_2$ $4H_2O$ system in wet CH_3CN. *Orient J Chem*, **27**, 991-996.

129 Schmidt, S., Rock, K., Sahre, M., Burkhardt, O., Brunner, M., Lobmeyer, M.T. and Derendorf, H. (2008) Effect of protein binding on the pharmacological activity of highly bound antibiotics. *Antimicrob Agents Chem*, **52**, 3994-4000.

130 Travis, B.R., Sivakumar, M., Hollist, G.O. and Borhan, B. (2003) Facile oxidation of aldehydes to acids and esters with Oxone. *Org Lett*, **5**, 1031-1034.

131 Biava, M., Porretta, G.C., Poce, G., Battilocchio, C., Alfonso, S., De Logu, A., Serra, N., Manetti, F. and Botta, M. (2010) Identification of a novel pyrrole derivative endowed with antimycobacterial activity and protection index comparable to that of the current antitubercular drugs streptomycin and rifampin. *Bioorganic Med Chem*, **18**, 8076-8084.

132 Leber, A. (2016) Synergism Testing: Broth Microdilution Checkerboard and Broth Macrodilution Methods. *In Clinical Microbiology Procedures Handbook, Fourth Edition.*, **5**, 1-23.

Appendix 1. Publications, posters and oral communications

Publications in peer-reviewed journals

2018 Poce, G.; Cocozza, M.; Alfonso, S.; Consalvi, S.; **Venditti, G**.; Fernandez-Menedez, R.; Bates, H. R.; Barros Aguirre, D.; Ballel, L.; De Logu, A.; Vistoli, G.; Biava, M. *Eur. J. Med. Chem.* **2018**,145, 539-550.

2017 **Venditti, G.**; Poce, G.; Consalvi, S.; Biava, M. *Chem. Heterocycl. Compd.* **2017**, Vol 53, No 3 281-291.

Posters presentations/oral presentations

11/2018 Poster: **Venditti, G.**; Poce, G.; Consalvi, S.; Boshoff, H.; Rubin, E.J.; Biava, M. "Derivatives of 2-amino-6-fluorobenzoic acid as inhibitors of Mycobacterium tuberculosis tryptophan biosynthetic pathway". 9th BeMM Symposium, Roma.

07/2018 Poster: Poce, G.; **Venditti, G.;** Consalvi, S.; Audette, B.; Rubin, EJ.; Boshoff, H.; Biava, M. "FABA derivatives as anti-mycobacterials targeting tryptophan biosynthetic pathway", MedChemSicily2018, Palermo (PA).

07/2018 Poster: Poce, G., Consalvi, S.; **Venditti, G**.; Scarpecci, C.; Ballell, L.; Bates, RH.; Fernandez-Menendez, R.; De Logu, A.; Rubin, EJ.; Biava, M. "MmpL3 inhibitors forthe treatment of tuberculosis", Second workshop on research, Department of Chemistry and Technologies of Drug, Sapienza, Rome (RM).

Poster: Poce, G., Consalvi, S.; **Venditti, G**.; Scarpecci, C.; De Logu, A.; Rubin, EJ.; Biava, M., "Novel inhibitors of the tryptophan biosynthetic

pathway as anti-mycobacterial agents", Second workshop on research, Department of Chemistry and Technologies of Drug, Sapienza, Rome (RM).

07/2018 Oral presentation: **Venditti, G.**; Poce, G.; Consalvi, S.; Scarpecci, C.; Ballell, L.; Bates, RH.; Fernandez-Menendez, R.; De Logu, A.; Rubin, EJ.; Biava, M. "Anti-mycobacterial compounds targeting MmpL3 and tryptophan biosynthetic pathway" , Second workshop on research, Department of Chemistry and Technologies of Drug, Sapienza, Rome (RM).

07/2018 Poster: **Venditti, G.,** Consalvi, S.; Boshoff, H., Rubin, EJ., Poce, G., Biava, M. "New aryl hydrazide inhibitors of Mycobacterium tuberculosis tryptophan biosynthetic pathway", XXXVIII European School of Medicinal Chemistry, Urbino (PU).

09/2017 Poster: **Venditti**, **G.**; Consalvi, S.; Boshoff, H.; Biava, M.; Poce, G. "Derivatives of 2-amino-6-fluorobenzoic acid as inhibitors of *Mycobacterium tuberculosis* tryptophan biosynthetic pathway", XXVI National Congress of Società Chimica Italiana, Paestum (SA).

06/2017 Poster: Poce, G.; **Venditti, G.;** Consalvi, S.; De Logu, A.; Boshoff, H.; Rubin, E.; Biava, M.; "Anthranilate like-inhibitors as potent antitubercular agents", Gordon Research Conferences, Lucca.

09/2016 Poster: Poce, G.; Consalvi, S.; **Venditti, G.**; Boshoff, H.; Rubin, E. J.; Biava, M. "Anthranilate-like inhibitors as potent antitubercular agents". 24th National meeting on medicinal chemistry, Perugia.

09/2016 Oral Presentation: **Venditti, G.**; Poce, G.; Alfonso, S.; Consalvi, S.; Fernandez-Menedez, R.; Bates, H. R.; Barros Aguirre, D.; Ballel, L.; De Logu, A.; Vistoli, G.; Biava, M. "New Pyrazole Compounds as Valuable Pre-Clinical Candidates for TB Treatment", 24th National meeting on medicinal chemistry, Perugia.

05/2016 Poster: **Venditti, G.;** Consalvi, S.; Boshoff, H.; Biava, M.; Poce, G. "Novel inhibitors of Mycobacterium tuberculosis tryptophan biosynthetic pathway to treat tuberculosis". Sixth Edition of European Workshop in Drug Synthesis, Certosa di Pontignano, Siena.